Supporting Information

to the manuscript

Synthesis and Catalytic Performance of Nickel Phosphinite Pincer Complexes in Deoxygenative Hydroboration of Amides

by Aziza Adilkhanova,[a] Valeriya F. Frolova,[a,§] Azamat Yessengazin,[a,§] Özgür Öztopçu,[a] Kristina A. Gudun,[a] Medet Segizbayev,[b] Nikita A. Matsokin,[c] Anton Dmitrienko,[b,d] Melanie Pilkington[b] and Andrey Y. Khalimon*[,a,e]

[a] Department of Chemistry, School of Sciences and Humanities, Nazarbayev University, 53 Kabanbay Batyr Ave., Astana 010000, Kazakhstan
[b] Department of Chemistry, Brock University, 1812 Sir Isaac Brock Way, St. Catharines, Ontario L2S 3A1, Canada.
[c] Department of Chemistry, Lomonosov Moscow State University, Leninskie Gory 1-3, Moscow 119991, Russia.
[d] Department of Chemistry and Biochemistry, University of Windsor, 401 Sunset Avenue, Windsor, Ontario N9B 3P4, Canada.
[e] The Environment and Resource Efficiency Cluster (EREC), Nazarbayev University, 53 Kabanbay Batyr Ave., Astana 010000, Kazakhstan

[§] These authors contributed equally

E-mail: andrey.khalimon@nu.edu.kz

Table of Contents:

1. Experimental details

All manipulations were carried out using conventional inert atmosphere glovebox and Schlenk techniques. All protonated and deuterated solvents were dried by distillation from appropriate drying agents. NMR spectra were obtained with a Bruker Avance 300, 400 and 600 MHz and JEOL ECA-500 MHz instruments (^{1}H: 300, 400, 500 and 600 MHz; ^{13}C: 75.5, 125.8 and 151 MHz; ^{31}P: 121.5, 202.5 and 243 MHz; ^{11}B: 160 MHz and ^{19}F: 471 MHz). ^{1}H and ^{13}C chemical shifts were referenced to residual proton and naturally abundant ^{13}C resonance of the deuterated solvent, respectively. ^{31}P-NMR spectra were referenced to 85% H_3PO_4 externally. NMR analysis was done at room temperature unless specified. IR spectra were measured using Nicolet iS10 FT-IR spectrometer. Elemental analyses were performed in the "Nazarbayev University Core Facilities" laboratories using Perkin Elmer 2400 Series II CHNS/O elemental analyzer and Elementar Unicube CNHS/O elemental analyzer. X-ray crystallographic analysis was performed using Bruker D8 Quest and Bruker Apex II CCD diffractometers by Nikita A. Matsokin (Lomonosov Moscow State University) and Dr. Anton Dmitrienko (University of Windsor) and Prof. Dr. Melanie Pilkington (Brock University). Full details can be found in the independently deposited crystallography information files (CIFs). Iminophosphinite,[1] aminophosphinite[1] and bis(phosphinite)[2,3] ligands, and the corresponding bromide complexes **1-Br**–**4-Br**,[1] **6-Br**,[2] as well as **1-BF$_4$**[4] and **1-BH$_4$**[4] were synthesized according to literature procedures. **6-H** was obtained from **6-Br** by modified literature procedure[5,6] using a stoichiometric amount of $LiBHEt_3$ instead of a large excess $LiAlH_4$. Unless noted otherwise, all reagents and substrates for catalysis were purchased from Sigma-Aldrich and used without further purification. All catalytic hydroboration reactions were performed under inert atmosphere using either NMR tubes equipped with Teflon valves (J. Young NMR tubes) or 10 mL pressure vials (Supelco headspace vials) equipped with magnetic screw caps having PTFE-faced butyl septa. The NMR yields for products and conversions of the substrates were determined by ^{1}H-NMR against either mesitylene or 1,3,5-trimethoxybenzene as internal standards.

Preparation of (POCN$^{i\text{-}Pr2}$)NiBr (5-Br)

A solution of the aminophosphinite ligand 1-($^{i}Pr_2PO$)-3-(CH_2-N$^{i}Pr_2$)-C_6H_4 (177 mg, 0.599 mmol) in toluene was added at room temperature to a suspension of [$NiBr_2(CH_3CN)_2$] (180 mg, 0.593 mmol) in toluene, followed by the addition of an excess of NEt_3 (0.4 mL, 0.725 mmol). The resulting mixture was heated at 100 °C for 4 days. The mixture was filtered through a pad of silica gel, the solvent was pumped off and the residue was dried in vacuum to give a yellow powder (205 mg, 75%).

^{1}H-NMR (500 MHz; C_6D_6; δ, ppm): 1.02 (d, J = 6.4 Hz, 6H, 2 CH_3 of N$^{i}Pr_2$); 1.20 (dd, J = 14.4 Hz, 7.0 Hz, 6H, 2 CH_3 of N$^{i}Pr_2$); 1.53 (dd, J = 17.1 Hz, 7.2 Hz, 6H, 2 CH_3 of N$^{i}Pr_2$); 1.80 (d, J = 6.5 Hz, 6H, 2 CH_3 of N$^{i}Pr_2$); 2.26-2.38 (m, 2H, 2 CH of N$^{i}Pr_2$); 3.20-3.34 (m, 2H, 2 CH of P$^{i}Pr_2$); 3.49 (s, 2H, NCH_2); 6.43 (d, J = 7.5 Hz, 1H, C_6H_3); 6.61 (d, J = 7.8

Hz, 1H, *C*$_6$*H*$_3$); 6.92 (t, *J* = 7.7 Hz, 1H, *C*$_6$*H*$_3$). ^{13}C{^{1}H}-NMR (125.8 MHz; C_6D_6; *δ*, ppm): 16.9 (d, *J* = 2.0 Hz); 18.5 (d, *J* = 3.5 Hz); 19.3 (s); 22.7 (s); 28.9 (d, *J* = 24.6 Hz); 57.7 (s); 60.8 (s); 107.7 (d, *J* = 13.0 Hz); 114.0 (s); 126.8 (s); 155.4 (s); 157.0 (s); 159.8 (s). ^{31}P{^{1}H}-NMR (202.5 MHz; C_6D_6; *δ*, ppm): 192.9 (s, O*P*^{i}Pr$_2$).

(**A**)

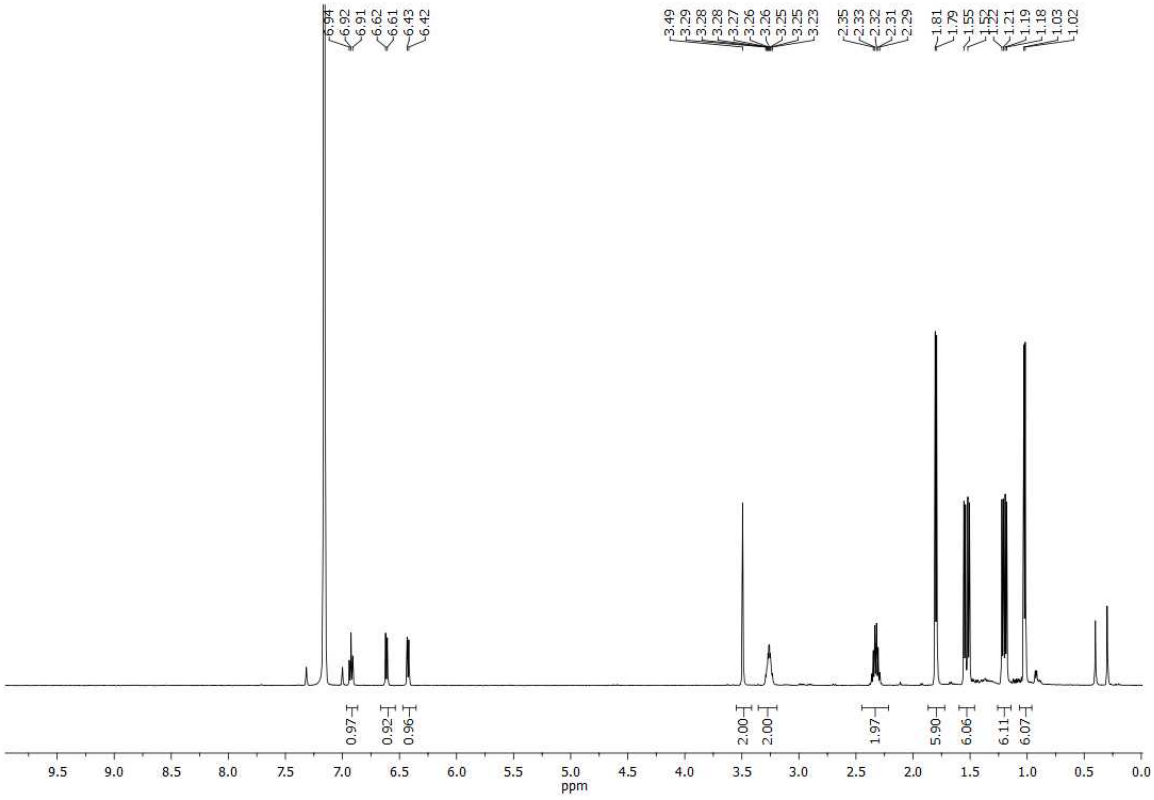

(**B**)

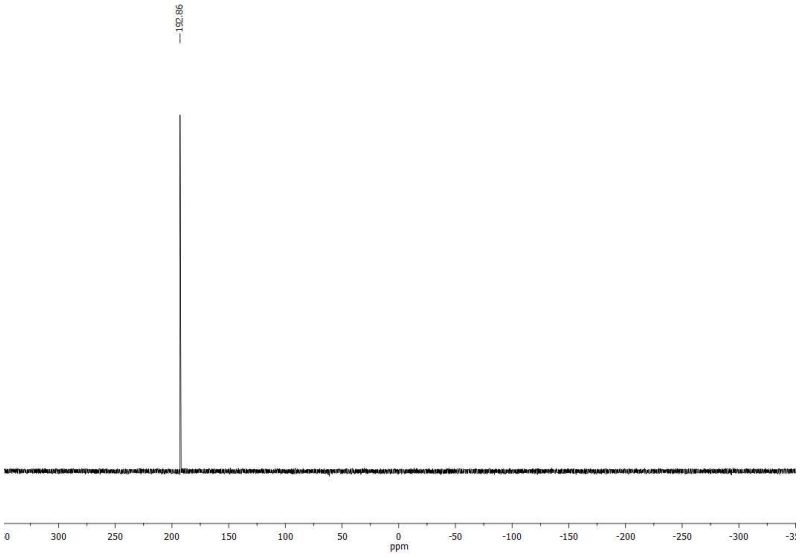

(**C**)

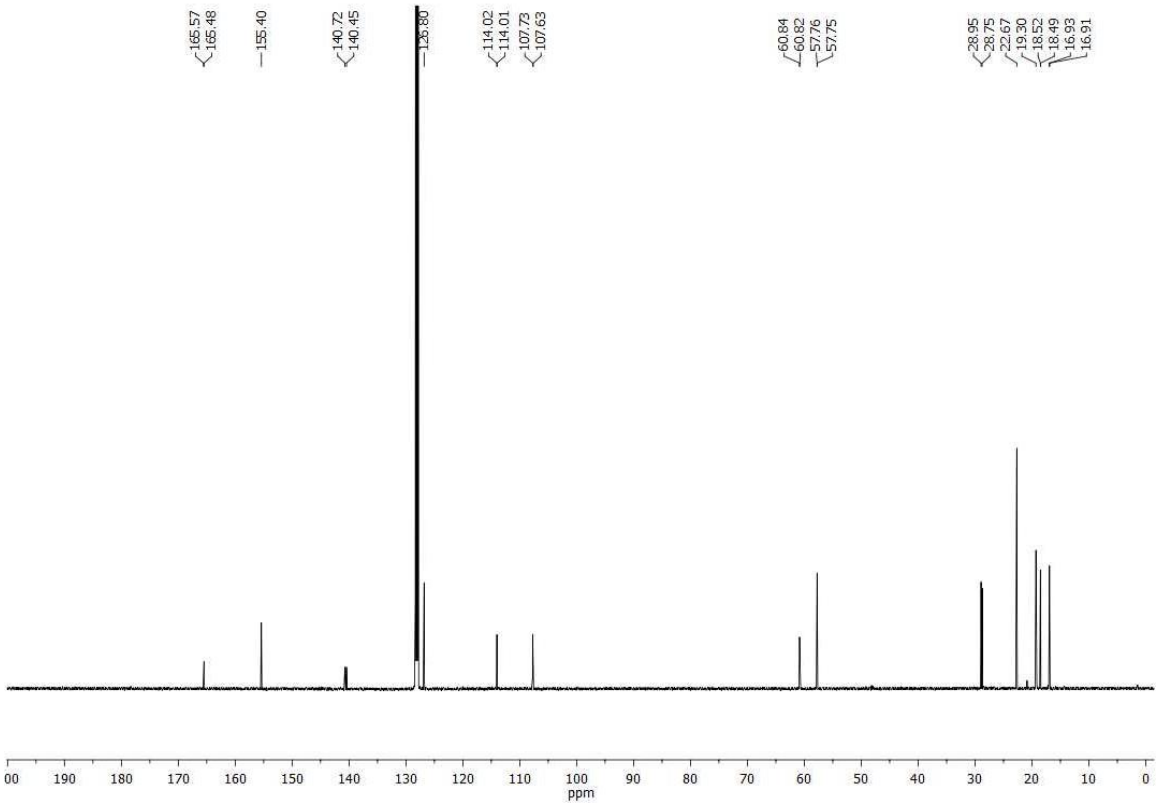

Figure S1. ^{1}H- (**A**), ^{31}P{^{1}H}- (**B**) and ^{13}C{^{1}H}-NMR (**C**) spectra of **5-Br** in C_6D_6.

Reaction of (POCN^{Dipp})NiBr (1-Br) with NaO^{t}Bu

A solution of **1-Br** (15.6 mg, 0.029 mmol) in 0.6 mL of THF was added at room temperature to solid NaO^{t}Bu (2.8 mg, 0.029 mmol). The color of the solution changed to red-brown immediately and the formation of a white precipitate of NaBr was observed. The mixture was transferred to an NMR tube, left for 10 minutes at room temperature, and was checked by NMR spectroscopy showing quantitative conversion of **1-Br** to (POCN^{Dipp})Ni(O^{t}Bu) (**1-O^{t}Bu**). Ian an attempt to isolate complex **1-O^{t}Bu**, all volatiles were pumped off, and the residue was dried and extracted with hexanes. Hexanes were removed under reduced pressure to give an oily red material, which by NMR analysis turned out to be a mixture of the target complex **1-O^{t}Bu** and unknown decomposition products. All attempts to separate this mixture and obtain **1-O^{t}Bu** in analytically pure form were unsuccessful.

^{1}H-NMR (300 MHz; C_6D_6; δ, ppm): 1.04 (s, 9H, 3 *CH$_3$* of NiO^{t}*Bu*); 1.13 (d, *J* = 6.8 Hz, 6H, 2 *CH$_3$* of N*Ar*); 1.23 (dd, *J* = 13.6 Hz and 7.0 Hz, 6H, 2 CH$_3$ of P^{i}*Pr$_2$*); 1.46 (dd, *J* = 17.9 Hz and 7.2 Hz, 6H, 2 *CH$_3$* of P^{i}*Pr$_2$*); 1.55 (d, *J* = 6.8 Hz, 6H, 2 *CH$_3$* of N*Ar*); 2.21 (m, 2H, 2 CH of P^{i}*Pr$_2$*); 3.91 (sept, *J* = 6.8 Hz, 2H, 2 *CH* of N*Ar*); 6.58 (d, *J* = 7.6 Hz, 1H); 6.65 (d, *J* = 7.3 Hz, 1H); 6.75 (t, *J* = 7.4 Hz, 1H); 7.09-7.26 (m, 3H); 7.66 (d, *J* = 4.6 Hz,

1H, C*H*=NAr). $^{13}C\{^{1}H\}$-NMR (125.8 MHz; C_6D_6; δ, ppm): 17.1 (d, J = 3.0 Hz); 18.0 (d, J = 5.6 Hz); 23.9 (s); 25.7 (s); 29.0 (d, J = 20.3 Hz); 29.1 (s); 36.2 (s); 68.8 (s); 111.9 (d, J = 11.6 Hz); 121.8 (s); 123.3 (s); 125.6 (s); 126.6 (s); 142.1 (s); 146.6 (s); 148.2 (s); 154.5 (d, J = 37.5 Hz); 166.5 (d, J = 10.1 Hz); 171.0 (d, J = 3.1 Hz). $^{31}P\{^{1}H\}$-NMR (121 MHz; C_6D_6; δ, ppm): 185.9 (s, O*P*^{i}Pr$_2$).

Reaction of (POCN^{Dmp})NiBr (2-Br) with LiCH$_2$SiMe$_3$

A solution of $LiCH_2SiMe_3$ in pentane (120.6 μL, 1M, 0.1206 mmol) was added in one portion to a solution of **2-Br** (52.5 mg. 0.11 mmol) in 5.0 mL of toluene at -78 °C. Immediately, the color of the reaction mixture changed to dark red. The mixture was left in the cooling bath to slowly warm up to room temperature and stirred overnight at room temperature. NMR analysis overnight showed the exclusive formation of (POCN^{Dmp})Ni(CH_2TMS) (**2-CH$_2$TMS**). The reaction mixture was filtered and all volatiles were pumped off to give a dark red solid, which was dried in vacuum (39.1 mg, 73%). NMR analysis of this material showed 71% of **2-CH$_2$TMS** in a mixture with an unidentified decomposition product. Attempts to isolate **2-CH$_2$TMS** in analytically pure form by recrystallization from hexanes and/or Et_2O solutions were unsuccessful.

^{1}H-NMR (500 MHz; C_6D_6; δ, ppm): -0.91 (d, J = 5.2 Hz, 2H, CH_2 of Ni*CH$_2$*TMS); 0.10 (s, 9H, 3 CH_3 of NiCH$_2$*TMS*); 1.18 (d, J = 6.9 Hz, 3H, CH_3 of P^{i}*Pr$_2$*); 1.20 (d, J = 6.9 Hz, 3H, CH_3 of P^{i}*Pr$_2$*); 1.26 (d, J = 7.2 Hz, 3H, CH_3 of P^{i}*Pr$_2$*); 1.29 (d, J = 7.2 Hz, 3H, CH_3 of P^{i}*Pr$_2$*); 2.17-2.25 (m, 2H, 2 CH of P^{i}*Pr$_2$*); 2.28 (s, 6H, 2 CH_3 of N*Dmp*); 6.76-6.81 (m, 1H); 6.84-6.90 (m, 2H); 6.96-7.03 (m, 3H); 7.19 (d, J = 4 Hz, 1H). $^{13}C\{^{1}H\}$-NMR (125.8 MHz; C_6D_6; δ, ppm): -6.3 (d, J = 17.3 Hz); 4.6 (s); 17.3 (d, J = 1.7 Hz); 18.3 (d, J = 4.8 Hz); 19.6 (s); 28.9 (d, J = 22.7 Hz); 112.6 (d, J = 12.2 Hz); 121.0 (d, J = 1.4 Hz); 125.6 (s); 126.1 (s); 128.6 (s); 130.8 (s); 147.4 (d, J = 1.6 Hz); 148.9 (s); 164.1 (d, J = 10.2 Hz); 165.4 (d, J = 30.3 Hz); 176.9 (d, J = 2.7 Hz). $^{31}P\{^{1}H\}$-NMR (202.5 MHz; C_6D_6; δ, ppm): 195.3 (s, O*P*^{i}Pr$_2$).

Reaction of (POCN^{Dmp})NiBr (2-Br) with PhMgBr

A solution of PhMgBr in THF (1.0 M, 26.0 μL, 0.026 mmol) was added via syringe to a solution of **2-Br** (12.7 mg, 0.026 mmol) in 0.6 mL of C_6D_6 in an NMR tube. Immediate color change to a darker tint of red and formation of small amounts of precipitate were observed. The reaction mixture was left at room temperature for 2 h showing by NMR complete conversion of **2-Br** to (POCN^{Dmp})NiPh (**2-Ph**). The mixture was filtered through a plug of glass wool and all volatiles were pumped off to leave a red residue, which was dried in vacuum. NMR analysis of this residue revealed partial decomposition of **2-Ph** to a mixture of unidentified products. All attempts to obtain **2-Ph** in the analytically pure form via recrystallization from different solvents were unsuccessful.

^{1}H-NMR (500 MHz; C_6D_6; δ, ppm): 7.50 (d, J = 7.5 Hz, 2H); 7.20 (d, J = 4.1 Hz, 1H); 7.16 (s, 1H); 6.98 (t, J = 7.4 Hz, 2H); 6.92 – 6.79 (m, 4H); 6.78 – 6.68 (m, 2H); 2.22 (s,

6H, 2 *CH*$_3$ of N*Dmp*); 2.13 – 2.03 (m, 2H, 2 *CH* of P^i*Pr*$_2$); 1.16 (d, *J* = 6.9 Hz, 3H, *CH*$_3$ of P^i*Pr*$_2$); 1.13 (d, *J* = 6.9 Hz, 3H, *CH*$_3$ of P^i*Pr*$_2$); 1.02 (d, *J* = 7.2 Hz, 3H, *CH*$_3$ of P^i*Pr*$_2$); 0.98 (d, *J* = 7.2 Hz, 3H, *CH*$_3$ of P^i*Pr*$_2$). ^{13}C{^{1}H}-NMR (125.8 MHz; C_6D_6; *δ*, ppm): 16.8 (d, *J* = 1.3 Hz); 17.8 (d, *J* = 4.7 Hz); 19.2 (s); 27.8 (d, *J* = 24.2 Hz); 112.9 (d, *J* = 12.1 Hz); 121.3 (d, *J* = 1.5 Hz); 122.4 (s); 125.6 (s); 125. 8 (d, *J* = 1.6 Hz); 126.4 (s); 127.5 (s); 127.7 (s); 129.1 (s); 129.8 (s); 138.0 (s); 148.0 (d, *J* = 1.9 Hz); 148.8 (s); 164.5 (d, *J* = 3.5 Hz); 164.6 (d, *J* = 11.9 Hz); 166.7 (d, *J* = 29.1 Hz); 177.3 (d, *J* = 2.6 Hz). ^{31}P{^{1}H}-NMR (202.5 MHz; C_6D_6; *δ*, ppm): 196.9 (s, O*P*^{i}Pr$_2$).

Reaction of (POCN^{Dmp})NiBr (2-Br) with KO^{t}Bu

A solution of **2-Br** (147.4 mg, 0.308 mmol) in 20 mL of PhMe was added slowly to a suspension of KO^{t}Bu (35 mg, 0.312 mmol) in 10 mL of PhMe at -40 °C (CH_3CN / liq. N_2 bath). The colour change to a darker tint of red was observed almost immediately. The reaction mixture was stirred at -40 °C for 30 mins, slowly warmed up to room temperature, and stirred for additional 2 hours. NMR analysis of the reaction mixture showed a complete conversion of **2-Br** to (POCN^{Dmp})Ni(O^{t}Bu) (**2-O^{t}Bu**). All volatiles were pumped off and the residue was extracted with cold (-41 °C; liq. N_2/CH bath) hexanes to afford dark-red oily material (126.5 mg, 87%). NMR analysis of this substance revealed a mixture of **2-O^{t}Bu** (61% by ^{31}P{^{1}H}-NMR) with unidentified decomposition products. All attempts to separate this mixture and obtain **2-O^{t}Bu** in analytically pure form were unsuccessful. When the reaction was repeated in THF, analogous partial decomposition of **2-O^{t}Bu** was observed upon its isolation by extraction with hexanes. However, for catalytic trials, **2-O^{t}Bu** was cleanly generated *in situ* in C_6D_6.

^{1}H-NMR (500 MHz; C_6D_6; *δ*, ppm): 6.98-7.02 (m, 3H); 6.78 (t, *J* = 7.8 Hz, 1H); 6.64 (d, *J* = 7.3 Hz, 1H); 6.60 (d, *J* = 7.8 Hz, 1H); 2.51 (s, 6H, 2 *CH*$_3$ of N*Dmp*); 2.17 – 2.24 (m, 2H, 2 *CH* of P^i*Pr*$_2$); 1.47 (d, *J* = 7.2 Hz, 3H, *CH*$_3$ of P^i*Pr*$_2$); 1.44 (d, *J* = 7.2 Hz, 3H, *CH*$_3$ of P^i*Pr*$_2$); 1.27 (d, *J* = 6.9 Hz, 3H, *CH*$_3$ of P^i*Pr*$_2$); 1.24 (d, *J* = 6.9 Hz, 3H, *CH*$_3$ of P^i*Pr*$_2$); 1.08 (s, 9H, 3 *CH*$_3$ of O^t*Bu*). ^{13}C{^{1}H}-NMR (125.8 MHz; C_6D_6; *δ*, ppm): 17.2 (d, *J* = 2.6 Hz); 17.9 (d, *J* = 5.5 Hz); 19.6 (s); 28.8 (d, *J* = 20.1 Hz); 35.9 (s); 68.8 (s); 111.9 (d, *J* = 11.5 Hz); 121.8 (s); 125.4 (s); 125.9 (s); 131.8 (s); 148.5 (s); 149.3 (s); 154.2 (s); 154.5 (s); 166.6 (d, *J* = 10.2 Hz); 171.8 (d, *J* = 3.2 Hz). ^{31}P{^{1}H}-NMR (202.5 MHz; C_6D_6; *δ*, ppm): 185.4 (s, O*P*^{i}Pr$_2$). ^{31}P{^{1}H}-NMR (202.5 MHz; toluene; *δ*, ppm): 185.0 (s, O*P*^{i}Pr$_2$).

Reaction of (POCN^{Me2})NiBr (3-Br) with KO^{t}Bu

In a glovebox, a solution of **3-Br** (18.8 mg,0.046 mmol) in 0.6 mL of C_6D_6 was added at room temperature to KO^{t}Bu (5.7 mg, 0.051 mmol) in a vial and stirred for 5 hours. After that, the reaction mixture was transferred to an NMR tube and was analysed by NMR showing complete conversion of **3-Br** and exclusive formation of (POCN^{Me2})Ni(O^{t}Bu) (**3-O^{t}Bu**). Filtration of the reaction mixture and removal of C_6D_6 in vacuum resulted in the partial decomposition of **3-O^{t}Bu** to a mixture of unidentified products. All attempts to

obtain **3-O^{t}Bu** in analytically pure form by recrystallization methods were also unsuccessful. For catalytic trials, **3-O^{t}Bu** was generated in situ prior to catalysis.

^{1}H-NMR (500 MHz; C_6D_6; δ, ppm): 1.22 (dd, J = 12.8 Hz, 6.9 Hz, 6H, 2 *CH$_3$* of P^i*Pr$_2$*); 1.45-1.55 (m, 15H, 2 *CH$_3$* of P^i*Pr$_2$* and 3 *CH$_3$* of NiO^t*Bu*); 2.15-2.25 (m, 2H, 2 *CH* of P^i*Pr$_2$*); 2.42 (s, 6H, 2 *CH$_3$* of N*Me$_2$*); 3.34 (s, 2H, N*CH$_2$*); 6.42 (d, J = 7.1 Hz, 1H, *C$_6$H$_3$*); 6.60 (d, J = 7.8 Hz, 1H, *C$_6$H$_3$*); 6.91 (t, J = 7.6 Hz, 1H, *C$_6$H$_3$*). ^{13}C{^{1}H}-NMR (125.8 MHz; C_6D_6; δ, ppm): 17.4 (d, J = 3.5 Hz); 18.9 (d, J = 6.0 Hz); 29.5 (d, J = 20.4 Hz); 36.7 (s); 48.2 (d, J = 2.0 Hz); 68.7 (s); 71.2 (d, J = 2.0 Hz); 107.2 (d, J = 10.0 Hz); 115.4 (d, J = 1.9 Hz); 126.1 (s); 138.8 (d, J = 34.9 Hz); 151.5 (s); 166.4 (d, J = 10.0 Hz). ^{31}P{^{1}H}-NMR (202.5 MHz; C_6D_6; δ, ppm): 190.0 (s, O*P*^{i}Pr$_2$).

Reaction of (POCN^{Et2})NiBr (4-Br) with KO^{t}Bu

A solution of **4-Br** (170 mg, 0.393 mmol) in 30 mL of THF was added via cannula to KO^{t}Bu (48.5 mg, 0.432 mmol). The colour immediately changed from yellow to orange. The reaction mixture was stirred at room temperature for 30 min and then analyzed by NMR. The ^{31}P{^{1}H}-NMR analysis of the sample taken directly from the reaction mixture showed a complete conversion of **4-Br** to (POCN^{Et2})Ni(O^{t}Bu) (**4-O^{t}Bu**). Partial decomposition of **4-O^{t}Bu** to a mixture of unidentified products was observed upon its isolation *via* extraction with hexanes and or toluene. The reaction of **4-Br** (10.5 mg, 0.024 mmol) with KO^{t}Bu (3.26 mg, 0.029 mmol) was also repeated on NMR scale in C_6D_6 (0.6 mL) showing exclusive *in situ* formation of **4-O^{t}Bu**.

^{1}H-NMR (500 MHz; C_6D_6; δ, ppm): 6.89 (t, J = 7.6 Hz, 1H); 6.56 (d, J = 7.8 Hz, 1H); 6.41 (d, J = 7.4 Hz, 1H); 3.48 (s, 2H, Et$_2$N*CH$_2$*); 3.16-3.24 (m, 2H, N*Et$_2$*); 2.22-2.30 (m, 2H, N*Et$_2$*); 2.04-2.13 (m, 2H, 2 *CH* of P^i*Pr$_2$*); 1.63 (t, J = 7.1 Hz, 6H, N*Et$_2$*); 1.56 (d, J = 7.2 Hz, 3H, *CH$_3$* of P^i*Pr$_2$*); 1.52 (d, J = 7.2 Hz, 3H, *CH$_3$* of P^i*Pr$_2$*); 1.37 (s, 9H, 3 *CH$_3$* of O^t*Bu*); 1.25 (d, J = 7.0 Hz, 3H, *CH$_3$* of P^i*Pr$_2$*); 1.22 (d, J = 7.0 Hz, 3H, *CH$_3$* of P^i*Pr$_2$*). ^{13}C{^{1}H}-NMR (125.8 MHz; C_6D_6; δ, ppm): 13.6 (s); 17.3 (d, J = 4.2 Hz); 19.5 (d, J = 6.1 Hz); 30.3 (d, J = 20.2 Hz); 32.6 (s); 36.3 (s); 54.7 (d, J = 1.8 Hz); 63.8 (d, J = 1.8 Hz); 107.0 (d, J = 12.5 Hz); 114.1 (d, J = 2.0 Hz); 125.8 (s); 138.3 (d, J = 34.3 Hz); 154.6 (d, J = 1.3 Hz); 165.9 (d, J = 10.3 Hz). ^{1}P{^{1}H}-NMR (202.5 MHz; C_6D_6; δ, ppm): 189.8 (s, O*P*^{i}Pr$_2$).

Reaction of (POCN$^{i\text{-}Pr2}$)NiBr (5-Br) with KO^{t}Bu

In a glovebox, 3.8 mg (0.033 mmol) of KO^{t}Bu was added to solution of 15 mg (0.032 mmol) of **5-Br** in approx. 2 mL of THF in a vial. The reaction mixture was left at room temperature with stirring overnight resulting in a color change from yellow to orange. The ^{31}P{^{1}H}-NMR analysis of the reaction mixture showed the almost exclusive formation of (POCN$^{i\text{-}Pr2}$)Ni(O^{t}Bu) (**5-O^{t}Bu**). All attempts to either crystallize **5-O^{t}Bu** from THF solution or isolate the product via extraction with hexanes resulted in its partial decomposition to a difficult-to-analyse mixture with unidentified compounds.

^{1}H-NMR (500 MHz; THF; δ, ppm; selected resonances, spectra are taken directly from the reaction mixture): 6.64 (t, J = 7.6 Hz, 1H, C_6H_3); 6.28 (d, J = 7.5 Hz, 1H, C_6H_3); 6.13 (d, J = 7.8 Hz, 1H, C_6H_3); 2.39-2.46 (m, 2H, 2 CH of ^{i}Pr); 1.28 (d, J = 6.9 Hz, 3H, CH_3 of ^{i}Pr); 1.26 (d, J = 6.8 Hz, 6H, 2 CH_3 of ^{i}Pr); other resonances are obscured by resonances of THF. ^{13}C{^{1}H}-NMR spectrum in THF turned out to be not informative. Attempts to evaporate THF and redissolve the product in C_6D_6 for ^{13}C-NMR analysis led to partial decomposition of the product and formation of a complex mixture of **5-O^{t}Bu** with unidentified compounds. ^{31}P{^{1}H}-NMR (202.5 MHz; THF; δ, ppm): 185.5 (s, O$P^{i}Pr_2$). ^{31}P{^{1}H}-NMR (202.5 MHz; C_6D_6; δ, ppm): 186.1 (s, O$P^{i}Pr_2$).

NMR scale reaction of (POCN^{Dipp})NiBr (1-Br) with L-Selectride

A solution of L-Selectride in THF (20.2 μL, 0.0202 mmol, 1.0 M solution) was added *via* syringe to a frozen in liq. N_2 solution of **1-Br** (10.8 mg, 0.0202 mmol) in 0.6 mL of C_6D_6 in an NMR tube. The mixture was allowed to warm up slowly to room temperature, left at room temperature for 10 min, and then was monitored by NMR at room temperature, showing after 10 min selective formation of **1-H** (16% conversion of **1-Br** by ^{31}P{^{1}H}-NMR). Monitoring the reaction mixture by NMR during the next 24 h at room temperature revealed decomposition of **1-H** to a mixture of unidentified products together with the release of POC(H)N ligand and H_2 and formation of a black precipitate of metallic nickel.

(POCN^{Dipp})NiH (**1-H**, selected NMR resonances, spectra are taken directly from the reaction mixture): ^{1}H-NMR (500 MHz; C_6D_6; δ, ppm): -9.72 (d, $^{2}J_{H-P}$ = 54 Hz, 1H, Ni*H*; coupled in the ^{1}H-^{31}P HSQC NMR spectrum to the ^{31}P resonance at 205.1 ppm); 1.16 (m, 6H, 2 CH_3 of P$^{i}Pr_2$; found by ^{1}H-^{31}P HSQC NMR); 2.15 (m, 2H, 2 CH of P$^{i}Pr_2$); 3.03 (sept, $^{2}J_{H-H}$ = 6.8 Hz, 2H, 2 CH of N*Ar*); 7.94 (s, 1H, C*H*=NAr; coupled in the ^{1}H-^{13}C HSQC NMR spectrum to the ^{13}C resonance at 161.1 ppm); other resonances are overlapped with the resonances of **1-Br**. ^{31}P{^{1}H}-NMR (202.5 MHz; C_6D_6; δ, ppm): 205.1 (s, O$P^{i}Pr_2$).

NMR scale reaction of (POCN^{Dipp})NiBr (1-Br) with LiHBEt$_3$

A solution of $LiHBEt_3$ in THF (20.0 μL, 0.02 mmol, 1.0 M solution) was added slowly *via* syringe to a cold (app. -30 °C) solution of **1-Br** (10.8 mg, 0.02 mmol) in 0.6 mL of PhMe-d_8 in an NMR tube. The mixture was slowly warmed up to room temperature and left for 10 minutes (during this time the colour change first to dark red and then to green was observed), and then the reaction was monitored by NMR, showing the formation of a mixture of **1-H** and **1-H'** (approx. 1:4 ratio by ^{1}H-NMR, respectively; app. 74% overall conversion of **1-Br** by ^{31}P{^{1}H}-NMR). Further monitoring of the reaction by NMR during 24 h at room temperature revealed decomposition of both **1-H** and **1-H'** to a mixture of unidentified products together with the release of POC(H)N ligand and H_2 and formation of a black precipitate of

metallic nickel. An attempted variable temperature NMR analysis of the reaction mixture (-80 °C to room temperature) gave a result identical to the room temperature experiment.

1-H' (selected NMR resonances, spectra are taken directly from the reaction mixture): ^{1}H-NMR (500 MHz; PhMe-d_8; δ, ppm): -15.00 (dt, J = 22 Hz and 23.8 Hz, 1H, Ni*H*); -8.17 (dt, J = 22 Hz, 101.5 Hz, 1H, Ni*H*); the CH_3 resonances of P^{i}*Pr*$_2$ and N*Ar* of **1-H'** (in the region of 0.93-1.51 ppm are overlapping with the corresponding resonances for **1-Br**, **1-H** and the residual CH_3 resonance of PhMe-d_8; 2.10 (m, 4 CH of P^{i}*Pr*$_2$, overlapping with the CH resonances of **1-H** and with the residual resonance of PhMe-d_8); 3.10 (m, 4 CH of N*Ar*; overlapping with the CH resonances of **1-H**); 7.64 and 7.71 (both s, 1H, C*H*=NAr); other resonances are overlapped with the resonances of **1-Br**, **1-H** and with the residual resonances of PhMe-d_8. ^{31}P{^{1}H}-NMR (202.5 MHz; PhMe-d_8; δ, ppm): 197.6 (br s, 1P, O*P*^{i}Pr$_2$); 208.5 (br s, 1P, O*P*^{i}Pr$_2$).

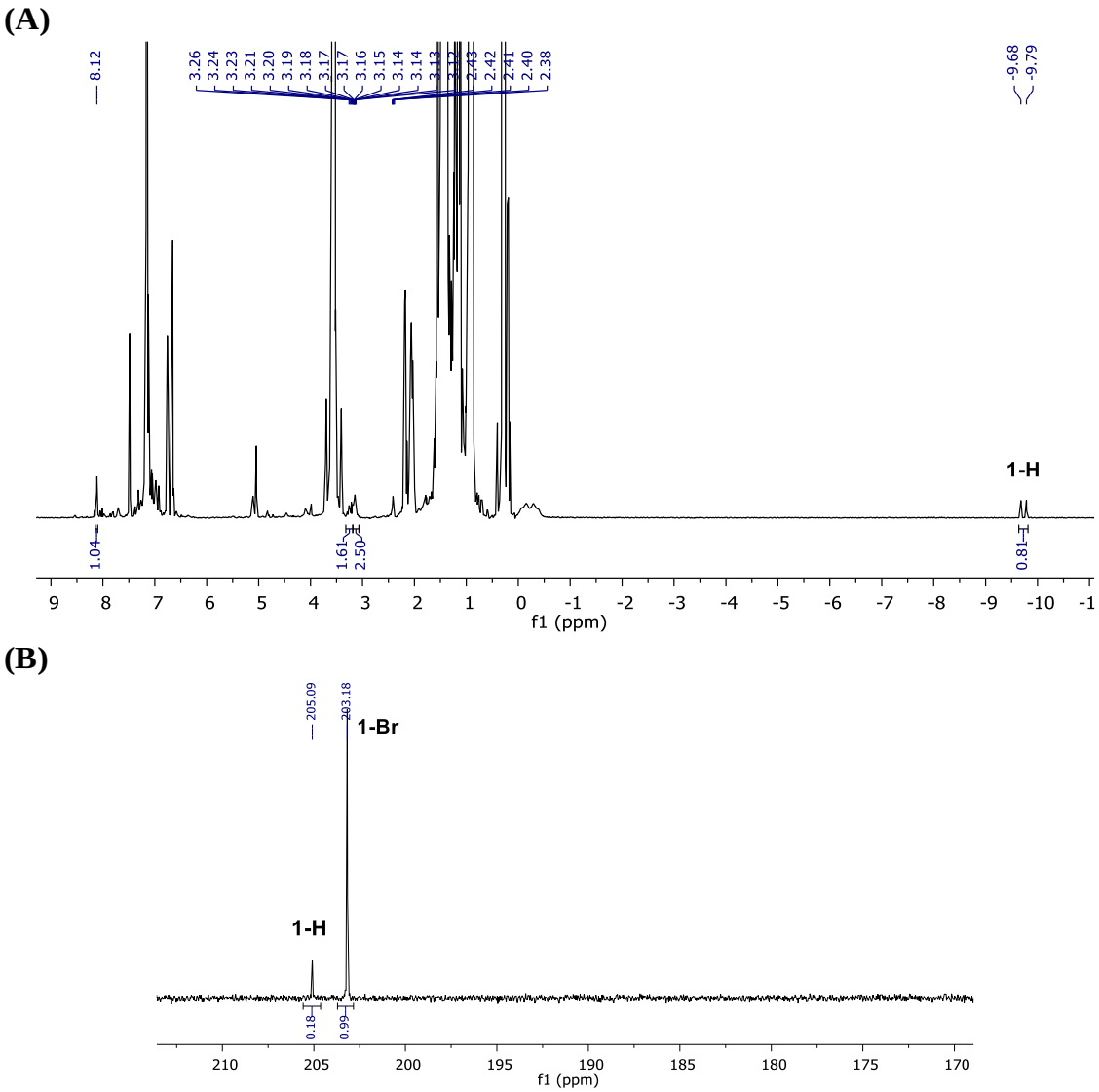

Figure S2. ^{1}H- (**A**) and ^{31}P{^{1}H}-NMR (**B**) spectra from the reaction of **1-Br** with L-Selectride in C_6D_6 taken after 10 min at room temperature, showing 16% conversion (by ^{31}P{^{1}H}-NMR) of **1-Br** to **1-H**.

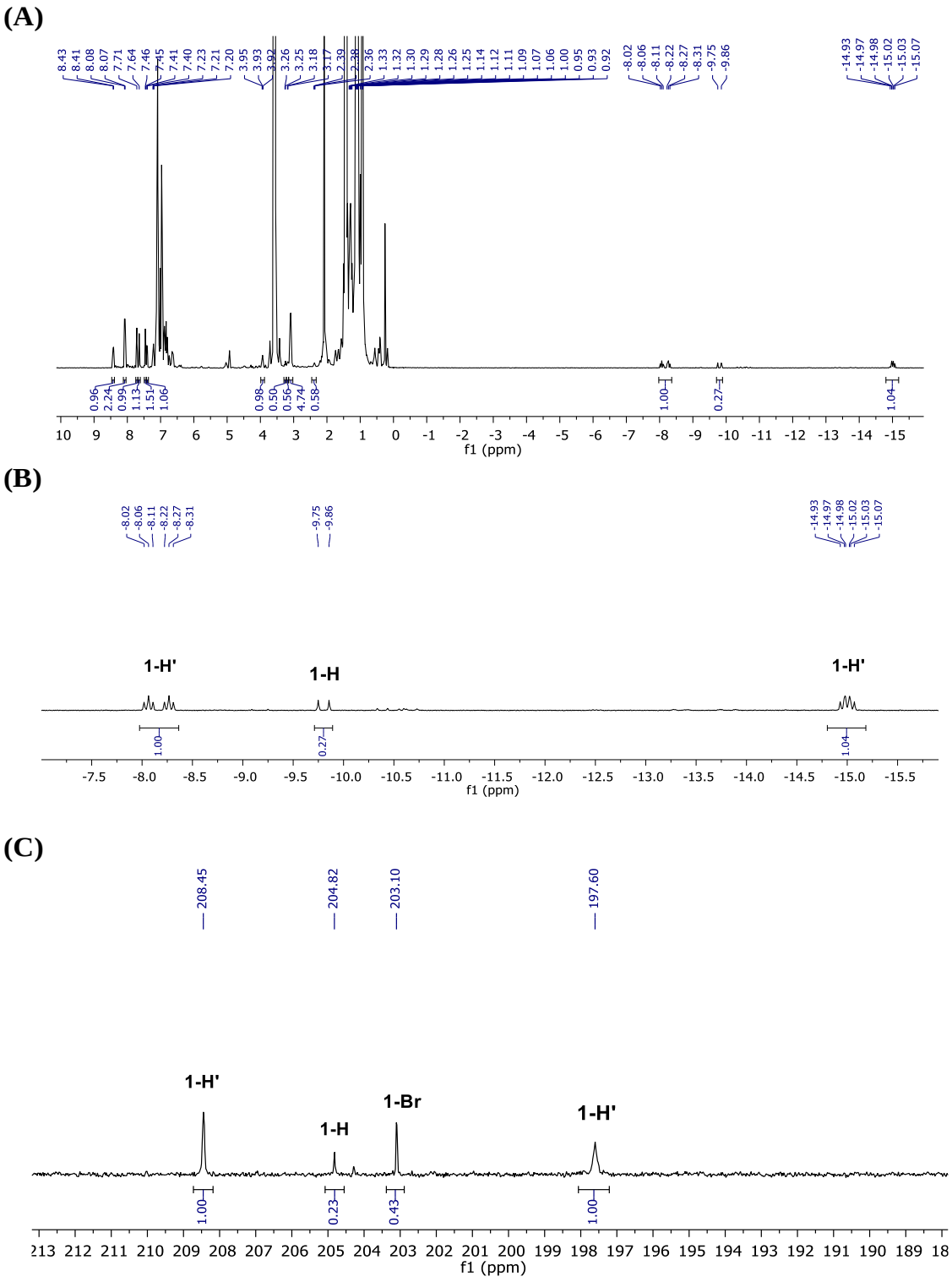

Figure S3. ^{1}H-NMR (**A**), expanded hydride region of ^{1}H-NMR (**B**) and ^{31}P{^{1}H}-NMR (**C**) spectra from the reaction of **1-Br** with $LiBHEt_3$ in PhMe-d_8 taken after 10 min at room temperature, showing 74% conversion (by ^{31}P{^{1}H}-NMR) of **1-Br** to a mixture of **1-H** and **1-H'** (approx. 1:4 ratio by ^{1}H-NMR, respectively).

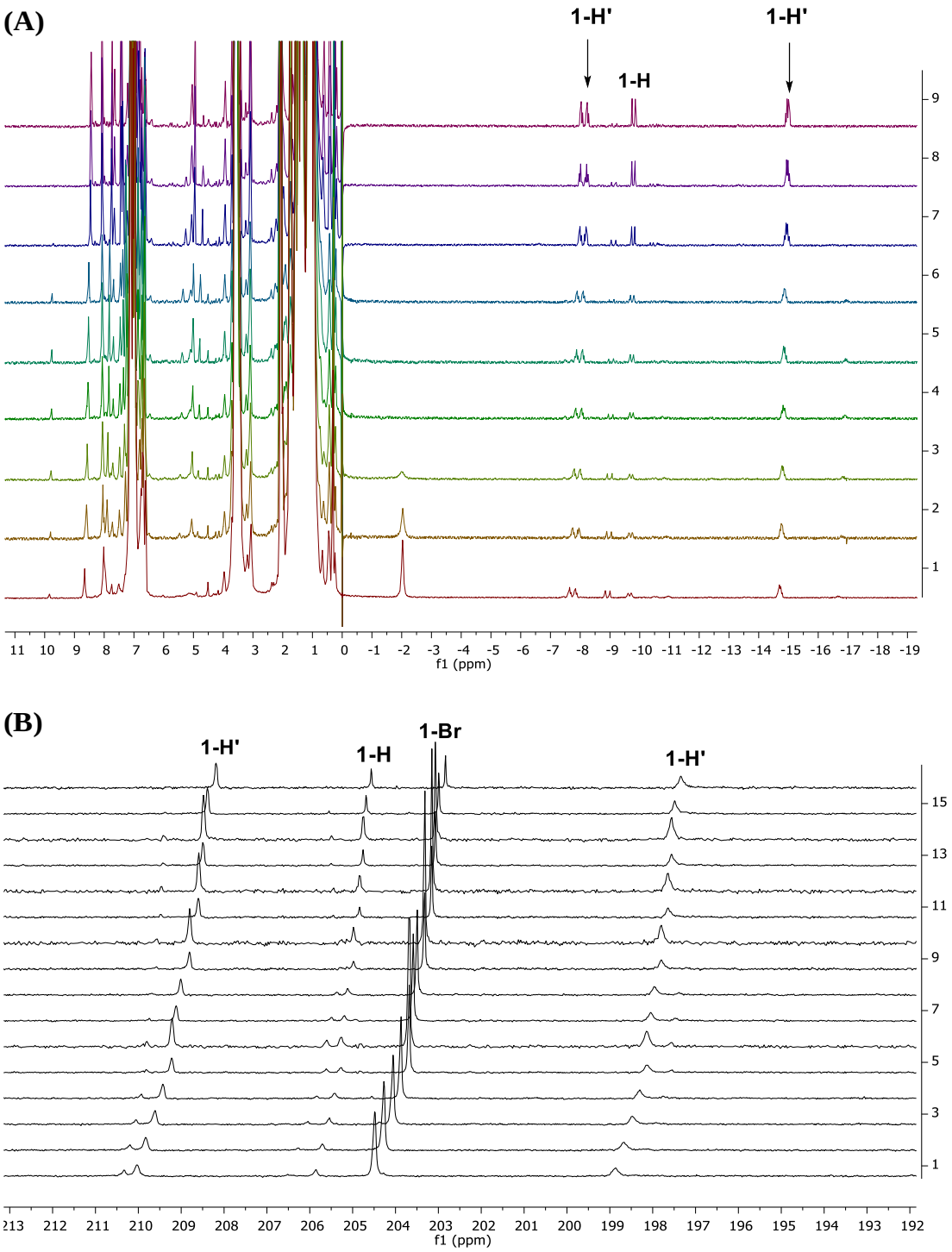

Figure S4. Variable temperature NMR analysis (-80 °C to room temperature) of the reaction of **1-Br** with $LiBHEt_3$ in PhMe-d_8, showing formation of a mixture of **1-H** and **1-H'**: ^{1}H-NMR spectra (**A**) and $^{31}P\{^{1}H\}$-NMR spectra (**B**).

NMR scale reaction of (POCN^{Dipp})NiMe (1-Me) with HBPin

HBPin (3.2 μL, 0.022 mmol) was added at room temperature to a solution of **1-Me** (12.2 mg, 0.022 mmol) in 0.6 mL of C_6D_6 in an NMR tube. The mixture was left at room temperature for 10 min and then the reaction was monitored by ^{1}H- and ^{31}P{^{1}H}-NMR at room temperature, showing after 24 h decomposition of **1-Me** (42% consumption of **1-Me** by ^{31}P{^{1}H}-NMR relative to **1-Br**, which is known to be unreactive towards HBPin and was used as an internal standard) and formation of small amounts of **1-H'** (7% by ^{31}P{^{1}H}-NMR). Further monitoring of the reaction by NMR showed only decomposition, along with H_2 release, to metallic Ni and unidentified products. The reaction at low temperatures showed an identical result.

NMR scale reaction of (POCN^{Dmp})Ni(O^{t}Bu) (2-O^{t}Bu) with HBPin

HBPin (5.7 μL, 0.039 mmol, 5 equiv.) was added at room temperature via syringe to a solution of **2-O^{t}Bu** (3.7 mg, 0.0783 mmol) in 0.6 mL of C_6D_6 in an NMR tube. Immediately after the HBPin addition, the colour of the reaction mixture changed from dark red to turquoise. The reaction mixture was left at room temperature for 15 min and then analyzed by NMR, which revealed the complete conversion of **2-O^{t}Bu** to [(POCN^{Dmp})Ni(μ$_2$-H)]$_2$ (**2-H'**) along formation with of ^{t}BuOBPin,[7] B_2Pin_2[8] and H_2. No intermediate formation of (POCN^{Dmp})NiH (**2-H**) was detected. Leaving the sample at room temperature for 18 h showed slow decomposition of **2-H'** and precipitation of nickel.

2-H' (spectra are taken directly from the reaction mixture): ^{1}H-NMR (500 MHz; C_6D_6; δ, ppm): -14.05 - -13.87 (m, 1H, Ni*H*); -8.90 (dt, J = 22.6 Hz, 96.3 Hz, 1H, Ni*H*); 0.70-0.83 (m, 6H, 2 *CH$_3$* of P^i*Pr$_2$*); 1.04-1.14 (m, 12H, 4 *CH$_3$* of P^i*Pr$_2$* overlapping with the CH_3 resonances of BPin group of ^{t}BuOBPin[7]); 1.29 – 1.43 (m, 6H, 2 *CH$_3$* of P^i*Pr$_2$* overlapping with the CH_3 resonances of ^{t}BuO group of ^{t}BuOBPin[7]); 1.81-1.90 (m, 1H, *CH* of P^i*Pr$_2$*); 1.97-2.14 (m, 3H, 3 *CH* of P^i*Pr$_2$* overlapping with the resonance for *CH$_3$* groups of N*Dmp*); 2.09 (s, 6H, 2 *CH$_3$* of N*Dmp* overlapping with the resonance for *CH* groups of P^i*Pr$_2$*); 2.20 (s, 3H, *CH$_3$* of N*Dmp*); 2.62 (s, 3H, *CH$_3$* of N*Dmp*); 6.70-7.73 (m, 1H, aromatic CH); 6.77-6.80 (m, 3H, aromatic CH); 6.82-6.84 (m, 1H, aromatic CH); 6.87-6.95 (m, 3H, aromatic CH); 7.00-7.03 (m, 2H, aromatic CH); 7.47 (br d, J = 7.1 Hz, 1H, aromatic CH); 7.79 (s, 1H, -C*H*=NDmp); 7.90 (s, 1H, -C*H*=NDmp); 8.46 (br d, J = 7.3 Hz, 1H, aromatic CH). ^{31}P{^{1}H}-NMR (202.5 MHz; C_6D_6; δ, ppm): 199.5 (br s, 1P, O*P*^{i}Pr$_2$); 210.3 (s, 1P, O*P*^{i}Pr$_2$).

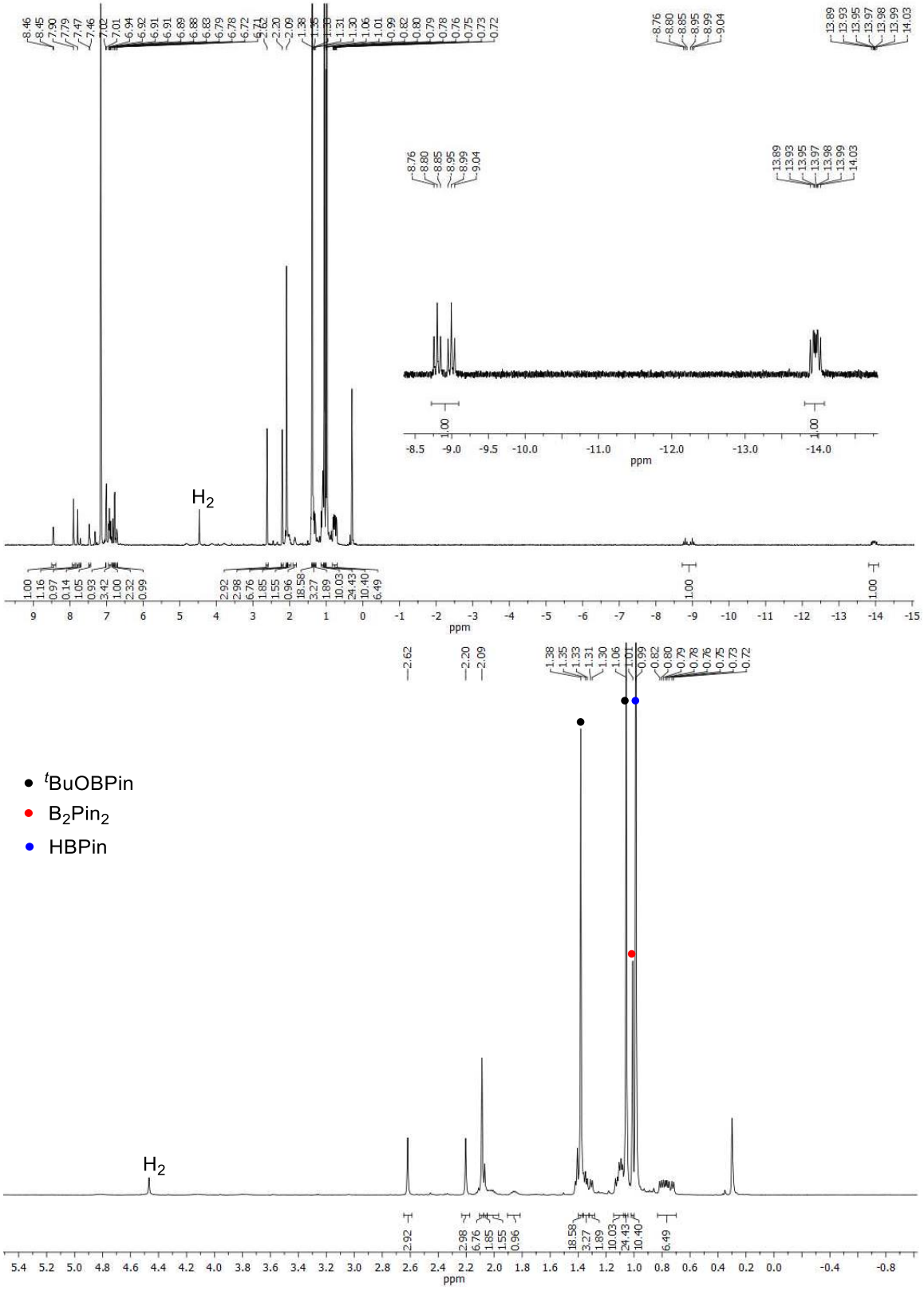

Figure S5. ^{1}H-NMR spectrum taken directly from the reaction of **2-O^{t}Bu** with 5 equiv. of HBPin in C_6D_6 and showing formation of **2-H'**, ^{t}BuOBPin, B_2Pin_2 and H_2.

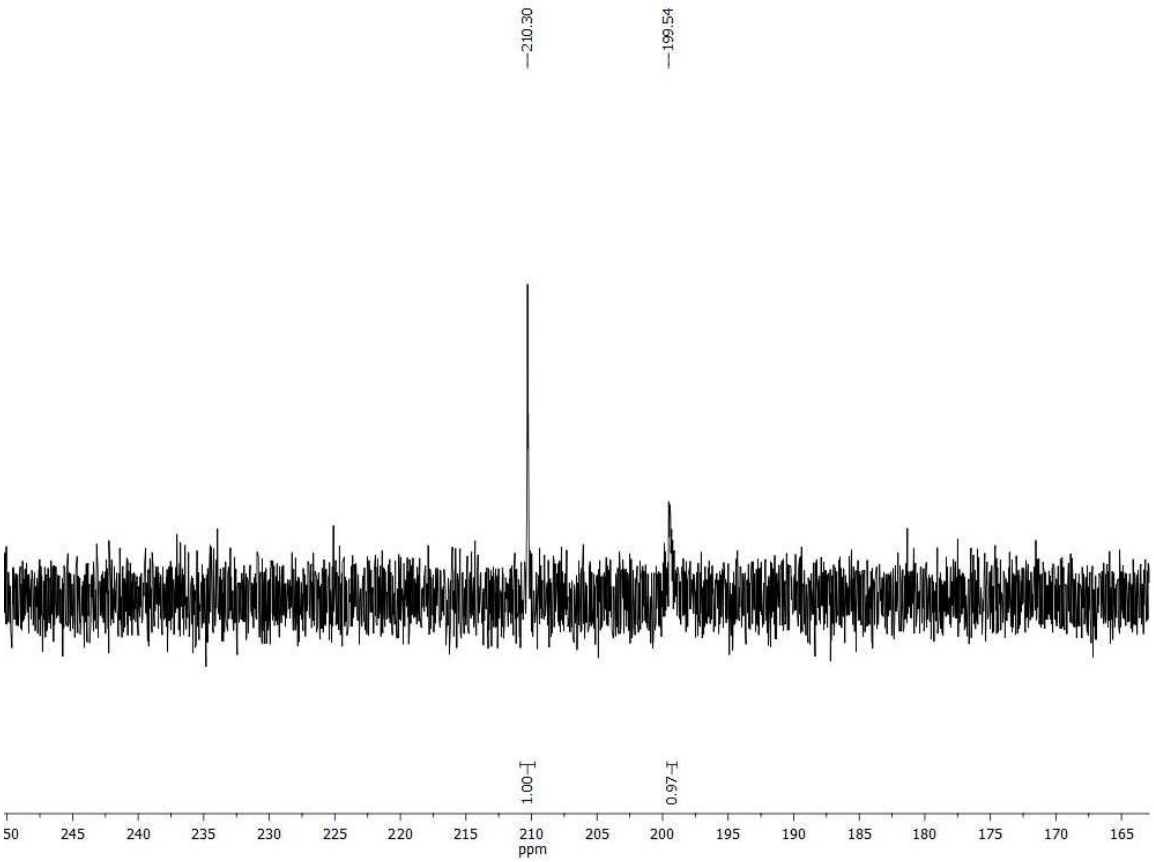

Figure S6. $^{31}P\{^{1}H\}$-NMR spectrum taken directly from the reaction of **2-O^{t}Bu** with 5 equiv. of HBPin in C_6D_6 and showing formation of **2-H'**.

NMR scale reactions of (POCN^{R2})Ni(O^{t}Bu) (R = Me: 3-O^{t}Bu; R = Et: 4-O^{t}Bu) with HBPin.

HBPin (4.0 µl, 0.028 mmol, 1.12 equivalents to Ni) was added at room temperature via syringe to a solution of (POCN^{Me2})Ni(O^{t}Bu) (**3-O^{t}Bu**) in 0.6 mL of C_6D_6 in an NMR tube (**3-O^{t}Bu** was generated in situ from 10 mg (0.025 mmol) of (POCN^{Me2})NiBr (**3-Br**) and 3.1 mg (0.0275 mmol) of KO^{t}Bu in C_6D_6). Immediately after the HBPin addition, the colour of the reaction mixture changed from orange to dark brown. The reaction mixture was left at room temperature for 15 minutes and then analyzed by NMR, showing the formation of a difficult-to-separate mixture of the hydride species [(POCN^{Me2})Ni(μ_2-H)]$_2$ (**3-H'**) and unidentified decomposition products. The formation of ^{t}BuOBPin[7] and H_2 was also detected by ^{1}H-NMR. No intermediate formation of a mononuclear hydride species akin to (POCN^{Me2})NiH (**3-H**) was detected. Full decomposition of **3-H'** was observed within 20 minutes at room temperature. The reaction of **4-O^{t}Bu** with HBPin was performed analogously. Notably, the formation of unstable **3-H'** was also observed by NMR upon treatment of (POCN^{Me2})NiBr (**3-Br**) (10.1 mg, 0.025 mmol) with L-Selectride (0.025 mmol, 25.0 µL of 1M solution in THF) in C_6D_6 at room temperature.

The reaction of (POCN^{Et2})Ni(O^{t}Bu) (**4-O^{t}Bu**) (generated in situ from (POCN^{Et2})NiBr (**4-Br**) (10.5 mg, 0.024 mmol) and 3.3 mg (0.029 mmol) of KO^{t}Bu in C_6D_6) with HBPin (4.2 µl, 0.029 mmol) was done analogously to dimethyl derivative **3-O^{t}Bu** and showed formation of small amounts of a similar dinuclear hydride species [(POCN^{Et2})Ni(µ$_2$-H)]$_2$ (**4-H'**).

[(POCN^{Me2})Ni(µ$_2$-H)]$_2$ (**3-H'**, the spectra are taken directly from the reaction mixture): selected characteristic NMR resonances: ^{1}H-NMR (500 MHz; C_6D_6; δ, ppm): -10.01 (dt, J = 21.8 Hz, 91.3 Hz, 1H, Ni*H*); -12.08 (m, 1H, Ni*H*). ^{31}P{^{1}H}-NMR (202.5 MHz; C_6D_6; δ, ppm): 189.5 (s,1P, OP^i*Pr*$_2$); 209.0 (s, 1P, OP^i*Pr*$_2$).

[(POCN^{Et2})Ni(µ$_2$-H)]$_2$ (**4-H'**, the spectra are taken directly from the reaction mixture): selected characteristic NMR resonances: ^{1}H-NMR (500 MHz; C_6D_6; δ, ppm): -9.82 – -10.15 (m, 1H, Ni*H*); -12.57 (ddd, J = 33.3 Hz, 26.6 Hz, 15.3 Hz, 1H, Ni*H*). ^{31}P{^{1}H}-NMR (202.5 MHz; C_6D_6; δ, ppm): 197.3 (s, 1P, OP^i*Pr*$_2$); 205.9 (s, 1P, OP^i*Pr*$_2$).

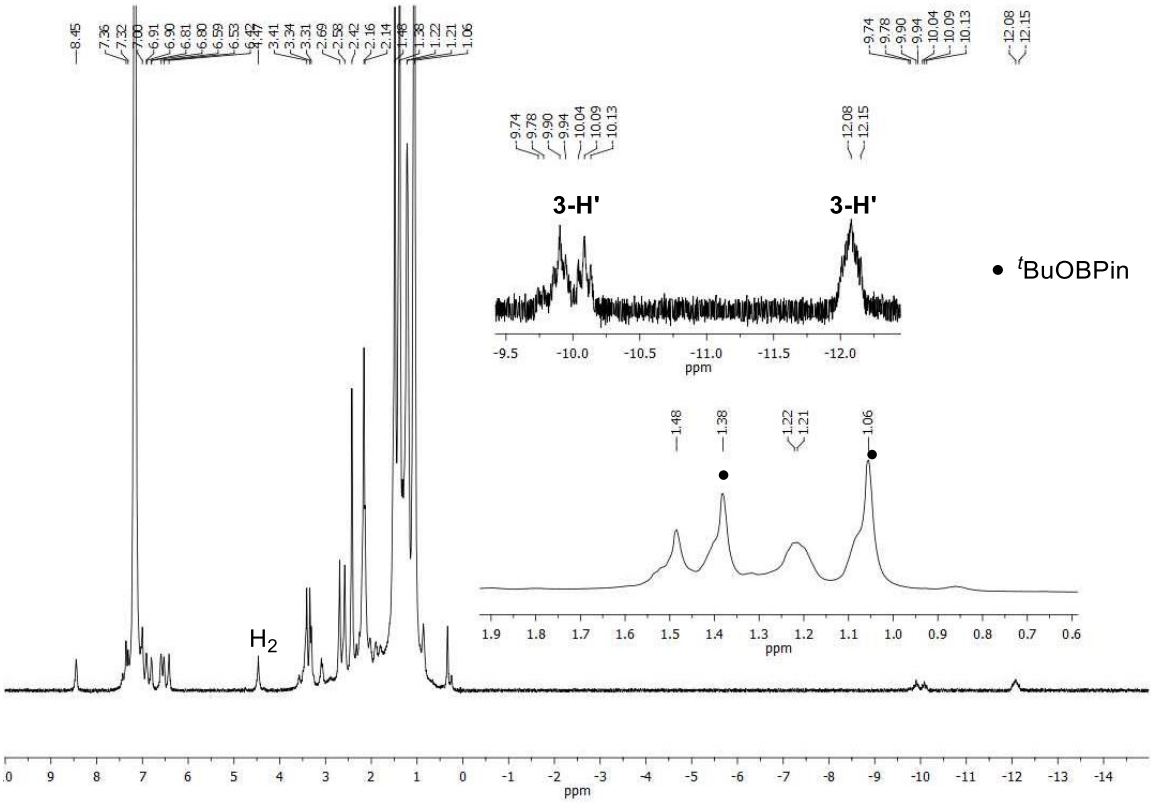

Figure S7. ^{1}H-NMR spectrum taken directly from the reaction of **3-O^{t}Bu** with HBPin in C_6D_6 and showing formation of **3-H'**, ^{t}BuOBPin and H_2.

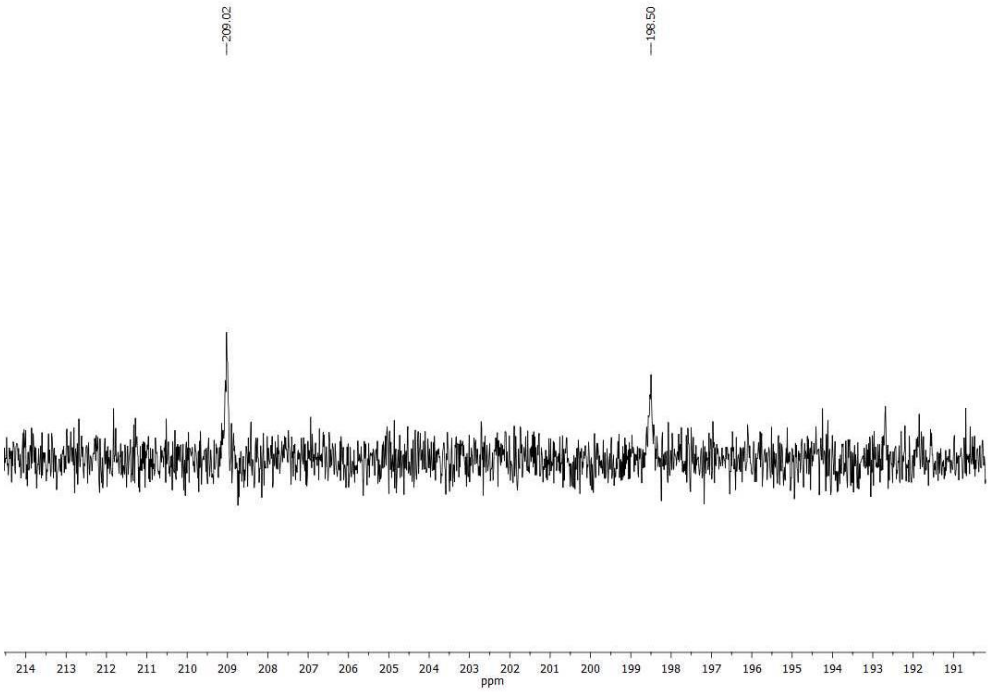

Figure S8. $^{31}P\{^{1}H\}$-NMR spectrum taken directly from the reaction of **3-O^{t}Bu** with HBPin in C_6D_6 and showing formation of **3-H'**.

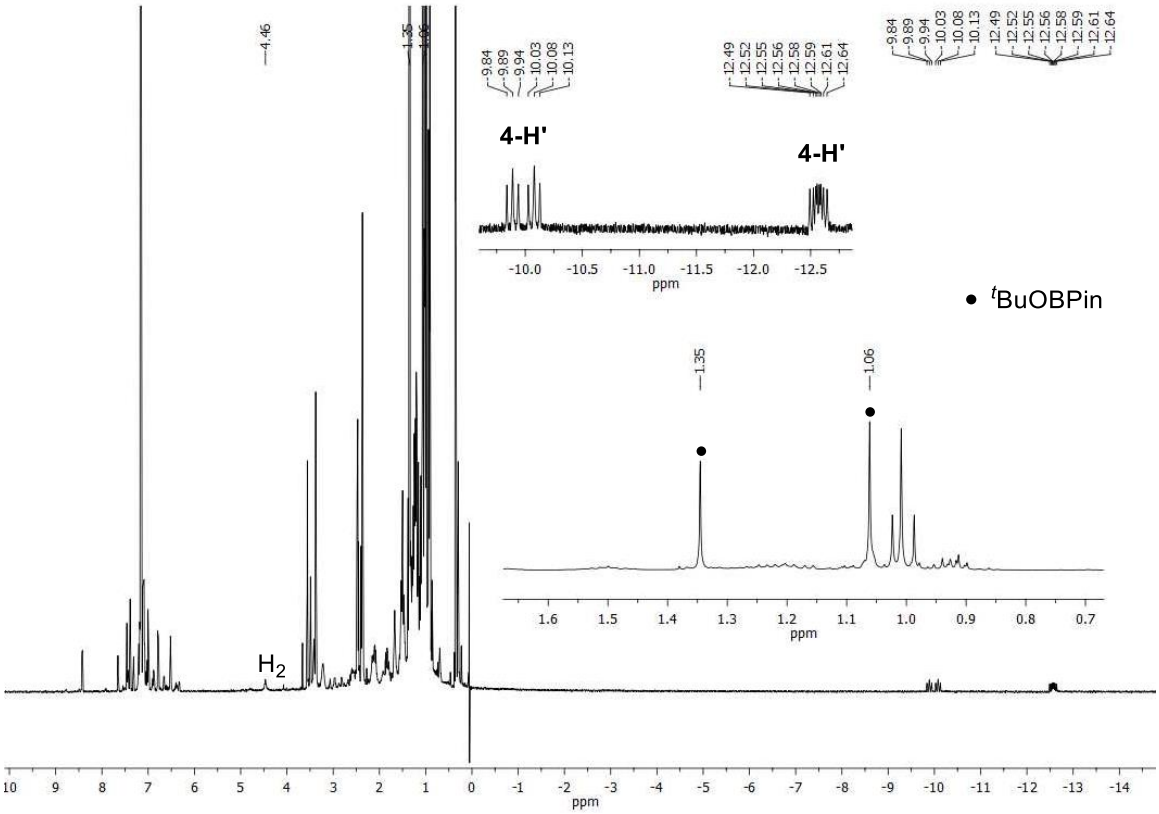

Figure S9. ^{1}H-NMR spectrum taken directly from the reaction of **4-O^{t}Bu** with HBPin in C_6D_6 and showing formation of **4-H'**, ^{t}BuOBPin and H_2.

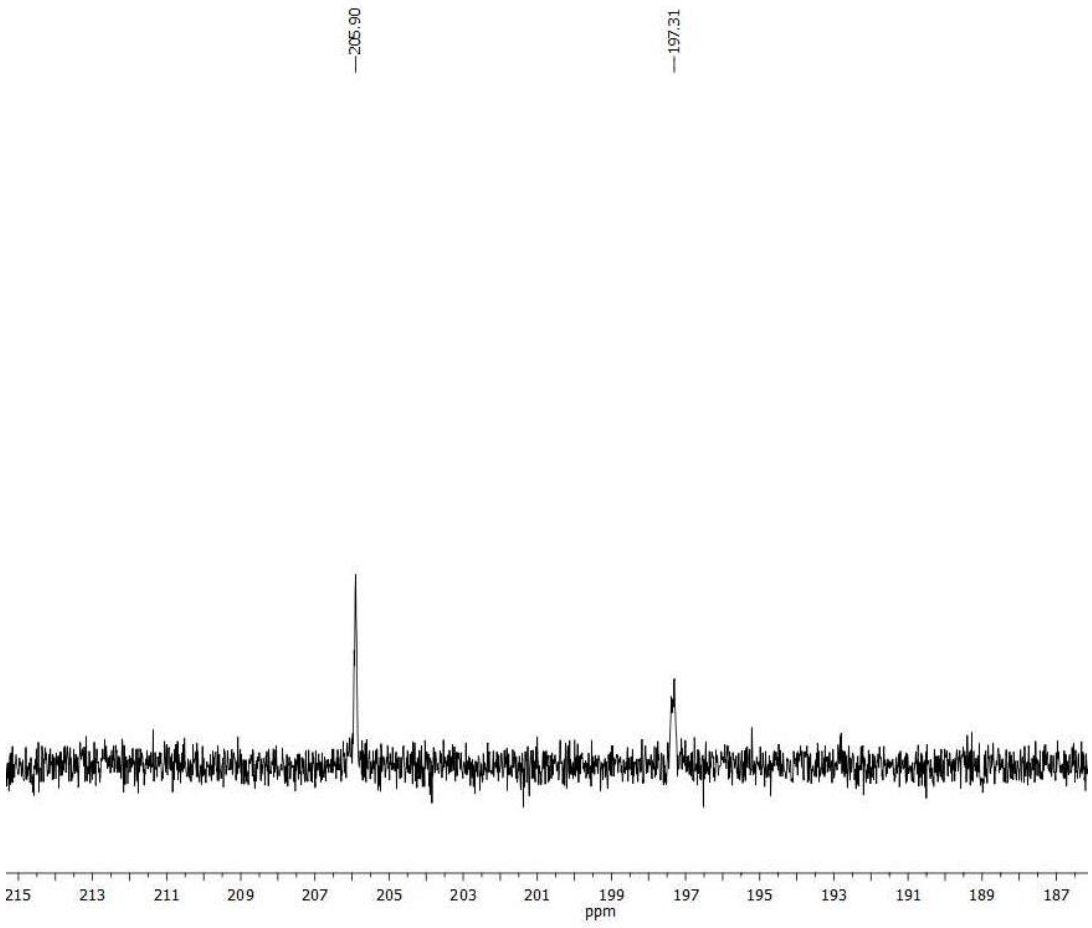

Figure S10. $^{31}P\{^{1}H\}$-NMR spectrum taken directly from the reaction of **4-O^{t}Bu** with HBPin in C_6D_6 and showing formation of **4-H'**.

NMR scale reaction of (POCN^{Me2})Ni(OAc) (3-OAc) with HBPin

HBPin (3.2 μl, 0.022 mmol) was added at room temperature via syringe to a solution of (POCN^{Me2})Ni(OAc) (**3-OAc**) (8.4 mg, 0.022 mmol) in 0.6 mL of C_6D_6 in an NMR tube. Immediately after HBPin addition the colour of the reaction mixture changed from yellow to brown. The reaction mixture was left at room temperature for 15 minutes and then analyzed by NMR, showing the formation of a difficult-to-separate mixture of the starting **3-OAc** and the hydride species [(POCN^{Me2})Ni(μ_2-H)]$_2$ (**3-H'**) (approx. 9:1 by $^{31}P\{^{1}H\}$-NMR, respectively).

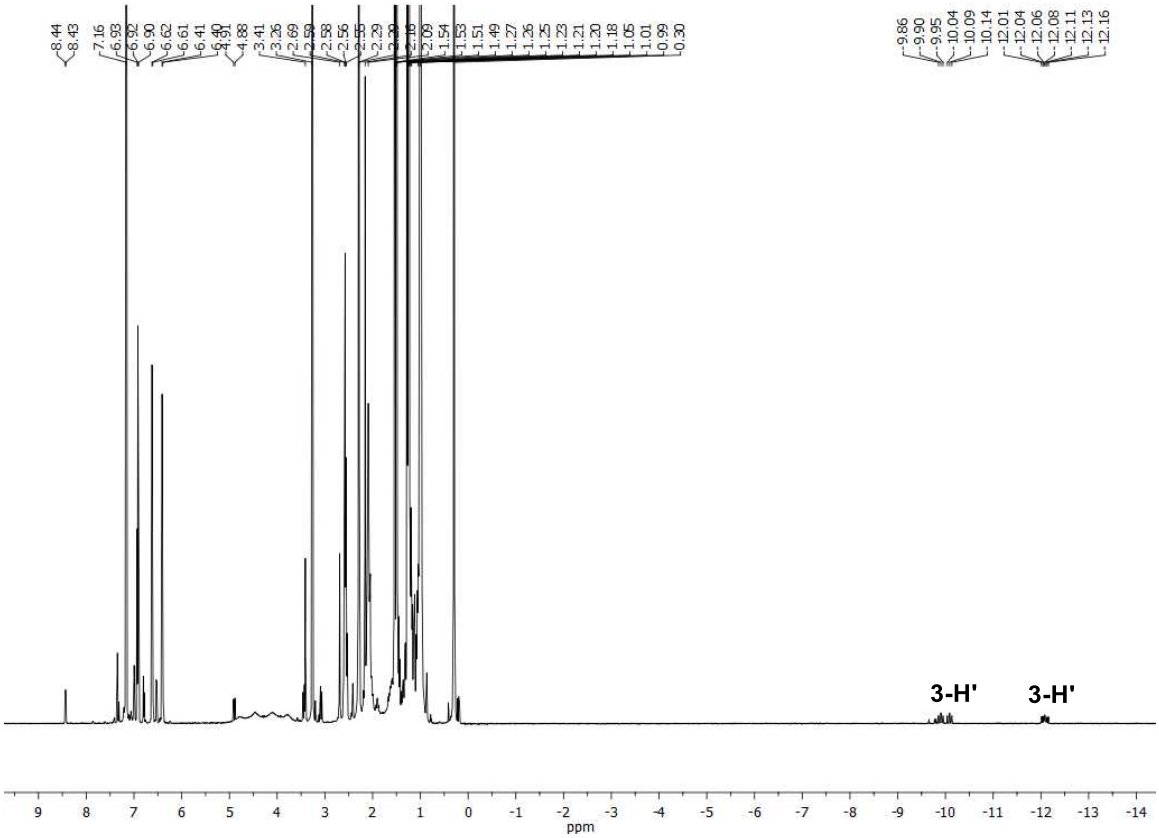

Figure S11. ^{1}H-NMR spectrum taken directly from the reaction of **3-OAc** with HBPin in C_6D_6 and showing formation of **3-H'**.

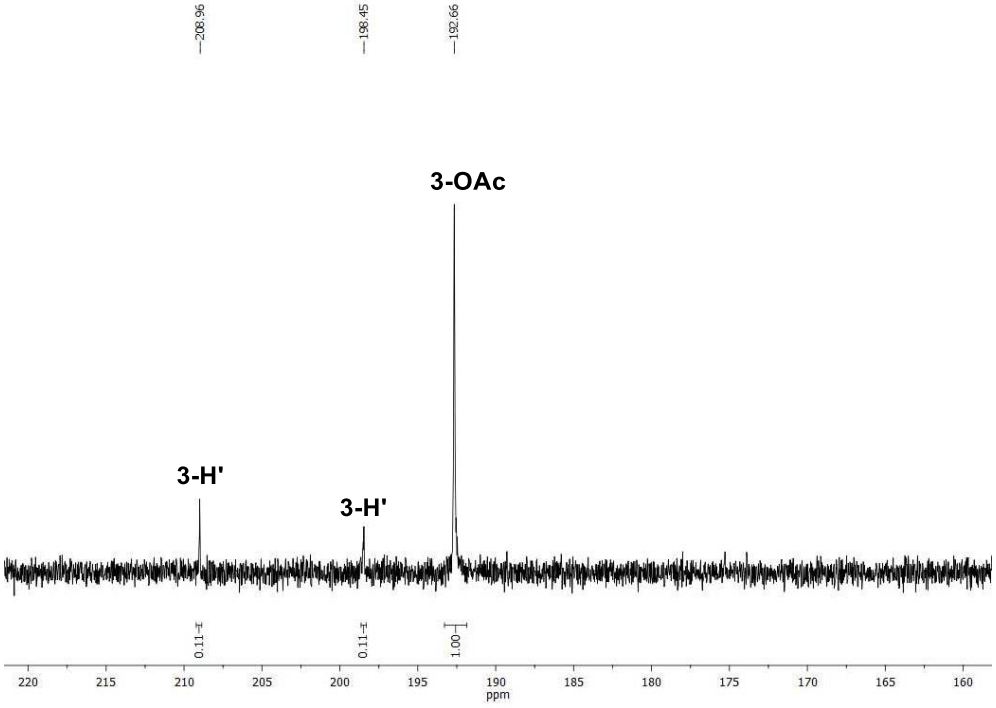

Figure S12. ^{31}P{^{1}H}-NMR spectrum taken directly from the reaction of **3-OAc** with HBPin in C_6D_6 and showing formation of **3-H'**.

NMR scale reaction of (POCN^{iPr2})NiBr (5-Br) with LiHBEt$_3$

A solution of LiBHEt$_3$ in THF (26.0 μL, 0.026 mmol, 1.0 M solution) was added by syringe at room temperature to a solution of **5-Br** (10.0 mg, 0.024 mmol) in 0.6 mL of C_6D_6 in an NMR tube. The reaction mixture was left at room temperature for 30 min and then was monitored by NMR, which showed slow (66% in 19 hours by $^{31}P\{^1H\}$-NMR) formation of (POCN^{iPr2})NiH (**5-H**). All attempts to fully convert **5-Br** to the hydride product **5-H** were unsuccessful resulting in difficult-to-separate mixtures of **5-H** and the starting bromide **5-Br**. Thus, repeating the reaction in either C_6D_6 or PhMe with increased concentration of LiBHEt$_3$ (up to 1.5 equiv. to **5-Br**) and under increased temperature (up to 50 °C) showed a maximum 80% conversion (by $^{31}P\{^1H\}$-NMR) of **5-Br** to **5-H**, with the best results achieved with 1.3 equiv. of LiBHEt$_3$ in at 30 °C. Leaving the obtained mixture of **5-Br** and **5-H** in mother liquor for several days at room temperature did not result in any significant decomposition of the hydride complex **5-H**. All attempts to separate the mixture of **5-Br** and **5-H** by recrystallization methods were unsuccessful.

(POCN^{iPr2})NiH (**5-H**, spectra were taken directly from the reaction mixture): ^{1}H-NMR (500 MHz; C_6D_6; δ, ppm): -10.26 (br d, $^2J_{H\text{-}P}$ = 78.5 Hz, 1H, Ni*H*); the resonance for two *CH*$_3$ groups of N^i*Pr*$_2$ substituent is overlapping with the resonances of B*Et*$_3$ groups; 1.20-1.26 (m, 6H, 2 *CH*$_3$ of P^i*Pr*$_2$); 1.27-1.34 (m, 2 *CH*$_3$ of P^i*Pr*$_2$); 1.61 (br m, 6H, 2 *CH*$_3$ of N^i*Pr*$_2$); 2.06-2.16 (m, 2H, 2 CH of N^i*Pr*$_2$); 3.02-3.13 (m, 2H, 2 CH of P^i*Pr*$_2$); 3.83 (s, 2H, N*CH*$_2$); 6.67 (d, *J* = 7.2 Hz, 1H of *C*$_6$*H*$_3$); 6.82 (d, *J* = 7.7 Hz, 1H of *C*$_6$*H*$_3$); 7.04 (m, 1H of *C*$_6$*H*$_3$). ^{1}H-NMR (500 MHz; THF-H$_8$; selected characteristic resonances δ, ppm): -11.67 (d, *J* = 81.0 Hz, 1H, Ni*H*). $^{31}P\{^1H\}$-NMR (202.5 MHz; C_6D_6; δ, ppm): 203.8 (s, O*P*^{i}Pr$_2$). $^{31}P\{^1H\}$-NMR (202.5 MHz; THF-H$_8$; δ, ppm): 202.2 (s, O*P*^{i}Pr$_2$)

NMR scale reaction of (POCN^{iPr2})Ni(O^{t}Bu) (5-O^{t}Bu) with HBPin

In a glovebox, HBPin (4.60 μL, 0.032 mmol) was added at room temperature via syringe to a solution of **5-O^{t}Bu** (14.3 mg, 0.032 mmol) in approx. 1.0 mL of THF in a vial. The reaction mixture was stirred at room temperature overnight, affording a dark brown solution, NMR analysis of which revealed only approx. 40% conversion (by $^{31}P\{^1H\}$-NMR) of **5-O^{t}Bu** to (POCN^{iPr2})NiH **5-H**. Increasing the temperature of the reaction up to 40 °C did not result in increased conversion of **5-O^{t}Bu** to **5-H**. No formation of binuclear species akin to [(POCN^{iPr2})Ni(μ_2-H)]$_2$ (**5-H'**) was observed by NMR.

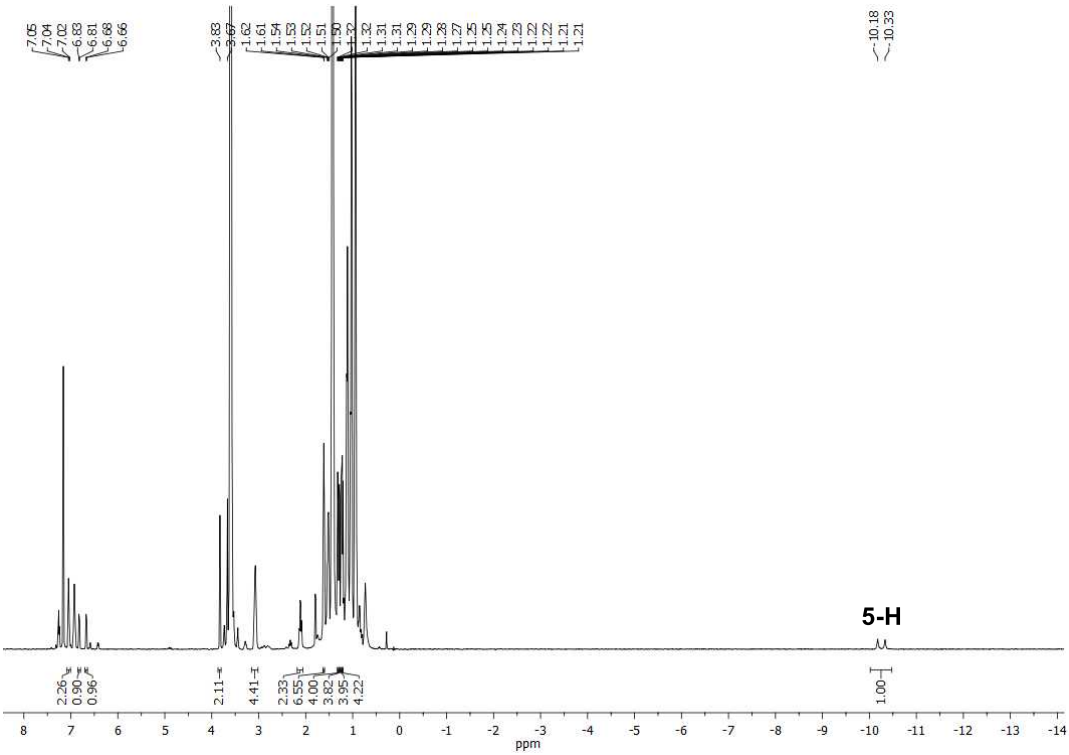

Figure S13. ^{1}H-NMR spectrum taken directly from the reaction of **5-Br** with 1.3 equiv. of $LiBHEt_3$ in C_6D_6 at 30 °C and showing formation of **5-H**.

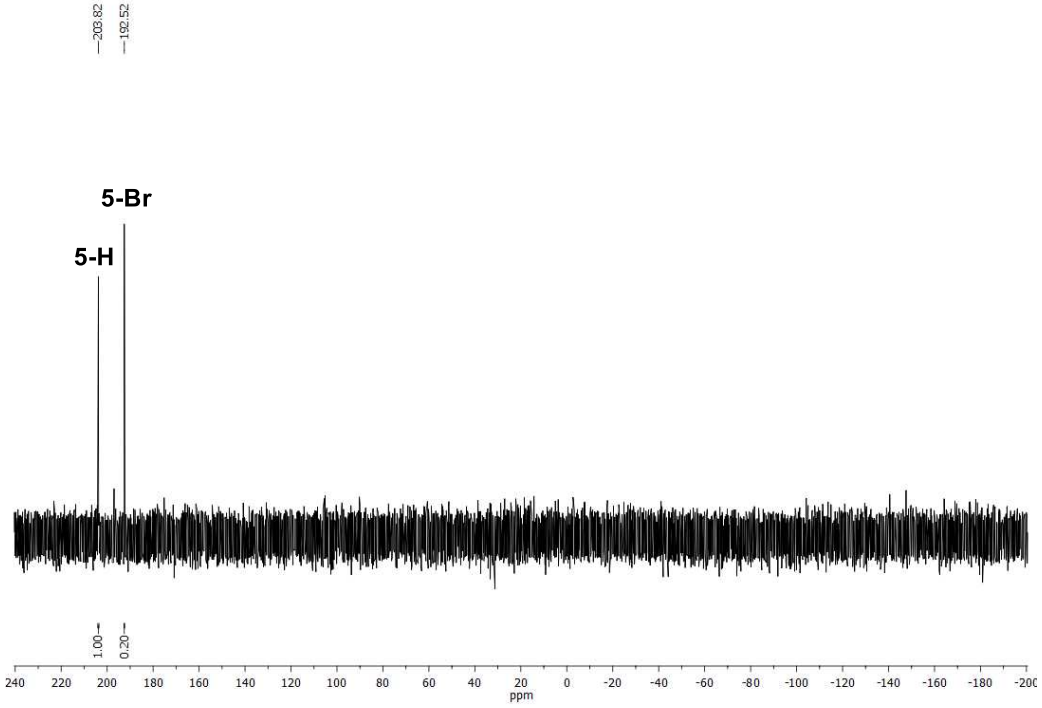

Figure S14. ^{31}P{^{1}H}-NMR spectrum taken directly from the reaction of **5-Br** (δ_P = 192.5 ppm) with 1.3 equiv. of $LiBHEt_3$ in C_6D_6 at 30 °C and showing formation of **5-H** (δ_P = 203.8 ppm).

General procedure for catalytic deoxygenative hydroboration of carboxamides

0.1 mmol of the amide substrate were added at room temperature to a solution of 5 mol% of either **6-H** (for reactions with 2° amides) or **2-CH$_2$TMS** (generated in situ from **2-Br** and LiCH$_2$TMS; for reactions with 1° amides) in 0.6-1.0 mL of C_6D_6 in a pressure vial (10 mL Supelco headspace vials equipped with magnetic screw caps having PTFE-faced butyl septa). This was followed by a room temperature addition of either 3.5 equiv. (0.35 mmol, 50.8 µL for 2° amides) or 5 equiv. (0.5 mmol, 72.6 µL for 1° amides) of HBPin. The vial was sealed and placed in an oil bath for 24 h at the appropriate temperature (40-100 °C). After 24 h, the reaction mixture was cooled down to room temperature and analyzed by ^{1}H-NMR using 0.2 equivalents (0.02 mmol) of either 1,3,5-trimethoxybenzene or mesitylene as internal standards. The yields of the *N*-borylamine products were calculated by the integration of NMR spectra.

Deoxygenative hydroboration of benzamide catalyzed by *tert*-butoxide complexes 2-O^{t}Bu, 3-O^{t}Bu and 4-O^{t}Bu.

The reactions were performed according to the above general procedure for catalytic deoxygenative hydroboration of amides. Due to the high moisture sensitivity of *tert*-butoxide complexes and their partial hydrolysis upon isolation, **2-O^{t}Bu**, **3-O^{t}Bu** and **4-O^{t}Bu** were generated in situ from the corresponding bromides, **2-Br**, **3-Br** and **4-Br**, and KO^{t}Bu (1:1 ratio) in either C_6D_6 or THF. The purity of the prepared tert-butoxide complexes was confirmed by NMR prior to catalytic trials. The results of the deoxygenative hydroboration of benzamide catalyzed by these complexes are summarized below. Despite moderate conversions of benzamide observed in these reactions, tert-butoxide complexes were excluded from further studies due to their high air- and moisture sensitivity as well as long reaction times for their in situ generation from the corresponding bromide precursors in C_6D_6 (up to 5h at room temperature; see the generation of these complexes described above).

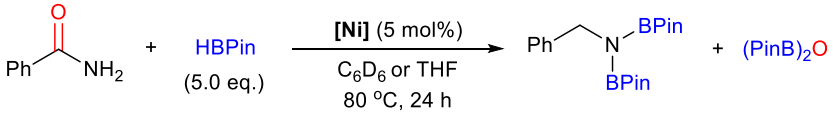

Entry	Cat. / Pre-cat.	Solvent	NMR yield[a], %
1	(POCN^{Dmp})Ni(O^{t}Bu) (**2-O^{t}Bu**)	C_6D_6	72
2	(POCN^{Me2})Ni(O^{t}Bu) (**3-O^{t}Bu**)	C_6D_6 THF	85 63
3	(POCN^{Et2})Ni(O^{t}Bu) (**4-O^{t}Bu**)	THF	66

Conditions: C(amide) = 0.21 mol/L; [Ni] loading 5 mol%.

[a] Determined using 1,3,5-trimethoxybenzene as internal standard.

General procedure for chemoselectivity studies of catalytic deoxygenative hydroboration reactions.

14.9 mg (0.1 mmol) of *N*-phenylpropenamide, 0.1 mmol of the competing substrate (bromobenzene, cyclohexene, styrene, *N*,*N*-dimethylbenzamide, benzamide), and 5 mol% of **6-H**, were mixed in 0.6 mL of C_6D_6 in a pressure vial (10 mL Supelco headspace vials equipped with magnetic screw caps having PTFE-faced butyl septa). This was followed by a room temperature addition of 3.0 equiv. (0.30 mmol, 43.5 μL for reactions with all competing substrates) or 5.0 equiv. (0.5 mmol, 72.6 μL; only for reaction in the presence of benzamide) of HBPin. The vial was sealed and placed in an oil bath for 12 h at the appropriate temperature (60 °C for the reaction in the presence of bromobenzene; 100 °C for reactions in the presence of cyclohexene, styrene, *N*,*N*-dimethylbenzamide and benzamide). After 12 h the reaction mixture was cooled down to room temperature and analyzed by ^{1}H-NMR using 0.2 equivalents (0.02 mmol) of 1,3,5-trimethoxybenzene. The yields of the *N*-borylamine products as well as hydroboration products from competing substrates were calculated by NMR analysis based on the integration of NMR resonances against the resonance of an internal standard. The results of the chemoselectivity tests are depicted in Scheme 9 in the manuscript.

2. Control Experiments

NMR reaction of (POCOP)NiH (6-H) with HBPin

HBPin (4.1 μL; 0.0284 mmol) was added via syringe at room temperature to a solution of (POCOP)NiH (**6-H**) (10.8 mg, 0.0284 mmol) in 0.6 mL of C_6D_6 in an NMR tube. The resulting mixture was left at room temperature for 15 min and then the reaction was monitored by NMR for 24 h at room temperature and then for 12 h at 40 °C. After 3 h at room temperature broadening of the hydride resonance of **6-H** equilibrium formation of an unknown borohydride species (approx. ratio of this species to **6-H** was 1:5) was observed (see Figure S15). The obtained borohydride species could be (POCOP)Ni(BH_2Pin). Heating the mixture for 13 h at 40 °C resulted in approx. ratio of the borohydride species to **6-H** = 1:3 (by ^{1}H-NMR; see Figure S16). The formation of trace amounts of B_2Pin_2 and H_2 was also observed. The addition of *N*-phenylpropanamide (one equivalent to **6-H**) resulted after 24 h at RT in the formation of small amounts of borylated *N*-phenylpropanamide, EtC(O)N(BPin)Ph, and borylated amine, PrN(BPin)Ph, products. Also, approx. 32% conversion of **6-H** to an unknown species characterized by δ_P = 188.5 ppm (s) (compare to δ_P = 206.9 ppm for **6-H**) was observed by ^{31}P{^{1}H}-NMR within 24 h at room temperature after addition of *N*-phenylpropanamide (see Figure S17).

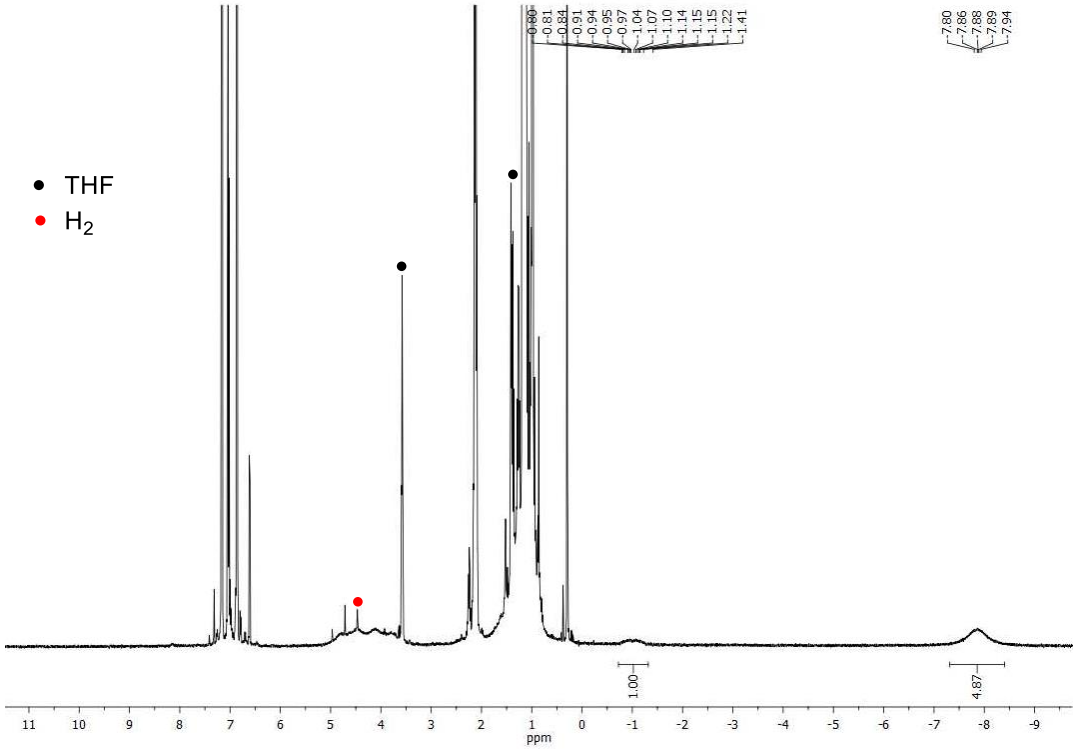

Figure S15. ^{1}H-NMR spectrum taken directly from the reaction of **6-H** with 1 equiv. of HBPin in C_6D_6 after 3 h at room temperature and showing formation of a new borohydride species (ratio to **6-H** is approx. 1:5) (δ -1.01 ppm; br d, J = 89.7 Hz).

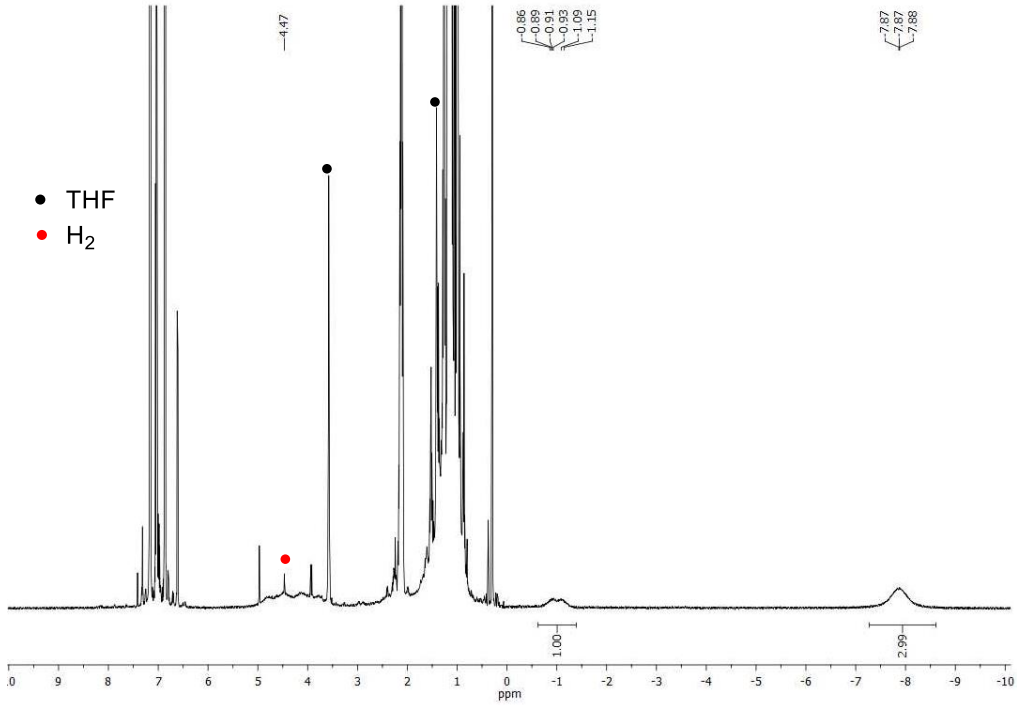

Figure S16. ^{1}H-NMR spectrum taken directly from the reaction of **6-H** with 1 equiv. of HBPin in C_6D_6 after 13 h at 40 °C and showing formation of a new borohydride species (ratio to **6-H** is approx. 1:3) (δ -1.01 ppm; br d, J = 89.7 Hz).

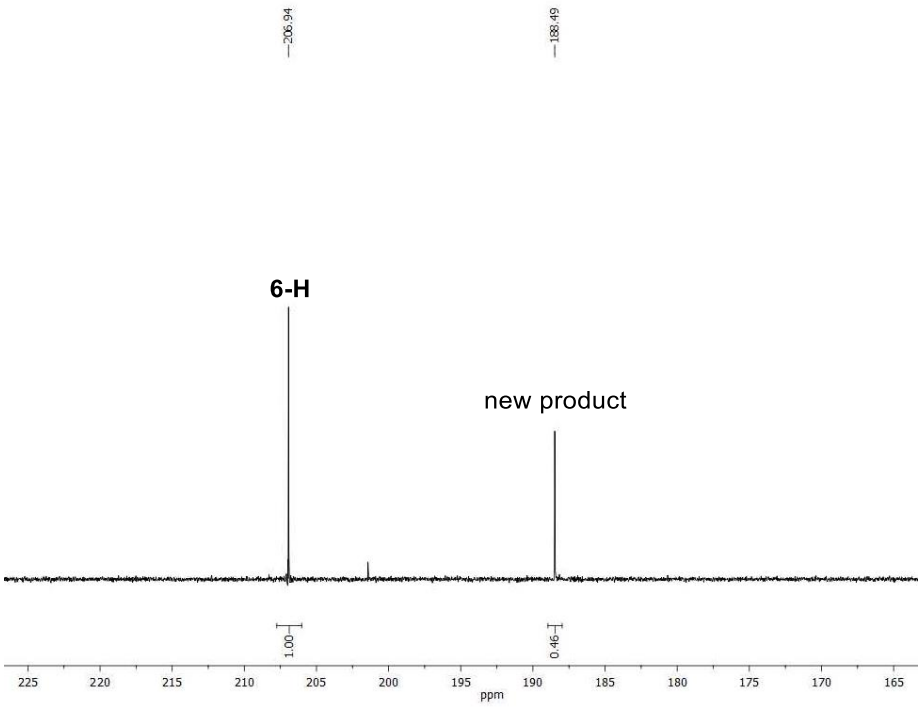

Figure S17. $^{31}P\{^{1}H\}$-NMR spectrum taken directly from the reaction of **6-H** with 1 equiv. of HBPin in C_6D_6 (13 h at 40 °C) followed by the treatment with 1 equiv. of *N*-phenylpropanamide (24 h at RT). The spectrum shows 32% conversion of 6-H to a new species at δ_P = 188.5 ppm.

NMR reaction of (POCOP)NiH (6-H) with *N*-phenylacetamide

A solution of (POCOP)NiH (**6-H**) (11.4 mg, 0.028 mmol) in 0.6 mL of C_6D_6 was added at room temperature to *N*-phenylacetamide (3.84 mg, 0.028 mmol). The resulting mixture was transferred to an NMR tube, left at room temperature for 15 min, and then monitored by NMR analysis for 22 h at room temperature and then at 80 °C for 2 days. At room temperature, a slow reaction was observed showing approx. 10% conversion of **6-H** to an unknown species (after 22 h) characterized by the resonance (singlet) in the $^{31}P\{^{1}H\}$-NMR spectra at δ_P = 188.5 ppm (compare to δ_P = 206.9 ppm for **6-H**), identical to the species produced in the reaction of **6-H** with 1 equiv. of HBPin followed by the addition of 1 equiv. of *N*-phenylpropanamide (see above) (see Figure S18). Notably, the formation of this unknown product is associated with the release of H_2 gas, which was observed in ^{1}H-NMR at δ_H = 4.47 ppm (in C_6D_6) (see Figure S19). Heating the mixture of **6-H** with *N*-phenylacetamide at 60-80 °C for 2 days did not result in any new products; however, the concentration of acetamide decreased and the concentration of H_2 and the initially formed species increased resulting in approx. 43% conv. of **6-H**. The addition of HBPin (1 equiv. to *N*-phenylacetamide) to this mixture results in the additional release of H_2 and formation of the borylated amine product, EtN(BPin)Ph (approx. 22% by ^{1}H-NMR after 3 days at room temperature). Further addition of

another 0.5 equiv. of HBPin leads to 46% of EtN(BPin)Ph in 24 h at room temperature.

Based on the above observations once could assume that this new species observed is (POCOP)Ni(N(Ph)C(O)R) (R = Me, Et), which is well supported by the observation of H_2 release upon reaction of (POCOP)NiH **6-H** and *N*-phenylacetamide (Figure S19). This species ai also identical to those observed upon **6-H**-catalyzed dehydrogenative borylation of *N*-phenylacetamide with 1 equiv. of HBPin (see below and Figures S22 and S23).

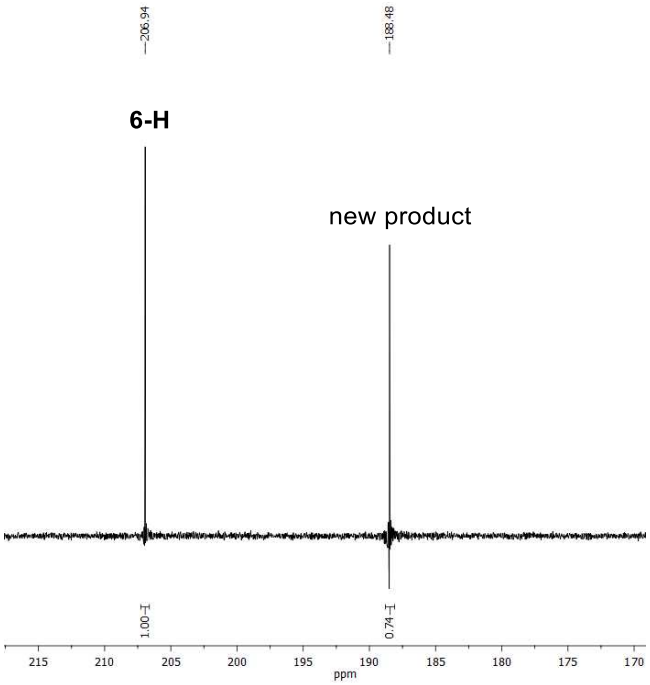

Figure S18. $^{31}P\{^{1}H\}$-NMR spectrum taken directly from the reaction of **6-H** with 1 equiv. of *N*-phenylacetamide in C_6D_6 after heating the reaction mixture for 2 days at 80 °C. The spectrum shows formation of a new species (δ_P = 188.5 ppm).

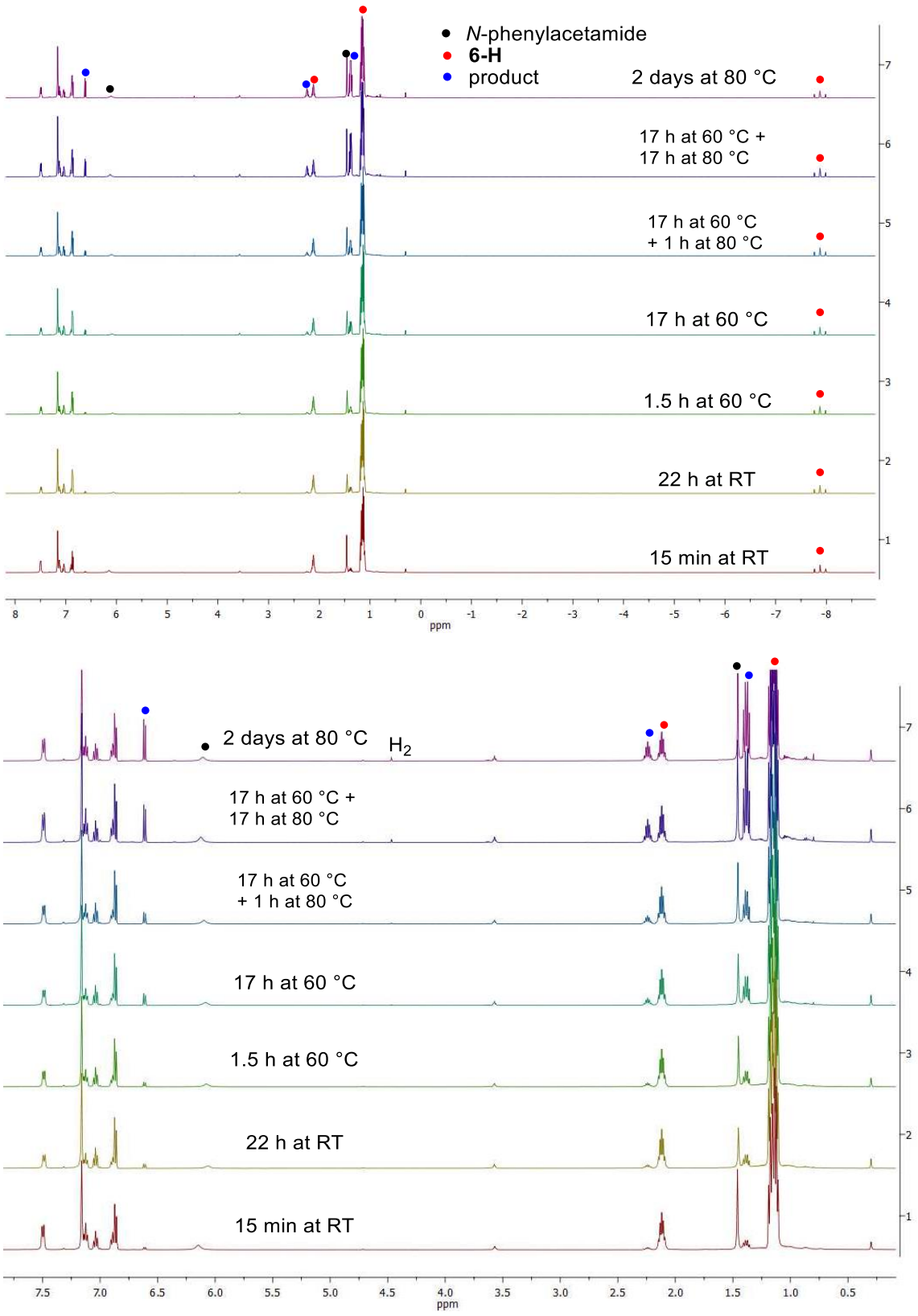

Figure S19. ^{1}H-NMR spectra taken directly from the reaction of **6-H** with 1 equiv. of *N*-phenylacetamide in C_6D_6 upon monitoring the reaction at RT and 80 °C.

NMR reaction of *N*-phenylbenzamide with HBPin in the absence of the catalyst

N-phenylbenzamide (19.7 mg, 0.1 mmol) and HBPin (14.5 μL, 0.1 mmol) were mixed in 0.6 mL of C_6D_6 in an NMR tube. The reaction mixture was left at room temperature for 2 h and checked by NMR, showing no reaction. After that the mixture was heated at 80 °C for 2 h and then checked by NMR again. NMR analysis revealed no reaction between N-phenylbenzamide and HBPin. Repeating the experiment with excess HBPin (up to 5 equivalents to *N*-phenylbenzamide) also did not show any productive reaction.

NMR reactions of *N*-phenylpropanamide with HBPin

A. With 1 equiv. of HBPin in the absence of the catalyst. *N*-phenylpropanamide (14.9 mg, 0.1 mmol) and HBPin (14.5 μL, 0.1 mmol) were mixed in 0.6 mL of C_6D_6 in an NMR tube. The mixture was left at room temperature for 15 min showing no reaction by NMR. Then, the reaction mixture was heated at 60 °C and monitored by ^{1}H-NMR analysis. No productive reaction and formation of only trace amounts of H_2 were observed in 2 h at 60 °C; however, 11% conversion of *N*-phenylpropanamide to the borylated *N*-phenylpropanamide, EtC(O)N(BPin)Ph (Figure S20) accompanied by the release of H_2 gas (δ_H = 4.47 ppm in C_6D_6) was detected after 24 h at 60 °C. Continuous heating of the reaction mixture at 60 °C for 2 days resulted in 35% conversion (by ^{1}H-NMR) of EtC(O)NHPh to EtC(O)N(BPin)Ph. For NMR data for EtC(O)N(BPin)Ph, see procedure B below.

B. With 1 equiv. of HBPin in the presence of 5 mol% of 6-H. HBPin (18.0 μL, 0.124 mmol) was added at room temperature via syringe to a mixture of *N*-phenylpropanamide (18.5 mg, 0.124 mmol) and (POCOP)NiH (**6-H**) (5 mol%, 2.5 mg, 0.0062 mmol, was added as a stock solution in C_6D_6) in 0.6 mL of C_6D_6 in an NMR tube. The reaction mixture was left at room temperature for 24 h showing 77% conversion (by ^{1}H-NMR) of *N*-phenylpropanamide to the borylated amide product, EtC(O)N(BPin)Ph, accompanied by the release of H_2 (δ_H = 4.47 ppm in C_6D_6). Repeating the reaction at 60 °C for 24 h resulted in 92% conversion to EtC(O)N(BPin)Ph (see Figure S21). The same 92% of EtC(O)NHPh was observed by ^{1}H-NMR after 12 h when the reaction was conducted at 80 °C. Formation of B_2Pin_2 (δ_H = 1.01 ppm in C_6D_6) and trace amounts of deoxygenated product, PrN(BPin)Ph, were also observed by NMR. Notably, the ^{31}P{^{1}H}-NMR spectrum taken directly from the reaction mixture revealed the presence of the same species observed upon the stoichiometric reaction of (POCOP)NiH (**6-H**) with N-phenylacetamide (see the procedure above and Figures S17, S18, S22, and S23), suggesting that this species is participating in dehydrogenative borylation of the amide.

EtC(O)N(BPin)Ph: ^{1}H-NMR (500 MHz; C_6D_6; δ, ppm): 0.93 (s, 12H, 4 *CH₃* of B*Pin*); 1.25 (t, *J* = 7.4 Hz, 3H, *CH₃* of *Et*C(O)-); 2.81 (q, *J* = 7.4 Hz, 2H, *CH₂* of *Et*C(O)-); 6.98-7.02 (m, 1H of N*Ph*); 7.11-7.16 (m, 4H of N*Ph*). ^{13}C{^{1}H}-NMR (125.8 MHz; C_6D_6; δ, ppm): 9.9 (s, *CH₃* of *Et*C(O)-); 24.3 (s, 4 *CH₃* of B*Pin*); 30.6 (s, *CH₂* of *Et*C(O)-); 83.7 (s, 2 C_q of B*Pin*); 126.7 (s, *CH* of N*Ph*); 128.8 (s, 2 *CH* of N*Ph*); 129.2 (s, 2 *CH* of N*Ph*); 141.5 (s, C_q of N*Ph*); 177.6 (s, *C*=O). ^{11}B{^{1}H}-NMR (160.5 MHz; C_6D_6; δ, ppm): 24.6 (br s, *B*Pin).

C. With 2 equiv. of HBpin in the presence of 5 mol% of 6-H. HBPin (36.0 μL, 0.248 mmol) was added at room temperature via syringe to a mixture of *N*-phenylpropanamide (18.5 mg, 0.124 mmol) and (POCOP)NiH (**6-H**) (5 mol%, 2.5 mg, 0.0062 mmol, was added as a stock solution in C_6D_6) in 0.6 mL of C_6D_6 in an NMR tube. The reaction mixture was left at room temperature for 24 h showing by ^{1}H-NMR formation of a mixture of the borylated amide, EtC(O)N(BPin)Ph (66%), N,O-bis(borylated) hemiaminal EtCH(OBPin)N(BPin)Ph (9%) and the deoxygenated product PrN(BPin)Ph (11%), accompanied by the release of H2 and formation of $(PinB)_2O$ (Figure S24). Heating this mixture at 80 °C for 12 h resulted in the complete conversion of the amide and formation of a mixture of EtC(O)N(BPin)Ph (50%) and PrN(BPin)Ph (49%).

EtCH(OBPin)N(BPin)Ph: ^{1}H-NMR (500 MHz; C_6D_6; selected characteristic resonances δ, ppm): 0.84 (t, *J* = 7.3 Hz, 3H, *CH₃* of *Et*CH(OBPin)-); 1.75-1.82 (m, 2H, *CH₂* of *Et*CH(OBPin)-); 5.99 (t, *J* = 6.9 Hz, 1H, CH of Et*CH*(OBPin)-).

NMR reactions of benzamide with HBPin in the absence of the catalyst

A: **Room temperature reaction.** HBPin (107.8 μL, 0.743 mmol; 5 equivalents) was added *via* syringe at room temperature to a suspension of benzamide (18.0 mg, 0.149 mmol) in 0.6 mL of C_6D_6 in an NMR tube. The formation of large gas was observed and the NMR tube was connected to the Schlenk line and depressurized. After that, the sample was left for 20 h at room temperature, and the reaction was analyzed by NMR, showing full conversion of benzamide and formation of a mixture of PhC(O)N(H)BPin (64%), an *O*-addict $PhC(O)NH_2$•HBPin (26%)[9] and PhC(H)=NBPin (9%)[10] (see Figure S25).

B: **Reaction at 80 °C.** HBPin (90.0 μL, 0.62 mmol; 5 equivalents) was added *via* syringe at room temperature to a suspension of benzamide (15.0 mg, 0.124 mmol) in 0.6 mL of C_6D_6 in an NMR tube. The NMR tube was sealed, connected to the Schlenk line, and placed in the (80 °C) oil bath for 24 hours. A vigorous release of H_2 gas was observed at the beginning of the reaction and the NMR tube was depressurized a few times using the Schlenk line. NMR analysis after 24 hours of heating at 80 °C showed full conversion of benzamide and formation of a mixture of PhC(O)N(H)BPin (80%),[10c] PhC(H)=NBPin (11%)[10] and $PhCH_2N(BPin)_2$ (9%)[11] (see Figure S26).

PhC(O)N(H)BPin: ^{1}H-NMR (500 MHz; C_6D_6; δ, ppm) 1.08 (s, 12H, 4 *CH*$_3$ of B*Pin*); 6.41 (br s, 1H, N*H*); 6.97 (t, *J* = 7.6 Hz, 2H, *m*-H of *C*$_6$*H*$_5$); 7.05 (t, *J* = 8.0 Hz, 1H, *p*-H of *C*$_6$*H*$_5$); 7.56 (d, *J* = 7.9 Hz, 2H, *o*-H of *C*$_6$*H*$_5$).

PhC(H)=NBPin was assigned based on characteristic imine resonance at 10.37 ppm in the ^{1}H-NMR spectrum (consistent with the previously reported data[10]).

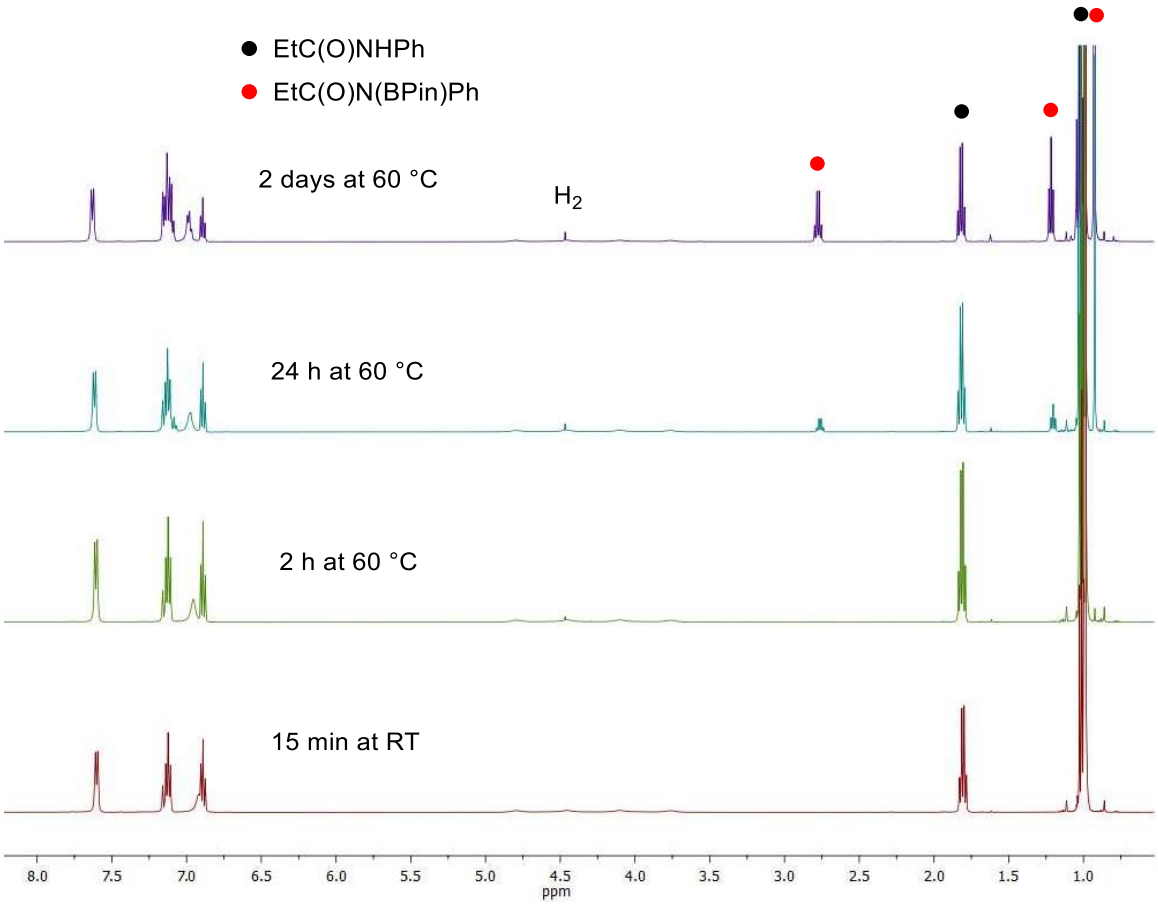

Figure S20. ^{1}H-NMR spectra taken directly from the catalyst-free reaction of *N*-phenylpropanamide with 1 equiv. of HBPin in C_6D_6 upon monitoring the reaction at room temperature and 60 °C.

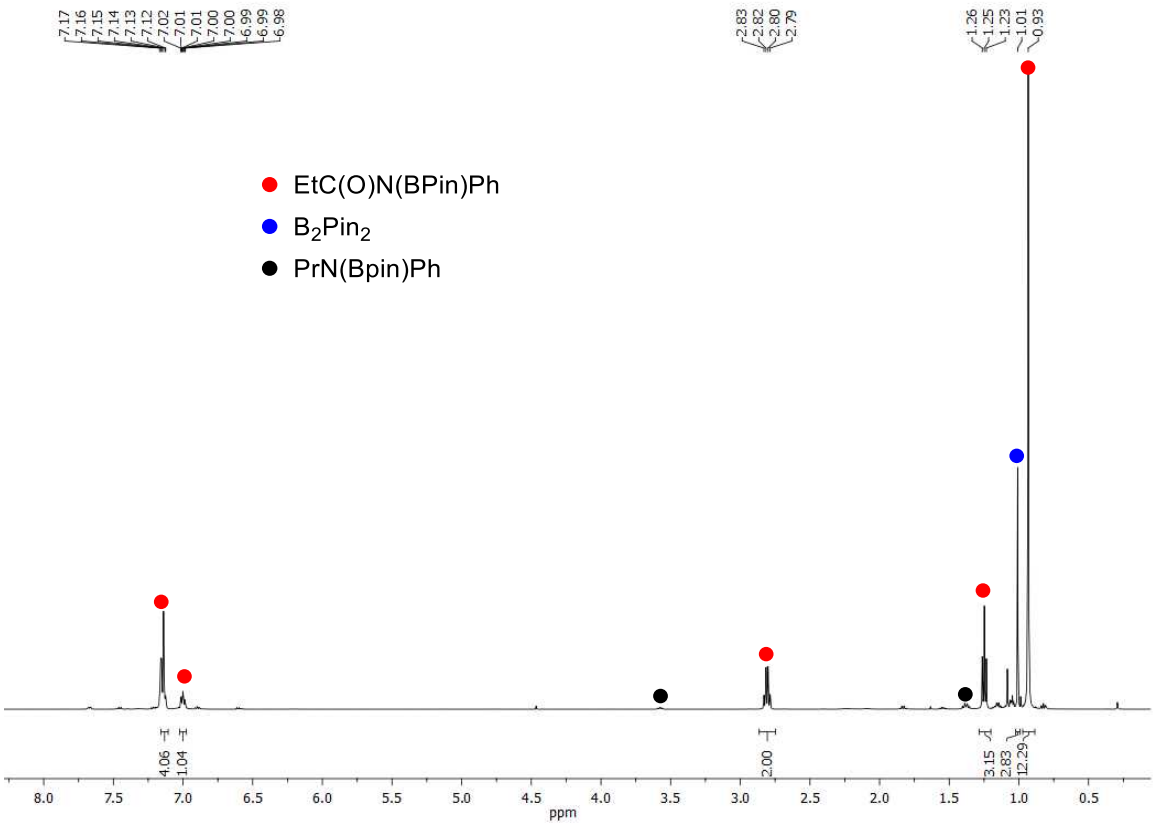

Figure S21. ^{1}H-NMR spectrum taken directly from the reaction mixture of **6-H**-catalyzed dehydrogenative borylation of *N*-phenylpropanamide with 1 equiv. of HBPin in C_6D_6 after 24 h at 60 °C, showing formation of EtC(O)N(BPin)Ph.

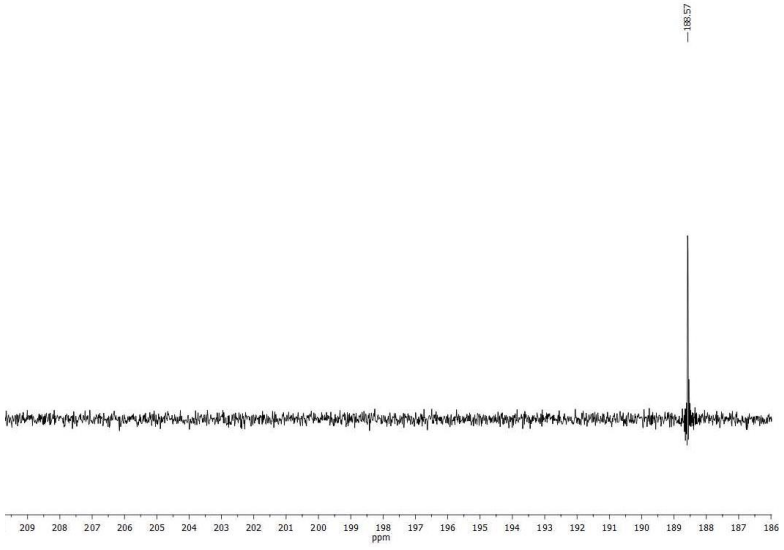

Figure S22. ^{31}P{^{1}H}-NMR spectrum taken directly from the reaction mixture of **6-H**-catalyzed dehydrogenative borylation of *N*-phenylpropanamide with 1 equiv. of HBPin in C_6D_6 after 24 h at 60 °C.

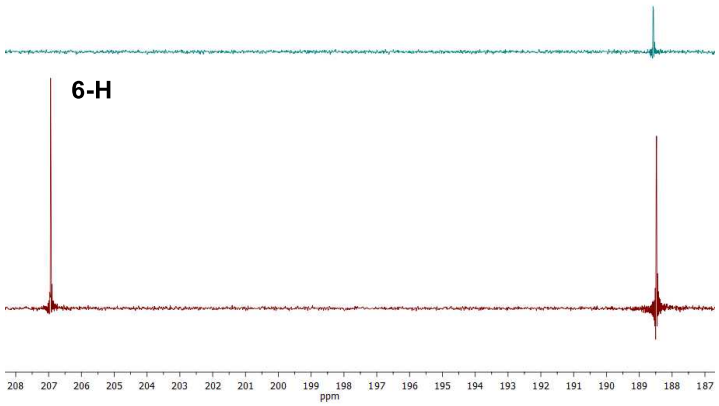

Figure S23. Comparison of the $^{31}P\{^{1}H\}$-NMR spectra from the reaction mixture of **6-H**-catalyzed dehydrogenative borylation of *N*-phenylpropanamide with 1 equiv. of HBPin in C_6D_6 after 24 h at 60 °C (*top spectrum*) and stoichiometric reaction of **6-H** with N-phenylacetamide (*bottom spectrum*).

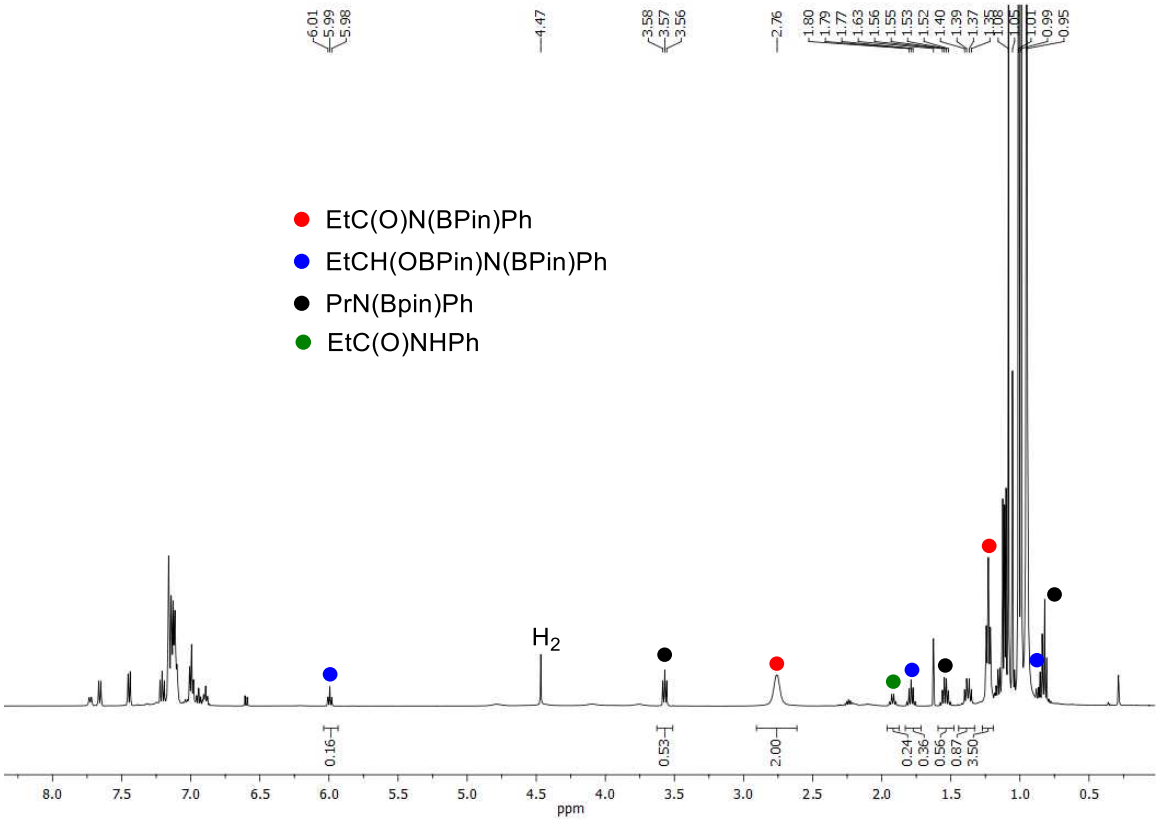

Figure S24. ^{1}H-NMR spectrum taken directly from the reaction mixture of **6-H**-catalyzed reaction of *N*-phenylpropanamide with 2 equiv. of HBPin in C_6D_6 after 24 h at room temperature.

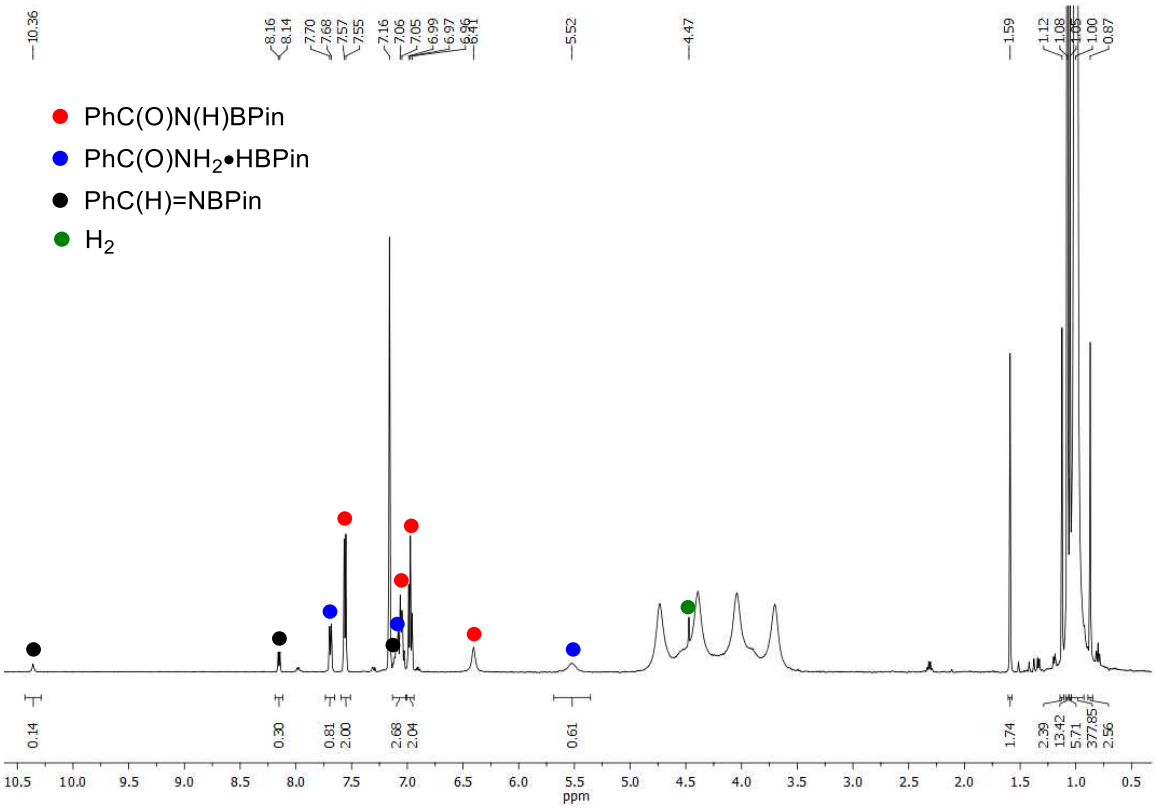

Figure S24. ^{1}H-NMR spectrum taken after 20 h directly from the reaction mixture from the reaction of benzamide with 5 equiv. of HBPin in C_6D_6 at room temperature.

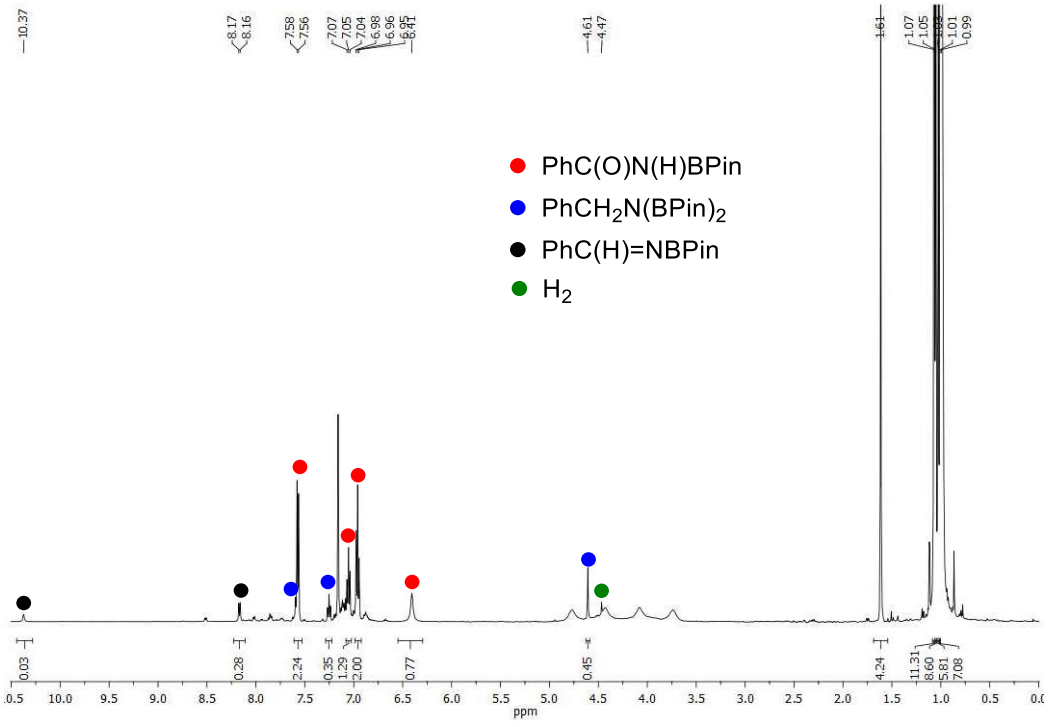

Figure S26. ^{1}H-NMR spectrum taken after 20 h directly from the reaction mixture from the reaction of benzamide with 5 equiv. of HBPin in C_6D_6 at 80 °C.

6-H-catalyzed hydroboration of a mixture of *N*-phenylbenzamide and *N*-(4-methoxybenzyl)acetamide

HBPin (94.3 μL, 0.65 mmol, 6.5 equivalents) was added at room temperature to a mixture of *N*-phenylbenzamide (19.7 mg, 0.1 mmol), *N*-(4-methoxybenzyl)acetamide (17.9 mg, 0.1 mmol) and (POCOP)NiH (**6-H**) (4.9 mg, 0.01 mmol, 10 mol%) in 0.6 mL of C_6D_6 in a pressure vial (10 mL Supelco headspace vials equipped with magnetic screw caps having PTFE-faced butyl septa). The resulting mixture was stirred at 80 °C for 24 h, then it was cooled down to room temperature and analyzed by NMR, which showed full conversions of both *N*-phenylbenzamide and *N*-(4-methoxybenzyl)acetamide formation of approx. 1:1 mixture of the corresponding amine products, $PhCH_2N(BPin)Ph$ and $CH_3CH_2N(BPin)CH_2$-C_6H_4-*p*-OMe (Figure S27).

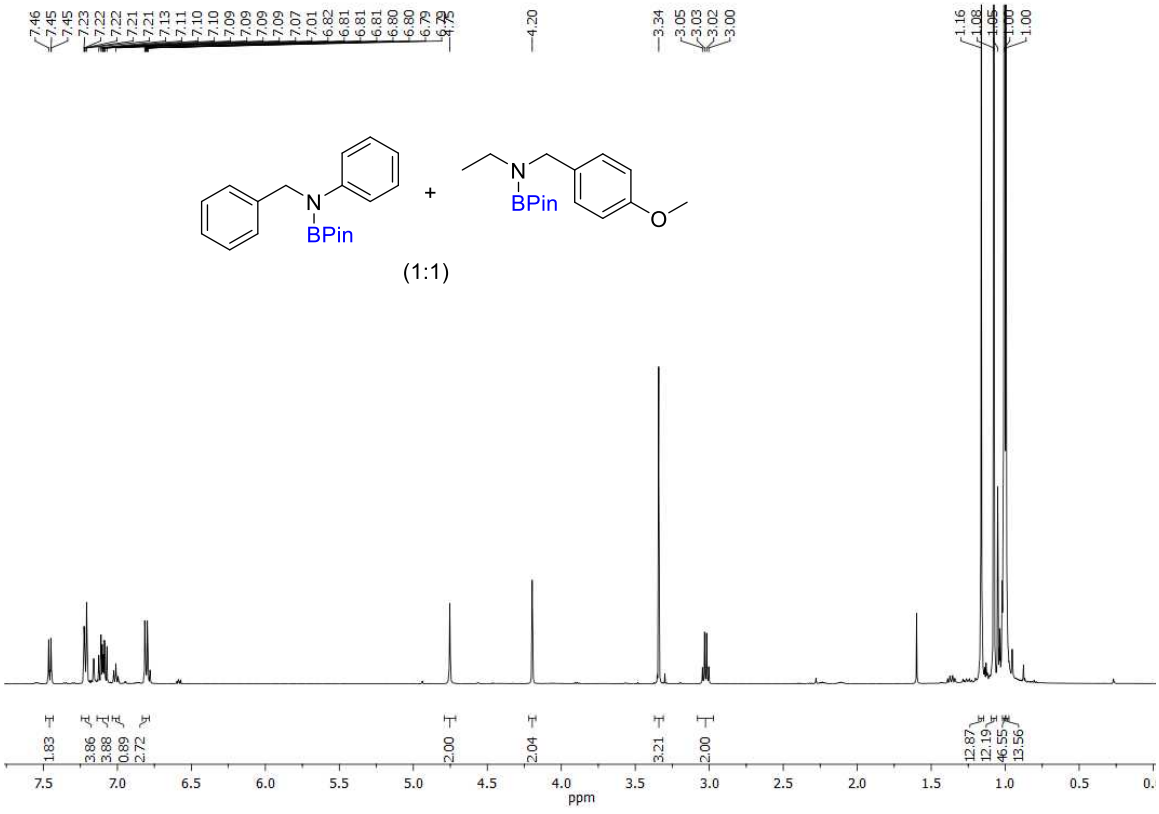

Figure S27. ^{1}H-NMR spectrum taken after 24 h from the **6-H**-catalyzed reaction of an equimolar mixture of *N*-phenylbenzamide and *N*-(4-methoxybenzyl)acetamide with 6.5 equiv. of HBPin at 80 °C.

6-H-catalyzed hydroboration of *N*-phenylbenzamide / cross-condensation with 4-methylbenzaldehyde

HBPin (45 μL, 0.3 mmol, 3 equivalents) was added to a solution of *N*-phenylbenzamide (19.7 mg, 0.1 mmol) and (POCOP)NiH (**6-H**) (2.4 mg, 0.05 mmol, was added from a stock solution in C_6D_6) in 0.6 mL of C_6D_6 in an NMR tube. The resulting mixture was heated at 80 °C for 1 hour, and after that 1 equivalent of 4-methylbenzaldehyde (11.8 μL, 0.1 mmol) was added to the reaction mixture. The resulting mixture was left at 80 °C overnight and then analyzed by NMR showing formation of an approx. 1:1 mixture of the borylamine product $PhCH_2N(BPin)Ph$ and *p*-Me-$C_6H_4CH_2OBPin$ (Figure S28). No formation of cross-condensation product akin to *p*-Me-$C_6H_4CH_2N(BPin)Ph$ was observed.

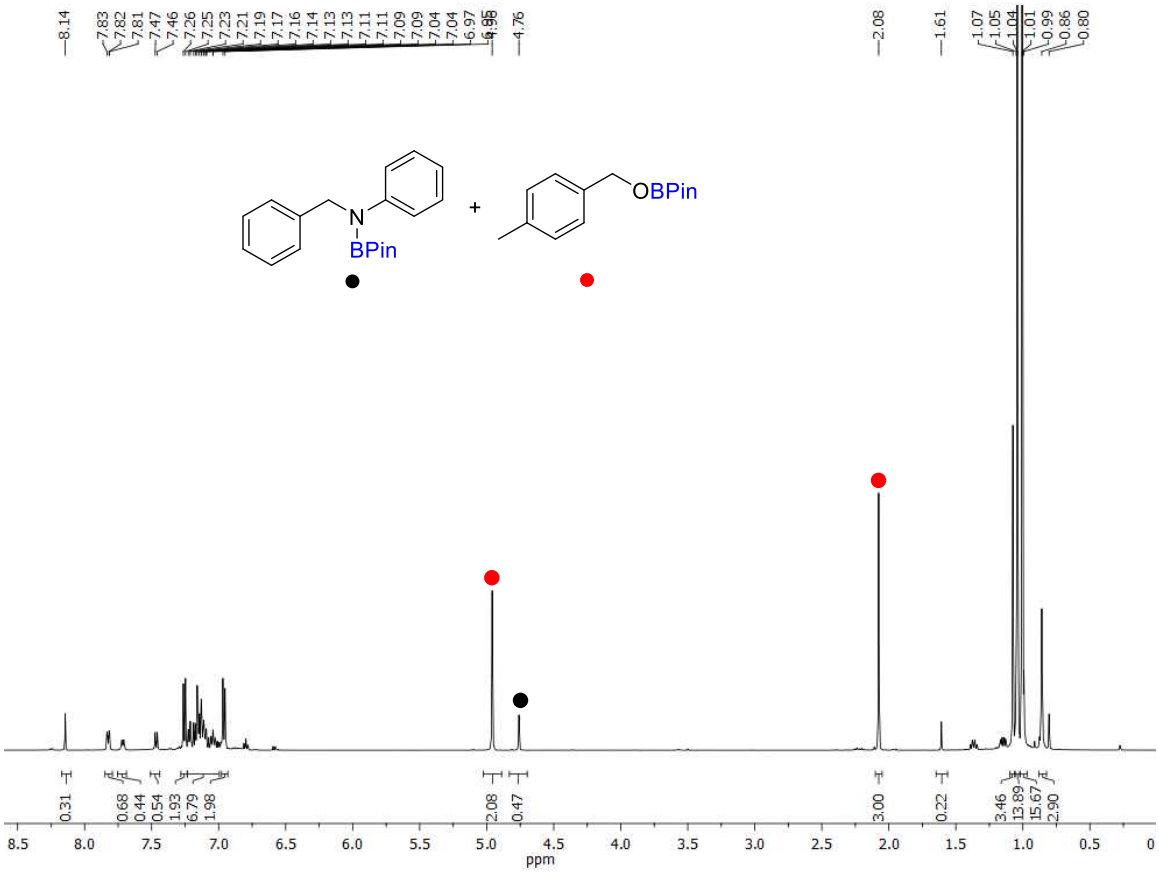

Figure S28. ^{1}H-NMR spectrum from the **6-H**-catalyzed reaction of *N*-phenylbenzamide with 3 equiv. of HBPin (80 °C, 1 h), followed by the reaction with 1 equiv. of 4-methylbenzaldehyde (overnight at 80 °C).

6-H-catalyzed hydroboration of *N*-(4-methoxybenzyl)acetamide / cross-condensation with 4-methylbenzaldehyde.

HBPin (45 μL, 0.3 mmol, 3 equivalents) was added to a solution of *N*-(4-methoxybenzyk)acetamide (17.9 mg, 0.1 mmol) and (POCOP)NiH (**6-H**) (2.4 mg, 0.05 mmol, was added from a stock solution in C_6D_6) in 0.6 mL of C_6D_6 in an NMR tube. The resulting mixture was heated at 80 °C for 1 hour, and after that 1 equivalent of 4-methylbenzaldehyde (11.8 μL, 0.1 mmol) was added to the reaction mixture. The resulting mixture was left at 80 °C overnight and then analyzed by NMR showing formation of a mixture of $CH_3C(O)N(BPin)CH_2C_6H_4$-*p*-OMe (approx. 25%), $CH_3CH_2N(BPin)CH_2C_6H_4$-*p*-OMe (approx. 25%) and *p*-Me-$C_6H_4CH_2OBPin$ (approx. 50%) (Figure S29). No formation of cross-condensation product akin to *p*-Me-$C_6H_4CH_2N(BPin)CH_2C_6H_4$-*p*-OMe was observed.

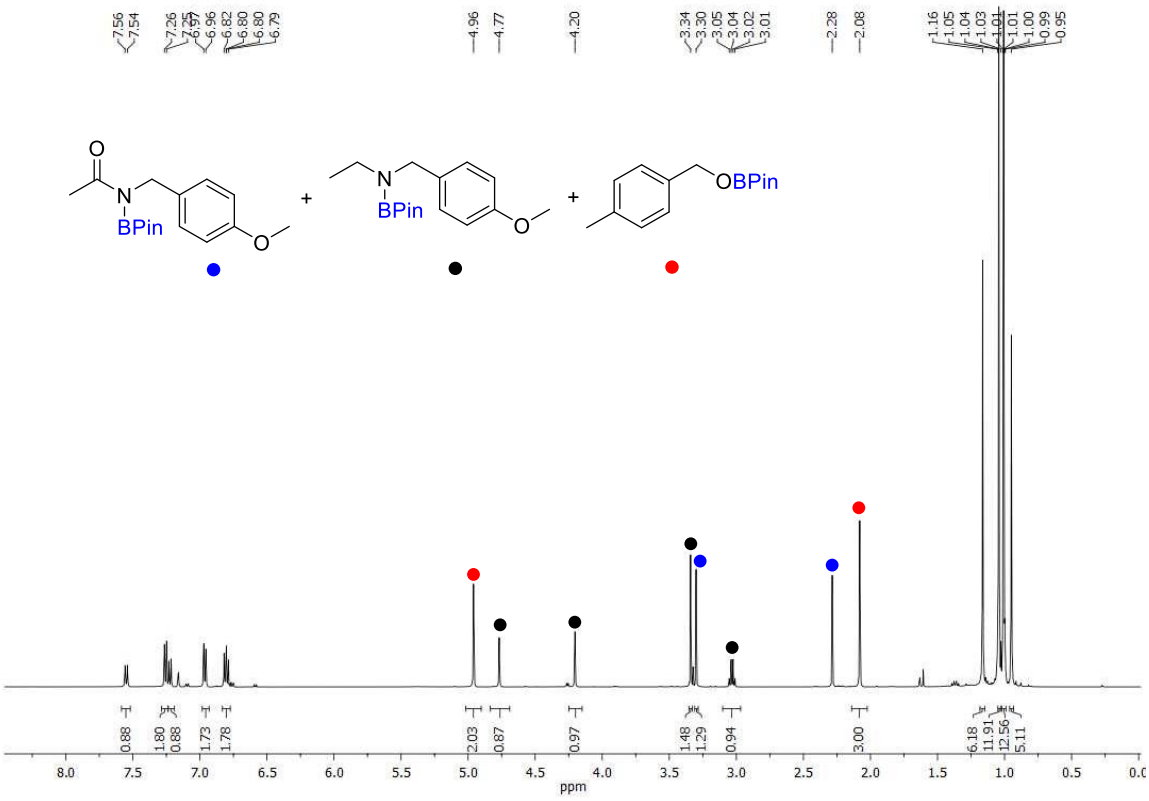

Figure S29. ^{1}H-NMR spectrum from the **6-H**-catalyzed reaction of *N*-(4-methoxybenzyl)acetamide with 3 equiv. of HBPin (80 °C, 1 h), followed by the reaction with 1 equiv. of 4-methylbenzaldehyde (overnight at 80 °C).

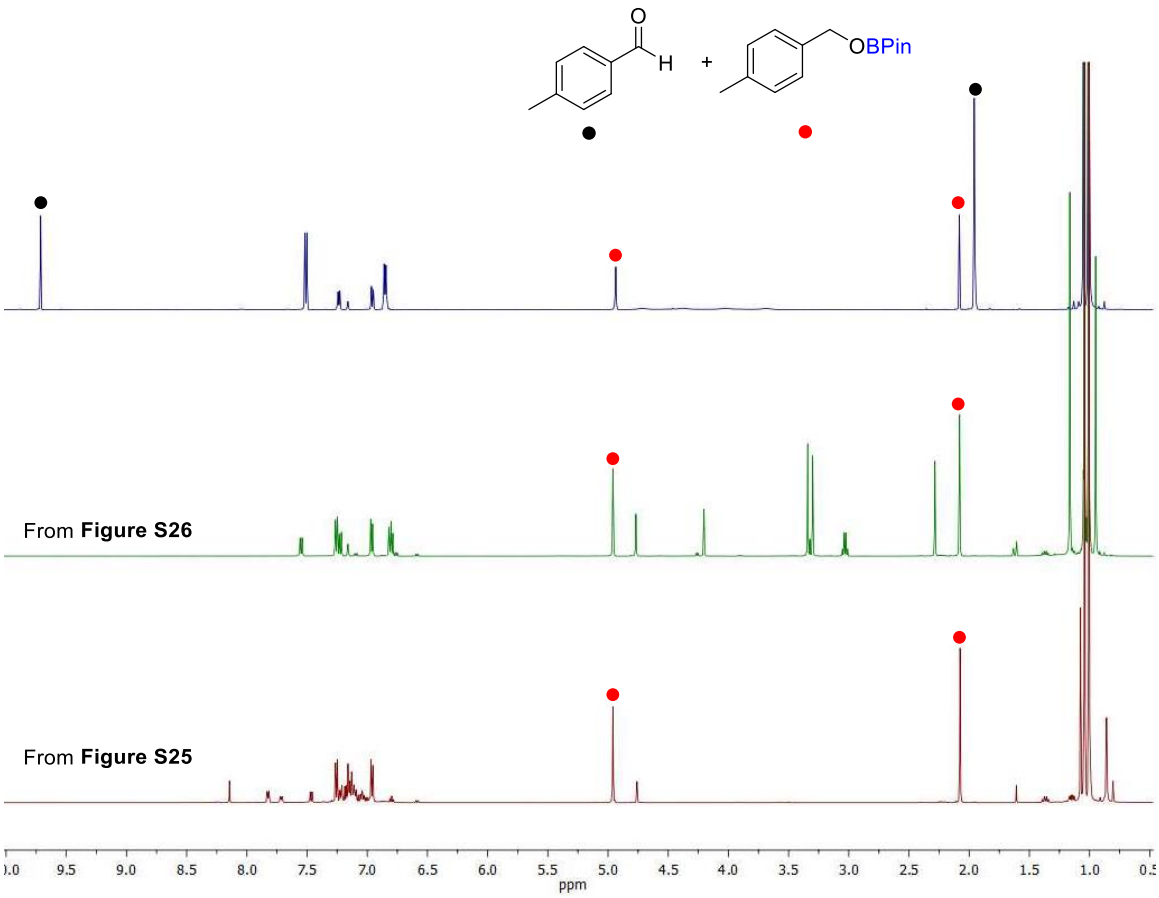

Figure S30. Comparison of ^{1}H-NMR spectra in Figures S25 and S26 to the ^{1}H-NMR spectrum from the reaction of 4-methylbenzaldehyde with 1 equiv. of HBPin (4 h at room temperature in C_6D_6).

Control experiments on deoxygenative hydroboration of benzamide in the presence of $LiCH_2SiMe_3$ and KO^tBu.

Since in hydroboration of benzamide with HBPin catalyzed by **2-CH_2TMS**, **2-O^tBu**, **3-O^tBu** and **4-O^tBu** pre-catalysts were generated in situ by the treatment of the corresponding bromide complexes **2-Br**, **3-Br** and **4-Br** with either $LiCH_2SiMe_3$ or KO^tBu, one can argue about a possibility that some residual amounts of $LiCH_2SiMe_3$ or KO^tBu were left in the reaction mixtures and were responsible for the observed catalytic activity. First, it should be noted that 1 equiv. of the base was used per 1 equiv. of the nickel bromide complex in our experiments, and complete conversions of bromide complexes and no residual $LiCH_2SiMe_3$ or KO^tBu were detected by NMR analysis prior to catalytic reactions. Nonetheless, to check the possibility of catalysis by $LiCH_2SiMe_3$ and KO^tBu, deoxygenative hydroboration of benzamide was probed using 0.5 mol% of $LiCH_2SiMe_3$ and 0.5 mol% of KO^tBu as catalysts. The reactions were performed using conditions identical to those for **2-CH_2TMS**, **2-O^tBu**, **3-O^tBu** and **4-O^tBu** pre-catalysts (C_{amide} = 0.21 mol/L, 80 °C, 24 h). Both experiments showed poor conversions of benzamide to benzylamine derivatives,

16% conv. for $LiCH_2SiMe_3$ and 38% conv. for KO^tBu. Considering the fact that no excess of $LiCH_2SiMe_3$ and KO^tBu was used to generate pre-catalysts **2-CH$_2$TMS**, **2-O^{t}Bu** – **4-O^{t}Bu** from the corresponding bromide complexes, as well as NMR confirmation of complete conversion of the latter compounds, these observations suggest unlikely involvement of $LiCH_2SiMe_3$ and KO^tBu in hydroboration by the in situ generated pre-catalysts **2-CH$_2$TMS**, **2-O^{t}Bu**, **3-O^{t}Bu** and **4-O^{t}Bu**.

3. Kinetic studies

Kinetic studies of 6-H-catalyzed deoxygenative hydroboration of *N*-phenylpropanamide with HBPin

In a J. Young NMR tube, *N*-phenylpropanamide (14.9 mg, 0.1 mmol), **6-H** (5 mol%, 0.005 mmol; was added from a stock solution of **6-H** in C_6D_6) and 3.4 mg 1,3,5-trimethoxybenzene (3.4 mg, 0.02 mmol; 0.2 equivalents to *N*-phenylpropanamide; was used as an internal standard) were mixed in 0.6 mL of C_6D_6. HBPin (2-15 equivalents to *N*-phenylpropanamide, 0.2-1.5 mmol) was added *via* syringe at room temperature and the samples were immediately placed into an NMR spectrometer preheated to 50 °C. The reactions were monitored by ^{1}H-NMR spectroscopy at 50 °C for 2-5 hours. The ^{1}H-NMR spectra were recorded every 5-10 mins (depending on each reaction). All the experiments were done in the same way by changing the concentration of HBPin. The product concentrations and conversions were measured by the integration of the NMR spectra against the resonances of the internal standard (1,3,5-trimethoxybenzene). The analysis was performed for the initial rates of up to 7% conversions of *N*-phenylpropanamide. Reaction rates (Table S1) were determined by the least-square fit of the product concentration versus time (errors were determined by linear regression analysis), and the plots are shown in Figures S28 and S29 below. The proposed mechanism is depicted in Scheme 11A in the manuscript and in Scheme S1 below. The data obtained from the NMR experiments show a linear dependence of the rate *vs.* concentration of HBPin with saturation behavior when large HBPin concentrations are applied (see Figure 11B in the manuscript and Figure S32 below). The obtained rate law for the mechanism presented in Scheme 11 and below qualitatively agrees with the observed kinetics, supporting the proposed mechanism.

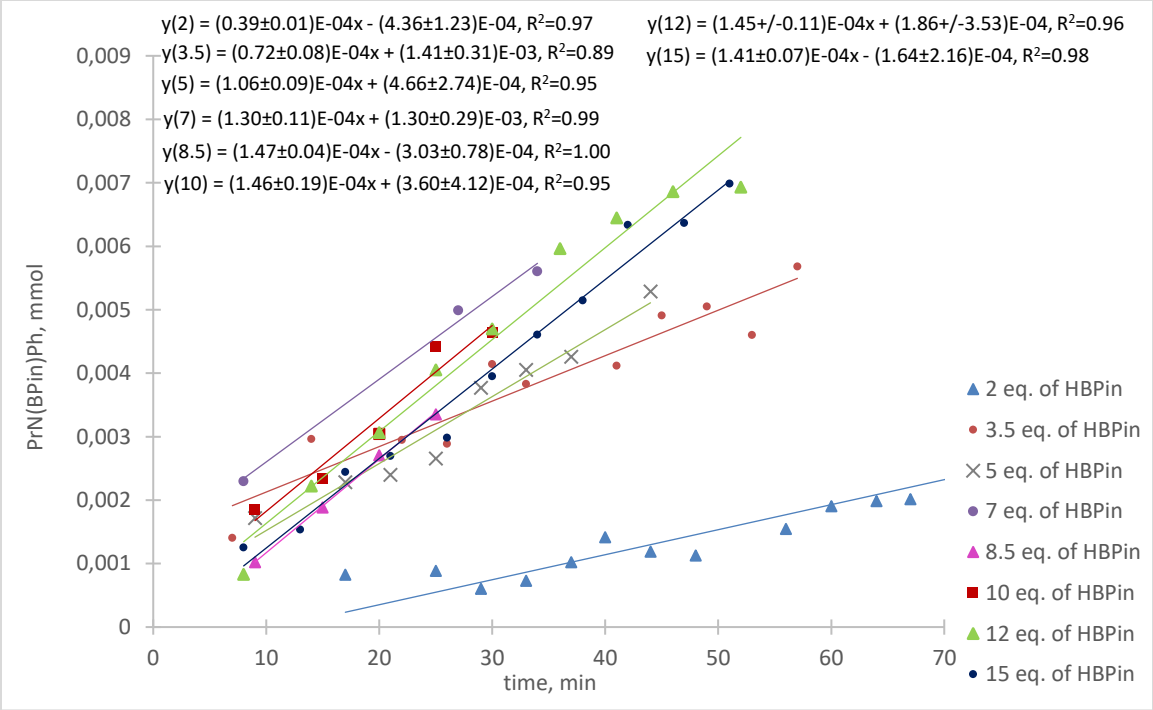

Figure S31. Product concentration vs. time plot for **6-H**-catalyzed deoxygenative hydroboration of *N*-phenylpropanamide with HBPin (2-15 equivalents to *N*-phenylpropanamide).

Table S1. Initial reaction rates for **6-H**-catalyzed hydroboration of *N*-phenylpropanamide with HBPin (0.2-15 equiv.)

HBPin, mmol	**Initial rate, 10^{-4} mmol/min**	**% Conversion of amide**
0.2	0.39±0.01	5
0.35	0.72±0.08	5
0.5	1.06±0.09	5
0.7	1.30±0.11	5
0.85	1.47±0.04	3
1	1.46±0.19	5
1.2	1.45±0.11	7
1.5	1.41±0.07	7

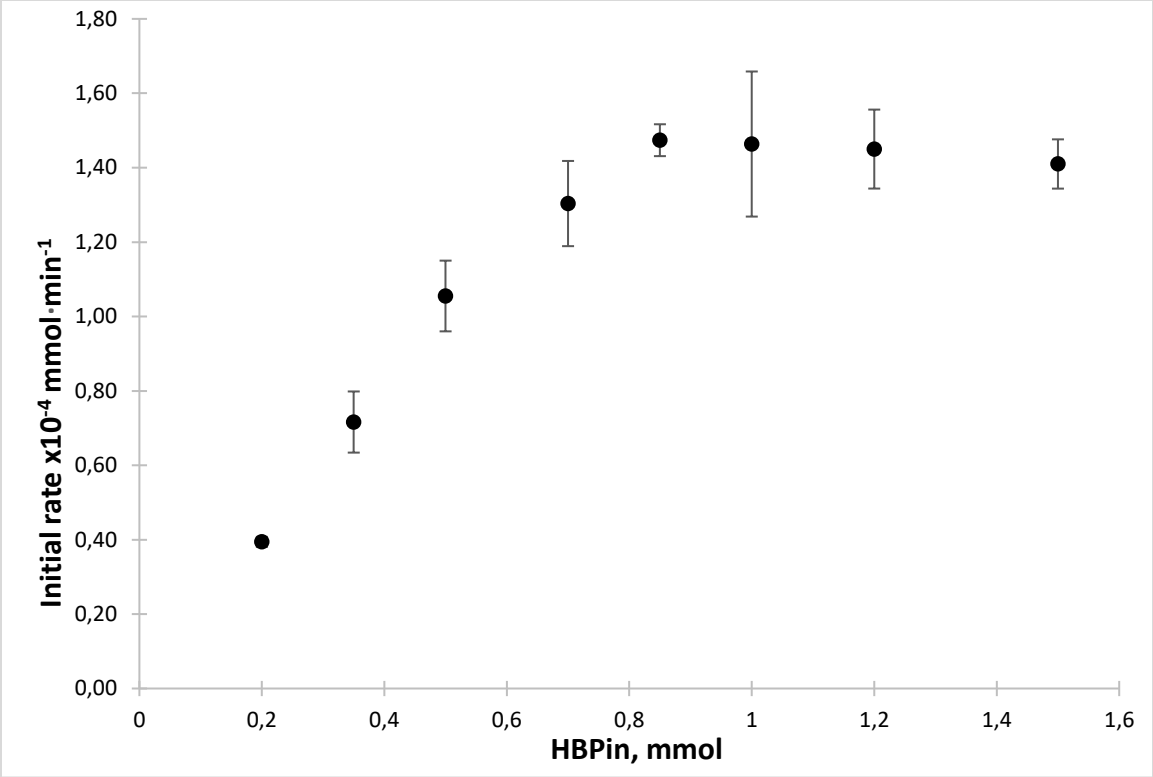

Figure S32. Dependence of the initial reaction rate *vs.* concentration of HBPin in **6-H**-catalyzed deoxygenative hydroboration of *N*-phenylpropanamide.

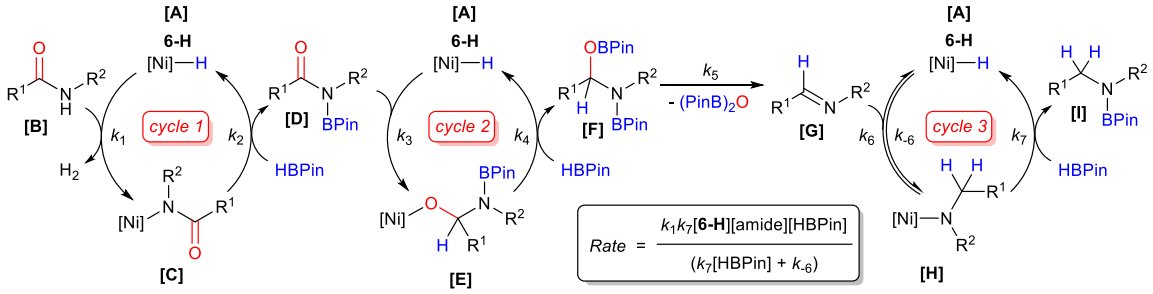

Scheme S1. Proposed mechanism of **6-H**-catalyzed deoxygenative hydroboration of secondary amides

The empirical rate law for 6-H-catalyzed deoxygenative hydroboration of secondary amides (the mechanism depicted in Scheme S1). Assuming a steady-state approximation for the following equations for [C], [D], [E], [F], [G], and [H]:

$d\rho/dt = k_7$ [H] [HBPin] **(*1*)**;

$d[H]/dt = k_6$ [A] [G] **-** k_{-6} [H] **-** k_7 [H] [HBPin] = 0 **(*2*)**; from **(*2*)**: [H] = k_6 [A] [G] / {k_{-6} [H] + k_7 [HBPin]} **(*3*)**;

Assuming that **6-H** ([A]) is not involved in conversion of the hemiaminal [F] to the imine [G]:
$d[G]/dt = k_5$ [A] [F] + k_{-6} [H] **-** k_6 [G] = 0 **(*4*)**; from **(*4*)**: [G] = {k_5 [F] + k_{-6} [H]} / k_6 [A] **(*5*)**;
$k_5 >> k_{-6}$, then [G] = k_5 [F] / k_6 [A] **(*6*)**;

From **(*3*)** and **(*6*)**: [H] = k_5 [F] / {k_{-6} [H] + k_7 [HBPin]} **(*7*)**;

$d[F]/dt = k_4$ [E] [HBPin] **-** k_5 [F] = 0 **(*8*)**; from **(*8*)**: [F] = k_4 [E] [HBPin] / k_5 **(*9*)**;

from **(*9*)** and **(*7*)**: [H] = k_4 [F] [HBPin] / {k_{-6} [H] + k_7 [HBPin]} **(*10*)**;

$d[E]/dt = k_3$ [A] [D] **-** k_4 [E] [HBPin] = 0 **(*11*)**; from **(*11*)**: [E] = k_3 [A] [D] / k_4 [HBPin] **(*12*)**;

from **(*12*)** and **(*10*)**: [H] = k_3 [A] [D] / {k_{-6} [H] + k_7 [HBPin]} **(*13*)**;

$d[D]/dt = k_2$ [C] [HBPin] **-** k_3 [A] [D] = 0 **(*14*)**; from **(*14*)**: [D] = k_2 [C] [HBPin] / k_3 [A] **(*15*)**;

from **(*15*)** and **(*13*)**: [H] = k_2 [C] [HBPin] / {k_{-6} [H] + k_7 [HBPin]} **(*16*)**;

$d[C]/dt = k_1$ [A] [B] **-** k_2 [C] [HBPin] = 0 **(*17*)**; from **(*17*)**: [C] = k_1 [A] [B] / k_2 [HBPin] **(*18*)**;

from **(*18*)** and **(*16*)**: [H] = k_1 [A] [B] / {k_{-6} [H] + k_7 [HBPin]} **(*19*)**;

Substitution of **(*19*)** into **(*1*)**: $d\rho/dt = k_1 k_7$ [A] [B] [HBPin] / {k_{-6} + k_7 [HBpin]} **(*20*)**;

Since [A] = [**6-H**]; [B] = [amide], $d\rho/dt = k_1 k_7$ [**6-H**] [amide] [HBPin] / {k_{-6} + k_7 [HBpin]} **(*21*)**;

At large concentrations of HBPin, k_7 [HBpin] >> k_{-6} and $d\rho/dt = k_1$ [**6-H**] [amide] **(*22*)** and the rate is independent of concentration of HBPin (see Figure S29).
Since only [HBPin] was varied, $k_1 k_7$ [**6-H**] [amide] is constant, then we get the following equation, which qualitatively agrees the observed experimental data:

Rate = A [HBPin] / {B + C [HBPin]} **(*23*)** where A = $k_1 k_7$ [**6-H**] [amide]; B = k_{-6} and C = k_7 (all constant).

The mechanism may also involve reversible formation of adducts of **6-H** ([A]) with the borylated amide [D] and an imine [G]. This does not change the dependence of the reaction rate on the concentration of HBPin and qualitatively agrees with the observed kinetics. We also considered alternative mechanisms which either involve catalyst-free formation of the borylated amide [D] or involve the initial addition of HBPin to **6-H** ([A]) to form the borohydride complex akin to (POCOP)Ni(η^2-H_2BPin), followed by its reaction with either secondary amide or with the borylated amide [D], but these mechanisms produced rate laws incompatible with the observed kinetics.

4. X-Ray diffraction analysis

The single crystals of **5-Br**, **3-Me**, **3-OTf**, **3-OAc**, **3-NO$_3$**, **3-SPh** and **3-BH$_4$** suitable for X-Ray diffraction analysis were obtained by appropriate crystallization methods (see Table S2 for details).

Table S2. Crystallization methods for single crystals of **5-Br**, **3-Me**, **3-OTf**, **3-OAc**, **3-NO$_3$**, **3-SPh** and **3-BH$_4$**.

Complex	Crystallization technique
5-Br	Crystallized from n-pentane solution at -28 °C
3-Me	Crystallized from Et_2O solution at -30 °C
3-OTf	Crystallized from Et_2O solution at -30 °C
3-OAc	Crystallized from Et_2O solution at -30 °C
3-NO$_3$	Crystallized from Et_2O solution at -30 °C
3-SPh	Crystallized from toluene solution layered with hexane at -28 °C.
3-BH$_4$	Crystallized from Et_2O solution at -28 °C

For **3-Me** and **3-BH$_4$**, suitable single crystals were mounted on a glass microloop covered with perfluoroether oil (Paratone® N). Crystallographic data were collected on Bruker APEX-II CCD diffractometer equipped with an Oxford Cryosystems lowtemperature device operating at 150.0(1) K. Generic φ and ω scans (MoKα, λ = 0.71073 Å) were used for the data measurement. The diffraction patterns were indexed, and the unit cells refined with SAINT (Bruker, V.8.34A, after 2013) software. Data reduction, scaling and absorption correction were performed with SAINT and SADABS software (Bruker, 8.34A after 2013). A multi-scan absorption correction was applied within SADABS-2014/4 (Bruker, 2014/4). Space group determination was based upon analysis of systematic absences, E statistics, and successful refinement of all structures. The structures were solved by ShelXT (Sheldrick, 2015) structure solution program with an Intrinsic phasing algorithm and refined with the Least squares method by minimization of $\Sigma w(F_0^2 - F_c^2)^2$. SHELXL weighting scheme was used under the 2018/3 version of ShelXL (Sheldrick, 2015). Structure solution, refinement, and CIF compilation were performed within Olex2SyS software (Dolomanov, 2009). All non-hydrogen atoms were refined anisotropically. The positions of the hydrogen atoms were calculated geometrically and refined using the riding model. Neutral atom scattering factors for all atoms were taken from the International Tables for Crystallography. For **3-Me**, analysis of residual electron density revealed the substitutional disorder at the C10 position which is represented by the presence of the bromide complex **3-Br** (Figure S34). The fraction of methyl and bromide complexes (**3-Me** and **3-Br**, respectively) was refined using free variables and comprised 0.91:0.09, respectively. The crystal of **3-**

BH_4 suitable for X-ray diffraction also contained the starting bromide complex **3-Br** (the ratio of BH_4 to Br is 0.84:0.16) (Figure S39).

Single crystals of **5-Br**, **3-OTf**, **3-OAc**, **3-NO_3** and **3-SPh**, were investigated on a Bruker D8 QUEST single-crystal X-ray diffractometer equipped with PHOTONII detector, charge-integrating pixel array detector (CPAD), laterally graded multilayer (Goebel) mirror and microfocus Mo-target X-ray tube (λ = 0.73071 Å). Data reduction and integration were performed with the Bruker software package SAINT (Version 8.40B) (SAINT, Version 8.40B; Bruker AXS Inc.: Madison, Wisconsin, USA, 2017.). A multi-scan absorption correction was applied within SADABS-2014/4 (Bruker, 2014/4). Crystal structure solution and refinement were performed using SHELX-2018 package. Atomic positions were located using dual methods and refined using a combination of Fourier synthesis and least-square refinement in isotropic and anisotropic approximations. The H atoms were positioned geometrically and refined as riding atoms with relative isotropic displacement parameters. The general view of **5-Br**, **3-Me**, **3-BH_4**, **3-OTf**, **3-OAc**, **3-NO_3**, and **3-SPh** are shown on the Figures S33-S39. Crystal data, data collection, and structure refinement details for **5-Br**, **3-Me**, **3-BH_4**, **3-OTf**, **3-OAc**, **3-NO_3**, and **3-SPh** are summarized in Tables S3 and S4. Structural parameters (bond distances (Å) and bond angles (°)) for complexes **5-Br**, **3-Me**, **3-BH_4**, **3-OTf**, **3-OAc**, **3-NO_3**, and **3-SPh** are listed in Tables S5-S18. The corresponding CIF files are also provided as separate supporting documents.

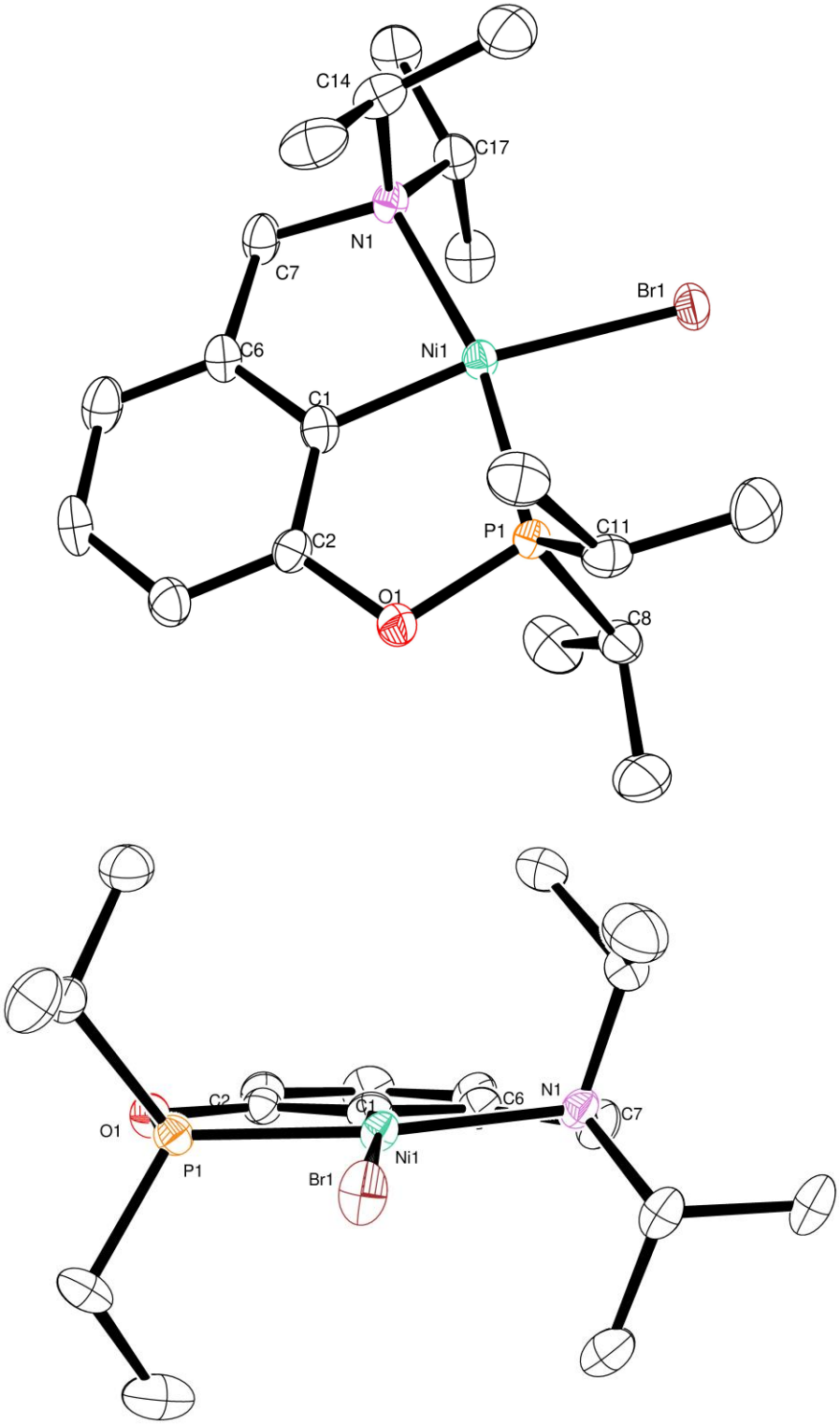

Figure 33. Molecular structure of (POCN$^{i\text{-Pr2}}$)NiBr (**5-Br**), depicted with 50% thermal ellipsoids probability level (hydrogen atoms are omitted for clarity).

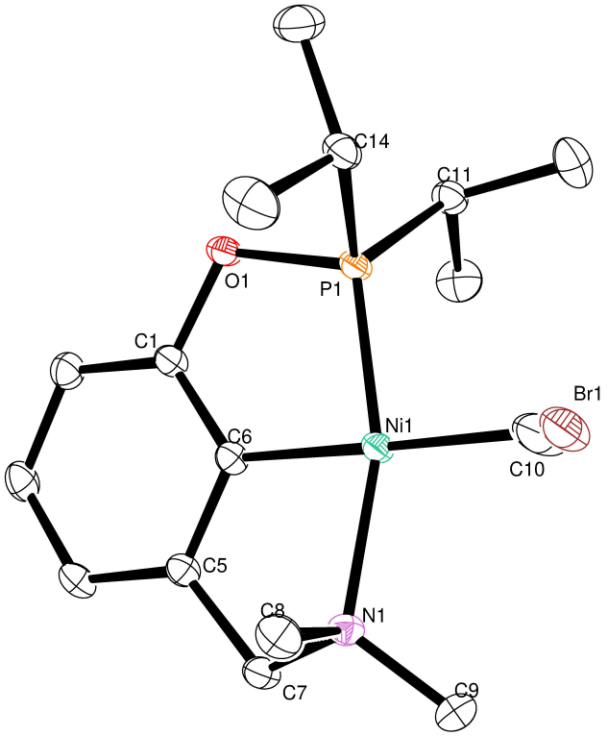

Figure 34. Molecular structure of (POCN^{Me2})NiMe (**3-Me**) co-crystallized with (POCN^{Me2})NiBr (**3-Br**) (0.9:0.1 fractions, respectively), depicted with 50% thermal ellipsoids probability level (hydrogen atoms are omitted for clarity).

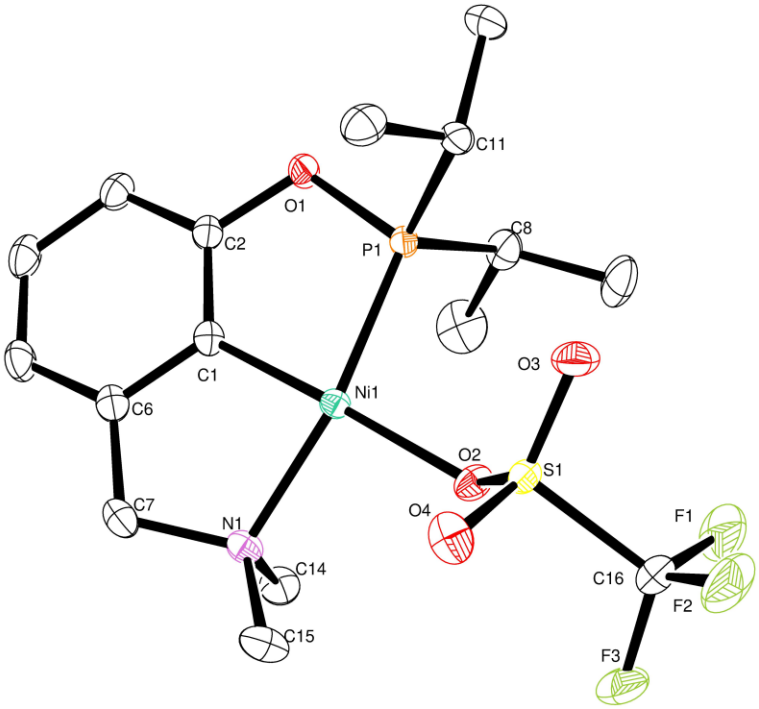

Figure 35. Molecular structure of (POCN^{Me2})Ni(OTf) (**3-OTf**), depicted with 50% thermal ellipsoids probability level (hydrogen atoms are omitted for clarity).

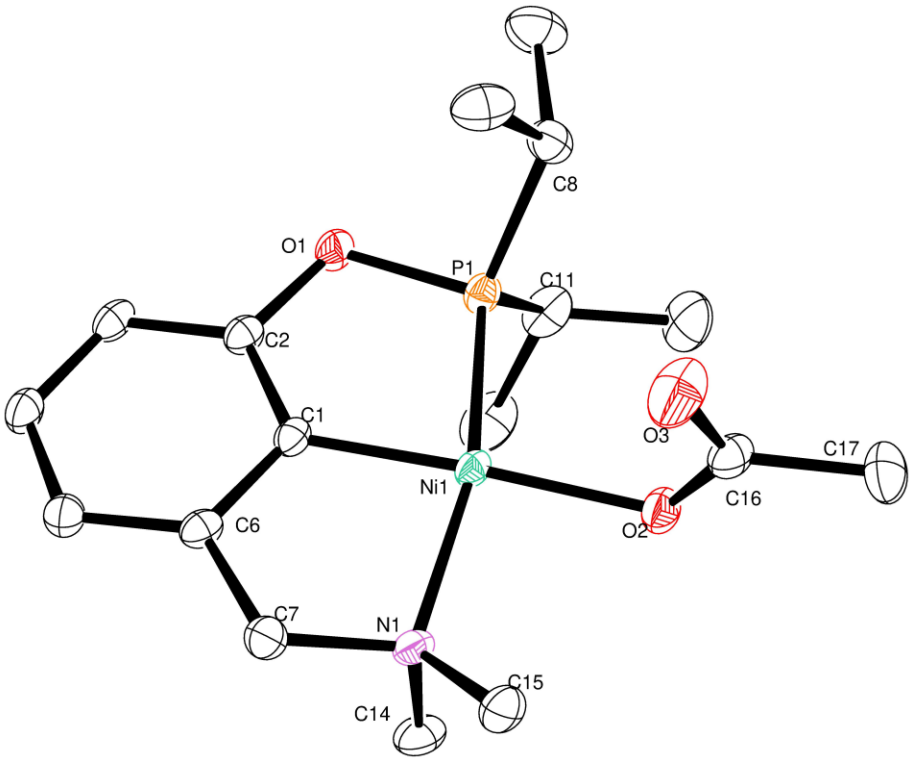

Figure 36. Molecular structure of (POCN^{Me2})Ni(OAc) (**3-OAc**), depicted with 50% thermal ellipsoids probability level (hydrogen atoms are omitted for clarity).

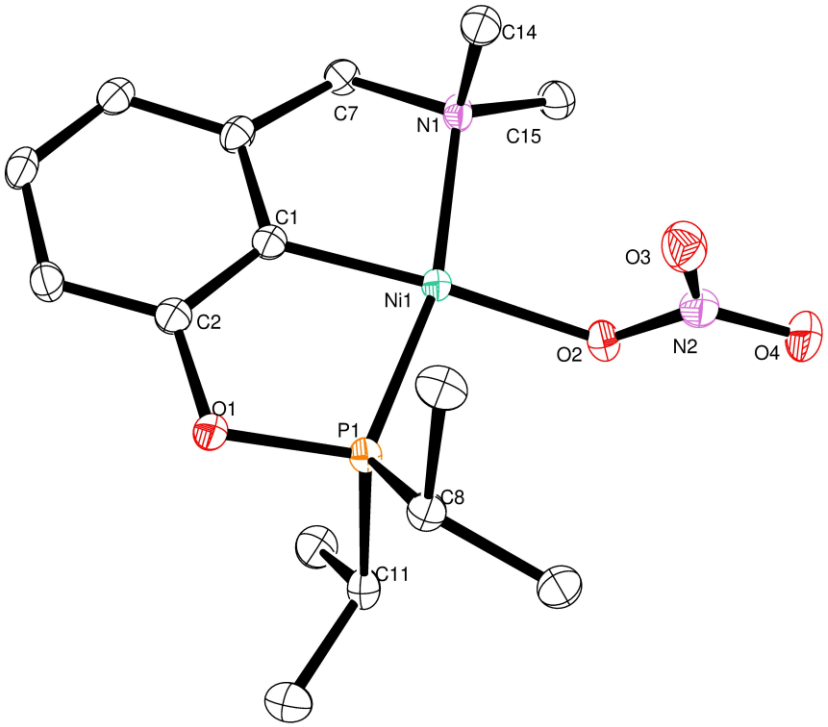

Figure 37. Molecular structure of (POCN^{Me2})Ni(ONO_2) (**3-NO_3**), depicted with 50% thermal ellipsoids probability level (hydrogen atoms are omitted for clarity).

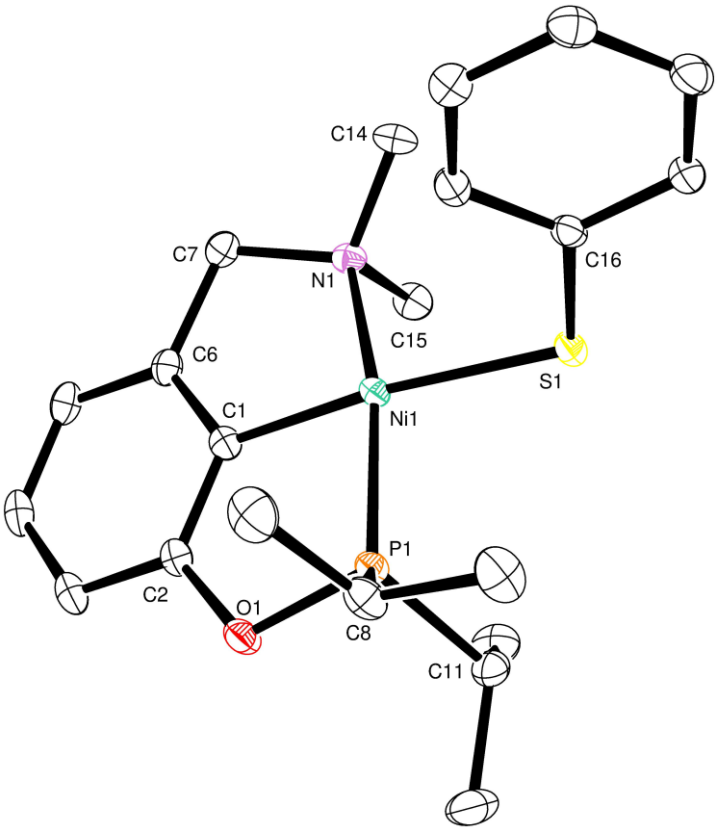

Figure 38. Molecular structure of (POCN^{Me2})Ni(SPh) (**3-SPh**), depicted with 50% thermal ellipsoids probability level (hydrogen atoms are omitted for clarity).

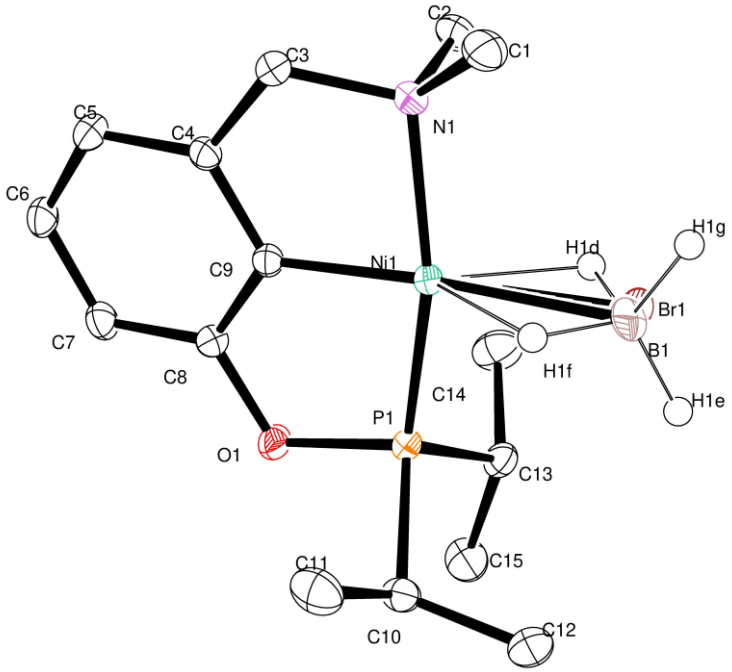

Figure 39. Molecular structure of (POCN^{Me2})Ni(η^2-BH_4) (**3-BH_4**), depicted with 50% thermal ellipsoids probability level (hydrogen atoms are omitted for clarity).

Table S3. X-ray crystallographic data and refinement details for complexes **5-Br**, **3-Me**, **3-BH_4** and **3-NO_3**.

	5-Br	**3-Me**	**3-BH_4**
Empirical formula	$C_{19}H_{33}BrNNiOP$	$C_{15.9}H_{27.72}Br_{0.11}NNiOP$	$C_{15}H_{28.36}B_{0.84}Br_{0.16}NNiOP$
Formula weight	461.05	347.03	350.29
Temperature (K)	100	150.0(1)	150.0(1)
Crystal system	Orthorhombic	Triclinic	Triclinic
Space group	P b c a	P -1	P -1
Z	8	2	2
Unit cell dimensions			
a, Å	14.8863(7)	9.3433(10)	9.3802(11)
b, Å	14.2089(7)	9.4438(10)	9.4495(11)
c, Å	19.6520(10)	10.8402(11)	10.9044(13)
α, °	90	66.371(3)	66.939(4)
β, °	90	78.720(3)	78.797(4)
γ, °	90	75.511(3)	75.715(4)
V, $Å^3$	4156.8(4)	843.52(15)	856.63(18)
d_{calc}, $g \cdot cm^{-3}$	1.469	1.366	1.358
μ, cm^{-1}	29.03	14.90	15.94
F(000)	1915	370	372
$2\theta_{max}$, °	60.00	51.12	57.114
Completeness	0.992	0.983	0.992
Refl. collected	27710	16798	21084
Refl. unique (R_{int})	6004 (0.0836)	4231 (0.0457)	4327 (0.0491)
Refl. with I > 2σ(I)	4324	3853	4017
Parameters	225	199	213
Final R_1 with I>2σ(I)	0.0461	0.0288	0.0278
wR_2 (all data)	0.0993	0.0717	0.0710
GOF	1.027	1.072	1.047
Largest difference in peak / hole ($e/Å^3$)	0.828/-0.464	0.484/-0.548	0.785/-0.605
CCDC number	2221358	2215530	2215529

Table S4. X-ray crystallographic data and refinement details for complexes **3-OTf**, **3-OAc** and **3-SPh**.

	3-OTf	**3-OAc**	**3-NO_3**	**3-SPh**
Empirical formula	$C_{16}H_{25}F_3NNiO_4PS$	$C_{17}H_{28}NNiO_3P$	$C_{15}H_{25}N_2NiO_4P$	$C_{21}H_{30}NNiOPS$
Formula weight	474.11	384.08	387.05	434.20
Temperature (K)	100	100	100	100
Crystal system	Monoclinic	Triclinic	Monoclinic	Triclinic
Space group	P 1 21/n 1	P -1	P 1 21/n 1	P -1
Z	4	2	4	2
Unit cell dimensions				
a, Å	7.8050(2)	7.7205(4)	11.2003(9)	9.1019(4)
b, Å	9.9384(3)	9.0830(5)	9.4423(8)	9.5253(4)
c, Å	26.7534(8)	14.8641(8)	16.3874(13)	13.2196(5)
α, °	90	76.7640(10)	90	109.0510(10)
β, °	96.5420(10)	81.7370(10)	101.156(3)	94.1800(10)
γ, °	90	66.2490(10)	90	102.8170(10)
V, $Å^3$	2061.73(10)	927.17(9)	1700.3(2)	1043.14(8)
d_{calc}, $g \cdot cm^{-3}$	1.527	1.376	1.512	1.382
μ, cm^{-1}	11.67	11.45	12.56	11.17
F(000)	984	408	816	460
$2\theta_{max}$, °	61.05	58.00	59.994	61.10
Completeness	0.998	0.969	1.00	0.983
Refl. collected	22476	7757	17214	15024
Refl. unique (R_{int})	6286 (0.0454)	4790 (0.0489)	4953 (0.1001)	6288 (0.0340)
Refl. with I > 2σ(I)	5116	4148	3413	5669
Variables	250	215	214	241
Final R_1 with I>2σ(I)	0.0324	0.0413	0.0613	0.0295
wR_2 (all data)	0.0746	0.0956	0.1084	0.797
GOF	1.024	1.034	1.054	1.059
Largest difference in peak / hole ($e/Å^3$)	0.421/-0.286	0.590/-0.475	0.594/-0.442	0.425/-0.473
CCDC number	2221356	2221354	2221357	2221355

Table S5. Selected bond distances (Å) for complex **5-Br**

Br1 Ni1 2.3588(5)	Ni1 C1 1.852(3)	Ni1 N1 2.067(2)	Ni1 P1 2.1037(8)
P1 O1 1.657(2)	P1 C8 1.817(3)	P1 C11 1.825(3)	O1 C2 1.395(3)
N1 C17 1.512(4)	N1 C7 1.513(4)	N1 C14 1.525(4)	C2 C3 1.380(4)
C2 C1 1.383(4)	C1 C6 1.396(4)	C6 C5 1.387(4)	C6 C7 1.500(4)
C11 C13 1.524(4)	C11 C12 1.527(4)	C8 C9 1.523(5)	C8 C10 1.532(4)
C17 C19 1.524(5)	C17 C18 1.524(4)	C3 C4 1.391(4)	C5 C4 1.395(5)
C14 C16 1.510(5)	C14 C15 1.520(4)		

Table S6. Selected bond angles (°) for complex **5-Br**

C1 Ni1 N1 85.54(11)	C1 Ni1 P1 81.48(10)	N1 Ni1 P1 166.42(7)
C1 Ni1 Br1 169.89(9)	N1 Ni1 Br1 102.05(7)	P1 Ni1 Br1 91.32(2)
O1 P1 C8 101.53(13)	O1 P1 C11 99.24(12)	C8 P1 C11 106.68(14)
O1 P1 Ni1 108.19(8)	C8 P1 Ni1 117.94(11)	C11 P1 Ni1 120.03(10)
C2 O1 P1 109.71(18)	C17 N1 C7 109.7(2)	C17 N1 C14 110.5(2)
C7 N1 C14 107.1(2)	C17 N1 Ni1 110.58(16)	C7 N1 Ni1 107.76(17)
C14 N1 Ni1 111.12(17)	C3 C2 C1 123.2(3)	C3 C2 O1 120.5(3)
C1 C2 O1 116.4(2)	C2 C1 C6 118.5(3)	C2 C1 Ni1 124.2(2)
C6 C1 Ni1 117.2(2)	C5 C6 C1 120.0(3)	C5 C6 C7 124.1(3)
C1 C6 C7 115.8(3)	C6 C7 N1 110.6(2)	C13 C11 C12 111.6(3)
C13 C11 P1 109.6(2)	C12 C11 P1 113.7(2)	C9 C8 C10 111.3(3)
C9 C8 P1 109.1(2)	C10 C8 P1 112.5(2)	N1 C17 C19 110.6(3)
N1 C17 C18 114.1(2)	C19 C17 C18 111.0(3)	C2 C3 C4 117.2(3)
C6 C5 C4 119.5(3)	C3 C4 C5 121.6(3)	C16 C14 C15 110.4(3)
C16 C14 N1 113.6(2)	C15 C14 N1 110.9(3)	

Table S7. Selected bond distances (Å) for complex **3-Me**

Ni1 P1 2.0739(5)	Ni1 C10 2.020(9)	Ni1 N1 2.0298(13)	Ni1 C6 1.8779(16)
Ni1 Br1 2.250(11)	P1 O1 1.6716(12)	P1 C11 1.8347(16)	P1 C14 1.8283(17)
O1 C1 1.3970(18)	N1 C7 1.500(2)	N1 C8 1.486(2)	N1 C9 1.475(2)
C1 C6 1.388(2)	C1 C2 1.384(2)	C6 C5 1.393(2)	C5 C7 1.508(2)
C5 C4 1.397(2)	C2 C3 1.401(2)	C4 C3 1.389(2)	C11 C12 1.532(2)
C11 C13 1.528(2)	C14 C16 1.527(2)	C14 C15 1.529(2)	

Table S8. Selected bond angles (°) for complex **3-Me**

P1 Ni1 Br1 96.8(2)	C10 Ni1 P1 98.2(3)	C10 Ni1 N1 96.3(3)
N1 Ni1 P1 163.47(4)	N1 Ni1 Br1 98.0(2)	C6 Ni1 P1 81.88(5)
C6 Ni1 C10 177.7(3)	C6 Ni1 N1 83.33(6)	C6 Ni1 Br1 178.6(2)
O1 P1 Ni1 108.51(4)	O1 P1 C11 100.00(7)	O1 P1 C14 101.81(7)
C11 P1 Ni1 121.26(6)	C14 P1 Ni1 116.18(5)	C14 P1 C11 106.18(7)
C1 O1 P1 110.03(10)	C7 N1 Ni1 109.01(9)	C8 N1 Ni1 103.88(10)
C8 N1 C7 109.00(12)	C9 N1 Ni1 116.82(10)	C9 N1 C7 109.15(13)
C9 N1 C8 108.68(13)	C6 C1 O1 115.81(13)	C2 C1 O1 121.24(14)
C2 C1 C6 122.95(14)	C1 C6 Ni1 123.46(11)	C1 C6 C5 118.51(14)
C5 C6 Ni1 117.93(12)	C6 C5 C7 113.39(14)	C6 C5 C4 120.37(14)
C4 C5 C7 126.18(14)	N1 C7 C5 108.26(12)	C1 C2 C3 117.31(15)
C3 C4 C5 119.40(14)	C4 C3 C2 121.46(15)	C12 C11 P1 111.57(12)
C13 C11 P1 108.96(11)	C13 C11 C12 111.37(15)	C16 C14 P1 113.64(12)
C16 C14 C15 111.26(15)	C15 C14 P1 109.02(11)	

Table S9. Selected bond distances (Å) for complex **3-BH$_4$**

Br1 Ni1 2.311(5)	Ni1 P002 2.1250(5)	Ni1 N1 2.0220(13)	Ni1 C9 1.8669(14)
Ni1 B1 2.270(10)	P002 O1 1.6642(11)	P002 C10 1.8332(15)	P002 C13 1.8301(15)
O1 C8 1.3921(17)	N1 C1 1.4838(19)	N1 C2 1.4931(19)	N1 C3 1.5018(18)
C3 C4 1.504(2)	C4 C5 1.397(2)	C4 C9 1.396(2)	C5 C6 1.395(2)
C6 C7 1.395(2)	C7 C8 1.3901(19)	C8 C9 1.392(2)	C10 C11 1.531(2)
C10 C12 1.536(2)	C13 C14 1.532(2)	C13 C15 1.532(2)	

Table S10. Selected bond angles (°) for complex **3-BH$_4$**

P002 Ni1 Br1 96.71(14)	P002 Ni1 B1 94.8(3)	N1 Ni1 Br1 98.26(15)
N1 Ni1 P002 162.74(4)	N1 Ni1 B1 100.5(3)	C9 Ni1 Br1 177.69(13)
C9 Ni1 P002 81.34(5)	C9 Ni1 N1 83.49(6)	C9 Ni1 B1 175.8(4)
O1 P002 Ni1 107.73(4)	O1 P002 C10 100.16(6)	O1 P002 C13 102.07(6)
C10 P002 Ni1 121.26(5)	C13 P002 Ni1 115.70(5)	C13 P002 C10 107.08(7)
C8 O1 P002 110.29(9)	C1 N1 Ni1 116.60(9)	C1 N1 C2 108.30(11)
C1 N1 C3 108.84(12)	C2 N1 Ni1 104.95(9)	C2 N1 C3 109.00(11)
C3 N1 Ni1 108.91(9)	N1 C3 C4 107.54(12)	C5 C4 C3 125.69(13)
C9 C4 C3 113.89(12)	C9 C4 C5 120.37(13)	C6 C5 C4 119.36(14)
C5 C6 C7 121.50(13)	C8 C7 C6 117.64(14)	O1 C8 C9 116.47(12)
C7 C8 O1 120.98(13)	C7 C8 C9 122.55(14)	C4 C9 Ni1 117.43(10)
C8 C9 Ni1 123.97(11)	C8 C9 C4 118.56(13)	C11 C10 P002 109.33(11)
C11 C10 C12 111.23(13)	C12 C10 P002 112.83(10)	C14 C13 P002 109.33(11)
C14 C13 C15 110.97(13)	C15 C13 P002 112.59(10)	

Table S11. Selected bond distances (Å) for complex **3-OTf**

Ni1 P1 2.1295(5)	Ni1 O2 1.9621(11)	Ni1 N1 1.9944(13)	Ni1 C1 1.8465(16)
S1 O2 1.4737(12)	S1 O3 1.4296(13)	S1 O4 1.4295(13)	S1 C16 1.8162(18)
P1 O1 1.6507(12)	P1 C11 1.8198(17)	P1 C8 1.8242(17)	F3 C16 1.324(2)
O1 C2 1.3886(19)	F1 C16 1.326(2)	F2 C16 1.329(2)	N1 C7 1.494(2)
N1 C15 1.479(2)	N1 C14 1.484(2)	C2 C1 1.388(2)	C2 C3 1.388(2)
C1 C6 1.395(2)	C6 C5 1.391(2)	C6 C7 1.494(2)	C5 C4 1.388(3)
C3 C4 1.391(2)	C11 C13 1.531(2)	C11 C12 1.523(2)	C8 C10 1.528(3)
C8 C9 1.525(3)			

Table S12. Selected bond angles (°) for complex **3-OTf**

O2 Ni1 P1 100.31(4)	O2 Ni1 N1 93.72(5)	N1 Ni1 P1 162.26(4)
C1 Ni1 P1 81.61(5)	C1 Ni1 O2 177.49(6)	C1 Ni1 N1 84.10(6)
O2 S1 C16 100.19(8)	O3 S1 O2 114.05(7)	O3 S1 O4 117.39(8)
O3 S1 C16 104.42(8)	O4 S1 O2 113.96(7)	O4 S1 C16 104.09(8)
O1 P1 Ni1 107.14(4)	O1 P1 C11 102.14(7)	O1 P1 C8 101.61(7)
C11 P1 Ni1 121.66(6)	C11 P1 C8 108.38(8)	C8 P1 Ni1 113.38(6)
S1 O2 Ni1 125.72(7)	C2 O1 P1 110.70(10)	C7 N1 Ni1 109.06(10)
C15 N1 Ni1 117.62(10)	C15 N1 C7 109.68(13)	C15 N1 C14 107.78(14)
C14 N1 Ni1 103.30(10)	C14 N1 C7 108.98(13)	C1 C2 O1 116.41(14)
C3 C2 O1 121.09(15)	C3 C2 C1 122.50(15)	C2 C1 Ni1 124.10(12)
C2 C1 C6 118.79(15)	C6 C1 Ni1 117.10(13)	C1 C6 C7 113.87(15)
C5 C6 C1 119.93(16)	C5 C6 C7 126.16(15)	C6 C5 H5 120.1
C4 C5 C6 119.78(16)	C2 C3 C4 117.52(16)	C13 C11 P1 108.50(12)
C12 C11 P1 112.76(13)	C12 C11 C13 111.99(15)	C6 C7 N1 107.82(13)
C5 C4 C3 121.48(16)	F3 C16 S1 111.71(12)	F3 C16 F1 107.89(15)
F3 C16 F2 108.13(15)	F1 C16 S1 111.31(12)	F1 C16 F2 107.44(15)
F2 C16 S1 110.19(13)	C10 C8 P1 111.32(13)	C9 C8 P1 108.83(13)
C9 C8 C10 112.20(17)		

Table S13. Selected bond distances (Å) for complex **3-OAc**

Ni1 P1 2.1043(6)	Ni1 O2 1.9270(14)	Ni1 N1 1.9997(17)	Ni1 C1 1.8493(18)
P1 O1 1.6510(14)	P1 C8 1.822(2)	P1 C11 1.827(2)	O2 C16 1.276(2)
O1 C2 1.394(2)	O3 C16 1.235(3)	N1 C15 1.475(2)	N1 C7 1.499(2)
N1 C14 1.485(3)	C2 C1 1.395(3)	C2 C3 1.385(3)	C1 C6 1.390(3)
C16 C17 1.510(3)	C6 C5 1.394(3)	C6 C7 1.501(3)	C3 C4 1.393(3)
C5 C4 1.393(3)	C8 C9 1.528(3)	C8 C10 1.529(3)	C11 C13 1.524(4)
C11 C12 1.523(3)			

Table S14. Selected bond angles (°) for complex **3-OAc**

O2 Ni1 P1 98.45(5)	O2 Ni1 N1 95.04(6)	N1 Ni1 P1 164.34(5)
C1 Ni1 P1 81.75(7)	C1 Ni1 O2 174.94(7)	C1 Ni1 N1 84.11(8)
O1 P1 Ni1 107.99(6)	O1 P1 C8 101.75(9)	O1 P1 C11 100.79(9)
C8 P1 Ni1 120.00(7)	C8 P1 C11 107.47(11)	C11 P1 Ni1 116.12(8)
C16 O2 Ni1 112.97(13)	C2 O1 P1 110.29(12)	C15 N1 Ni1 115.27(13)
C15 N1 C7 109.75(16)	C15 N1 C14 108.93(16)	C7 N1 Ni1 109.33(12)
C14 N1 Ni1 104.26(13)	C14 N1 C7 109.05(16)	O1 C2 C1 115.95(17)
C3 C2 O1 121.05(18)	C3 C2 C1 123.00(19)	C2 C1 Ni1 123.79(16)
C6 C1 Ni1 117.91(15)	C6 C1 C2 118.20(17)	O2 C16 C17 116.34(18)
O3 C16 O2 123.32(19)	O3 C16 C17 120.32(19)	C1 C6 C5 120.44(18)
C1 C6 C7 113.33(17)	C5 C6 C7 126.18(19)	C2 C3 C4 117.33(19)
C4 C5 C6 119.54(19)	N1 C7 C6 108.03(17)	C3 C4 C5 121.47(18)
C9 C8 P1 108.77(16)	C9 C8 C10 111.8(2)	C10 C8 P1 112.77(16)
C13 C11 P1 108.70(17)	C12 C11 P1 111.40(16)	C12 C11 C13 111.7(2)

Table S15. Selected bond distances (Å) for complex **3-NO_3**

Ni1 P1 2.1264(9)	Ni1 O2 1.946(2)	Ni1 N1 2.006(3)
Ni1 C1 1.849(3)	P1 O1 1.657(2)	P1 C8 1.821(3)
P1 C11 1.815(3)	O1 C2 1.391(4)	O2 N2 1.280(3)
O3 N2 1.243(4)	O4 N2 1.232(3)	N1 C14 1.493(4)
N1 C7 1.496(3)	N1 C15 1.474(4)	C1 C2 1.393(4)
C1 C6 1.391(4)	C2 C3 1.379(4)	C6 C5 1.391(4)
C6 C7 1.502(4)	C5 C4 1.385(4)	C8 C9 1.530(4)
C8 C10 1.534(4)	C3 C4 1.391(4)	C11 C12 1.530(4)
C11 C13 1.527(4)		

Table S16. Selected bond angles (°) for complex **3-NO_3**

O2 Ni1 P1 98.36(7)	O2 Ni1 N1 96.80(9)	N1 Ni1 P1 164.69(7)
C1 Ni1 P1 81.52(10)	C1 Ni1 O2 170.17(12)	C1 Ni1 N1 83.92(11)
O1 P1 Ni1 107.01(8)	O1 P1 C8 101.25(12)	O1 P1 C11 103.12(12)
C8 P1 Ni1 117.89(10)	C11 P1 Ni1 117.46(11)	C11 P1 C8 107.79(15)
C2 O1 P1 110.47(17)	N2 O2 Ni1 120.6(2)	C14 N1 Ni1 106.84(19)
C14 N1 C7 107.9(2)	C7 N1 Ni1 108.04(17)	C15 N1 Ni1 115.10(19)
C15 N1 C14 108.9(2)	C15 N1 C7 109.7(2)	O3 N2 O2 119.1(2)
O4 N2 O2 118.7(3)	O4 N2 O3 122.2(3)	C2 C1 Ni1 124.2(2)
C6 C1 Ni1 117.3(2)	C6 C1 C2 118.5(3)	O1 C2 C1 116.0(2)
C3 C2 O1 121.6(3)	C3 C2 C1 122.4(3)	C1 C6 C7 113.4(2)
C5 C6 C1 120.4(3)	C5 C6 C7 126.1(3)	C4 C5 C6 119.4(3)

C9 C8 P1 108.8(2)	C9 C8 C10 111.4(2)	C10 C8 P1 111.7(2)
C2 C3 C4 117.8(3)	C5 C4 C3 121.5(3)	N1 C7 C6 107.7(2)
C12 C11 P1 112.9(2)	C13 C11 P1 110.0(2)	C13 C11 C12 110.8(3)

Table S17. Selected bond distances (Å) for complex **3-SPh**

P1 O1 1.6604(10)	P1 C8 1.8264(14)	P1 C11 1.8235(14)	P1 Ni1 2.0947(4)
O1 C2 1.3904(16)	N1 C7 1.4920(18)	N1 C14 1.4766(17)	N1 C15 1.4861(17)
N1 Ni1 2.0171(11)	C1 C6 1.3883(18)	C1 C2 1.3939(18)	C1 Ni1 1.8641(13)
C6 C7 1.5017(19)	C6 C5 1.3928(19)	C17 C16 1.4014(18)	C17 C18 1.3951(19)
C8 C10 1.521(2)	C8 C9 1.529(2)	C16 C21 1.4018(18)	C16 S1 1.7596(14)
C18 C19 1.387(2)	C21 C20 1.393(2)	C2 C3 1.3831(19)	C19 C20 1.391(2)
C3 C4 1.398(2)	C11 C12 1.530(2)	C11 C13 1.529(2)	C5 C4 1.392(2)

Table S18. Selected bond angles (°) for complex **3-SPh**

O1 P1 C8 100.31(6)	O1 P1 C11 102.73(6)	O1 P1 Ni1 108.07(4)
C8 P1 Ni1 123.25(5)	C11 P1 C8 106.52(7)	C11 P1 Ni1 113.35(5)
C2 O1 P1 110.39(8)	C7 N1 Ni1 109.88(8)	C14 N1 C7 109.24(11)
C14 N1 C15 107.95(10)	C14 N1 Ni1 117.23(9)	C15 N1 C7 109.31(11)
C15 N1 Ni1 102.87(8)	C6 C1 C2 118.72(12)	C6 C1 Ni1 117.68(10)
C2 C1 Ni1 123.46(10)	C1 C6 C7 114.15(12)	C1 C6 C5 120.28(12)
C5 C6 C7 125.52(12)	N1 C7 C6 108.03(11)	C18 C17 C16 121.11(13)
C10 C8 P1 112.34(10)	C10 C8 C9 112.13(13)	C9 C8 P1 109.43(10)
C17 C16 C21 117.78(12)	C17 C16 S1 122.34(10)	C21 C16 S1 119.88(10)
C19 C18 C17 120.49(13)	C20 C21 C16 120.79(13)	O1 C2 C1 116.11(12)
C3 C2 O1 121.27(12)	C3 C2 C1 122.62(13)	C18 C19 C20 118.98(13)
C2 C3 C4 117.39(13)	C19 C20 C21 120.83(14)	C12 C11 P1 113.44(11)
C13 C11 P1 109.09(10)	C13 C11 C12 111.58(12)	C4 C5 C6 119.52(13)
C5 C4 C3 121.43(13)	P1 Ni1 S1 94.310(14)	N1 Ni1 P1 163.11(3)
N1 Ni1 S1 99.13(3)	C1 Ni1 P1 81.89(4)	C1 Ni1 N1 83.64(5)
C1 Ni1 S1 173.02(4)	C16 S1 Ni1 107.03(5)	

5. NMR data for deoxygenative hydroboration products

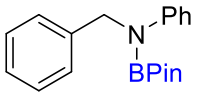

8a

>99% NMR yield. ^{1}H-NMR (500 MHz; C_6D_6; δ, ppm): 1.08 (s, 12H, 4 *CH*$_3$ of NB*Pin*); 4.77 (s, 2H, *CH*$_2$); 6.80 (t, *J* = 7.4 Hz, 1H, *p*-H of *Ph*); 7.01 (t, *J* = 7.3 Hz, 1H, *p*-H of *Ph*); 7.07-7.14 (m, 4H, 4 *m*-H of 2 *Ph*); 7.22 (d, *J* = 7.4 Hz, 2 *o*-H of *Ph*); 7.46-7.49 (m, 2H, 2 *o*-H of *Ph*). NMR data are consistent with those previously reported in the literature.[12]

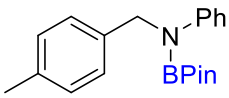

8b

>99% NMR yield. ^{1}H NMR (500 MHz; C_6D_6; δ, ppm): 1.09 (s, 12H, 4 *CH*$_3$ of NB*Pin*); 2.07 (s, 3H, *CH*$_3$ of *p-Tol*CH_2N); 4.78 (s, 2H, CH_2 of *p*-Tol*CH*$_2$N); 6.81 (t, *J* = 7.3 Hz, 1H, *p*-H of N*Ph*); 6.95 (d, *J* = 7.9 Hz, 2H, N*Ph* or NCH_2(*p-Tol*)); 7.09-7.14 (m, 2H, *m*-H of N*Ph*); 7.17 (d, *J* = 7.9 Hz, 2H, N*Ph* or NCH_2(*p-Tol*)); 7.48-7.53 (m, 2H, N*Ph* or NCH_2(*p-Tol*)). ^{13}C{^{1}H}-NMR (125.8 MHz; C_6D_6; δ, ppm): 21.0 (s); 24.9 (s); 51.3 (s); 83.0 (s); 121.1 (s); 121.7 (s); 126.7 (s); 128.9 (s); 129.5 (s); 136.0 (s); 137.9 (s); 146.9 (s). ^{11}B{^{1}H}-NMR (160.5 MHz; C_6D_6; δ, ppm): 24.3 (br s, N*B*Pin). NMR data are consistent with those previously reported in the literature.[13]

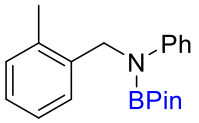

8c

8c was obtained in a complex mixture of unidentified compounds. The NMR yield (52%) was calculated based on the integral intensity of the characteristic CH_2 resonance of **8c** compared to the internal standard, 1,3,5-trimethoxybenzene. ^{1}H NMR (500 MHz; C_6D_6; δ, ppm): 1.04 (s, 12H, 4 *CH*$_3$ of NB*Pin*); 2.06 (s, 3H, *CH*$_3$ of *m-Tol*CH_2N); 4.96 (s, 2H, CH_2 of *m*-Tol*CH*$_2$N); aromatic resonances overlap with the resonances for other unidentified products. ^{11}B{^{1}H}-NMR (160.5 MHz; C_6D_6; δ, ppm): 24.1 (br s, N*B*Pin). Methanolysis of this mixture resulted in the conversion of **8c** to *N*-(2-methylbenzyl)aniline.[14]

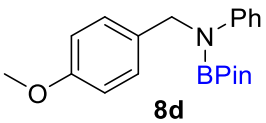

8d

94% NMR yield. ^{1}H NMR (500 MHz; C_6D_6; δ, ppm): 1.10 (s, 12H, 4 *CH*$_3$ of NB*Pin*); 3.27 (s, 3H, O*CH*$_3$); 4.77 (s, 2H, CH_2, *CH*$_2$N); 6.72-6.76 (m, 2H, *C*$_6$*H*$_4$ or N*Ph*); 6.83 (t, *J* = 7.3 Hz, 1H, *p*-H of N*Ph*); 7.11-7.18 (m, 4H, *C*$_6$*H*$_4$ or N*Ph*); 7.52 (d, *J* = 7.9 Hz, 2H, 2 *o*-H of N*Ph*). NMR data are consistent with those previously reported in the literature.[12]

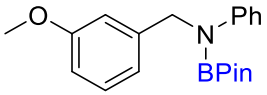

8e

92% NMR yield. ^{1}H NMR (500 MHz; C_6D_6; δ, ppm): 1.08 (s, 12H, 4 *CH*$_3$ of NB*Pin*); 3.28 (s, 3H, O*CH*$_3$); 4.78 (s, 2H, CH$_2$, *CH*$_2$N); 6.63-6.67 (m, 1H, *C*$_6$*H*$_4$); 6.81 (t, *J* = 7.3 Hz, 1H, *p*-H of N*Ph*); 6.89 (d, *J* = 7.5 Hz, 1H, C_6H_4); 6.96 (s, 1H, C_6H_4); 7.04-7.14 (m, 3H, 1 H of C_6H_4 and 2 *m*-H of N*Ph*); 7.51 (d, *J* = 7.9 Hz, 2H, 2 *o*-H of N*Ph*). ^{13}C{^{1}H}-NMR (125.8 MHz; C_6D_6; δ, ppm): 24.9 (s); 51.7 (s); 54.6 (s); 83.0 (s); 112.37 (s); 112.43 (s); 119.0 (s); 121.0 (s); 121.8 (s); 128.9 (s); 129.8 (s); 142.8 (s); 146.9 (s); 160.6 (s). ^{11}B{^{1}H}-NMR (160.5 MHz; C_6D_6; δ, ppm): 24.3 (br s, N*B*Pin). NMR data for the corresponding amine have been previously reported.[15]

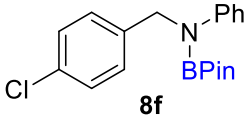

8f

8f was obtained in a complex and difficult-to-analyze mixture of compounds. The NMR yield (23%) was calculated based on the integral intensity of the characteristic CH_2 resonance of **8f** compared to the internal standard, 1,3,5-trimethoxybenzene. ^{1}H NMR (500 MHz; C_6D_6; δ, ppm): 1.06 (s, 12H, 4 *CH*$_3$ of NB*Pin*); 4.60 (s, 2H, CH$_2$, *CH*$_2$N); 6.82 (m, 1H, *C*$_6$*H*$_4$ / N*Ph*); 6.92 (m, 2H, *C*$_6$*H*$_4$ / N*Ph*); 7.03 (m, 2H, *C*$_6$*H*$_4$ / N*Ph*); 7.12 (m, 2H, *C*$_6$*H*$_4$ / N*Ph*); 7.38 (m, 2H, *C*$_6$*H*$_4$ / N*Ph*). NMR data are consistent with those previously reported in the literature.[12]

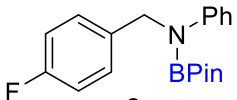

8g

98% NMR yield. ^{1}H NMR (500 MHz; C_6D_6; δ, ppm): 1.07 (s, 12H, 4 *CH*$_3$ of NB*Pin*); 4.63 (s, 2H, CH$_2$, *CH*$_2$N); 6.71-6.78 (m, 2H, *C*$_6$*H*$_4$ / N*Ph*); 6.82 (t, *J* = 7.3 Hz, 1H, *p*-H of N*Ph*); 6.96-7.01(m, 2H, *C*$_6$*H*$_4$ / N*Ph*); 7.10-7.14 (m, 2H, *C*$_6$*H*$_4$ / N*Ph*); 7.39-7.43 (m, 2H, *C*$_6$*H*$_4$ / N*Ph*). ^{13}C{^{1}H}-NMR (125.8 MHz; C_6D_6; δ, ppm): 24.9 (s); 50.8 (s); 54.6 (s); 83.1 (s); 115.3 (s); 115.5 (s); 121.1 (s); 122.0 (s); 128.9 (s); 136.5 (d, *J* = 3.0 Hz); 146.5 (s); 162.13 (d, *J* = 243.8 Hz). ^{11}B{^{1}H}-NMR (160.5 MHz; C_6D_6; δ, ppm): 24.0 (br s, N*B*Pin). ^{19}F{^{1}H}-NMR (471 MHz; C_6D_6; δ, ppm): -116.61 (s). NMR data are consistent with those previously reported in the literature.[13]

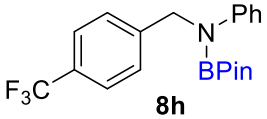

8h

82% NMR yield. ^{1}H NMR (500 MHz; C_6D_6; δ, ppm): 1.07 (s, 12H, 4 *CH*$_3$ of NB*Pin*); 4.63 (s, 2H, CH$_2$, *CH*$_2$N); 6.80-6.85 (m, 1H, N*Ph*); 7.03 (d, *J* = 8.0 Hz, 2H, *C*$_6$*H*$_4$); 7.09-7.14 (m, 2H, N*Ph*); 7.27 (d, *J* = 8.1 Hz, 2H, *C*$_6$*H*$_4$); 7.35-7.39 (m, 2H, N*Ph*). ^{19}F{^{1}H}-NMR (471 MHz; C_6D_6; δ, ppm): -61.93 (s). NMR data are consistent with those previously reported in the literature.[12]

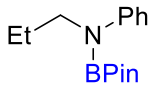

8i

>99% NMR yield. ^{1}H-NMR (500 MHz; C_6D_6; δ, ppm): 0.79 (t, J = 7.5 Hz, 3H, $CH_3CH_2CH_2N$); 1.08 (br s, 12H, B*Pin*); 1.49 (m, 2H, $CH_3CH_2CH_2N$); 3.51 (t, J = 7.2 Hz, 2H, $CH_3CH_2CH_2N$); 6.85 (t, J = 7.2 Hz, 1H, *p*-H of N*Ph*); 7.16 (t, J = 7.9 Hz, 2H, *m*-H of N*Ph*); 7.37 (d, J = 8.0 Hz, 2H, *o*-H of N*Ph*). ^{13}C{^{1}H}- NMR (128.5 MHz; C_6D_6; δ, ppm): 11.3 (s); 22.6 (s); 25.0 (s); 48.7 (s); 83.2 (s); 121.78 (s); 121.83 (s); 128.9 (s); 146.4 (s). ^{11}B{^{1}H}-NMR (160.5 MHz; C_6D_6; δ, ppm): 23.7 (br s, *B*Pin). NMR data are consistent with those previously reported in the literature.[4]

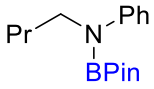

8j

>99% NMR yield. ^{1}H-NMR (500 MHz; C_6D_6; δ, ppm): 0.82 (t, J = 7.4 Hz, 3H, CH_3 of N*Bu*); 1.09 (br s, 12H, B*Pin*); 1.23-1.31 (m, 2H, CH_2 of N*Bu*); 1.48-1.55 (m, 2H, CH_2 of N*Bu*); 3.62 (t, J = 7.2 Hz, 2H, CH_2 of N*Bu*); 6.83-6.93 (m, 1H, *p*-H of N*Ph*); 7.17-7.25 (m, 2H, *m*-H of N*Ph*); 7.40-7.49 (m, 2H, *o*-H of N*Ph*). ^{13}C{^{1}H}- NMR (128.5 MHz; C_6D_6; δ, ppm): 14.1 (s); 20.2 (s); 24.7 (s); 31.7 (s); 46.8 (s); 82.3 (s); 122.0 (s); 122.1 (s); 128.9 (s); 146.4 (s). ^{11}B{^{1}H}-NMR (160.5 MHz; C_6D_6; δ, ppm): 23.6 (br s, *B*Pin).

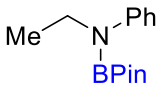

8k

>99% NMR yield. ^{1}H-NMR (500 MHz; C_6D_6; δ, ppm): 1.08 (br s, 12H, B*Pin*); 1.11 (t, J = 7.0 Hz, 3H, CH_3 of N*Et*); 3.60 (q, J = 7.0 Hz, 2H, CH_2 of N*Et*); 6.89 (t, J = 7.3 Hz, 1H, *p*-H of N*Ph*); 7.17-7.28 (m, 2H, *m*-H of N*Ph*); 7.43 (d, J = 7.8 Hz, 2H, *o*-H of N*Ph*). ^{13}C{^{1}H}- NMR (128.5 MHz; C_6D_6; δ, ppm): 15.6 (s); 24.7 (s); 42.0 (s); 82.6 (s); 121.5 (s); 121.8 (s); 129.0 (s); 146.4 (s). ^{11}B{^{1}H}-NMR (160.5 MHz; C_6D_6; δ, ppm): 23.7 (br s, *B*Pin). NMR data are consistent with those previously reported in the literature.[10b]

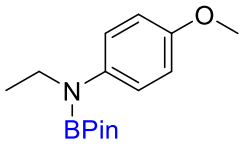

8l

>99% NMR yield. ^{1}H-NMR (500 MHz; C_6D_6; δ, ppm): 1.10 (s, 12H, B*Pin*); 1.12 (t, J = 7.0 Hz, 3H, CH_3 of N*Et*); 3.33 (s, 3H, O*Me*); 3.59 (q, J = 7.0 Hz, 2H, CH_2 of N*Et*); 6.80 (d, J = 9.0 Hz, 2H of C_6H_4); 7.28 (d, J = 9.0 Hz, 2H of C_6H_4). ^{13}C{^{1}H}-NMR (128.5 MHz; C_6D_6; δ, ppm): 15.7 (s); 24.8 (s); 42.9 (s); 55.0 (s); 82.4 (s); 114.4 (s); 124.2 (s); 139.4 (s); 155.7 (s). ^{11}B{^{1}H}-NMR (160.5 MHz; C_6D_6; δ, ppm): 23.6 (br s, *B*Pin).

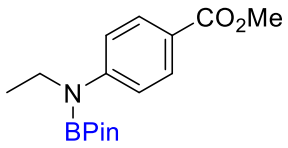

8m

>99% NMR yield. ^{1}H-NMR (500 MHz; C_6D_6; δ, ppm): 1.03 (s, 12H, B*Pin*); 1.05 (t, *J* = 7.0 Hz, 3H, *CH*$_3$ of N*Et*); 3.48 (q, *J* = 7.0 Hz, 2H, *CH*$_2$ of N*Et*); 3.53 (s, 3H, CO_2*Me*); 7.43 (d, *J* = 8.7 Hz, 2H of *C*$_6$*H*$_4$); 8.21 (d, *J* = 8.7 Hz, 2H of *C*$_6$*H*$_4$). ^{13}C{^{1}H}- NMR (128.5 MHz; C_6D_6; δ, ppm): 15.1 (s); 24.6 (s); 41.3 (s); 51.3 (s); 83.0 (s); 119.2 (s); 123.1 (s); 131.0 (s); 150.9 (s); 166.8 (s). ^{11}B{^{1}H}-NMR (160.5 MHz; C_6D_6; δ, ppm): 23.7 (br s, *B*Pin).

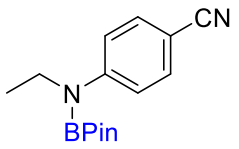

8n

69% NMR yield. **8n** was obtained in a mixture with EtN(BPin)$C_6H_4CH_2$N(BPin)$_2$ (25% by ^{1}H-NMR using 1,3,5-trimethoxybenzene as internal standard). ^{1}H-NMR (500 MHz; C_6D_6; δ, ppm): 0.94 (t, J = 7.0 Hz, 3H, *CH*$_3$ of N*Et*); 1.01 (s, 12H, B*Pin*); 3.34 (q, *J* = 7.0 Hz, 2H, *CH*$_2$ of N*Et*); 7.13-7.17 (m, 4H of *C*$_6$*H*$_4$). The corresponding 4-(ethylamino)benzonitrile has been previously reported.[16]

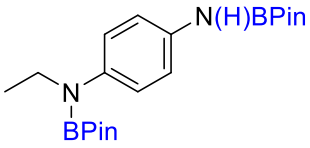

8o

81% NMR yield (with 9 equiv. of HBPin) in a mixture with unidentified products. ^{1}H-NMR (500 MHz; C_6D_6; δ, ppm): 1.01-1.06 (m, 27H, overlapping resonances of *CH*$_3$ groups of 2 N*BPin* and N*Et*); 3.46 (q, *J* = 7.1 Hz, 2H, *CH*$_2$ of N*Et*); 7.29 (d, *J* = 8.8 Hz, 2H of *C*$_6$*H*$_4$); 7.35 (d, *J* = 8.8 Hz, 2H of *C*$_6$*H*$_4$). ^{1}H-NMR (500 MHz; $CDCl_3$; δ, ppm): 1.15 (t, *J* = 7.0 Hz, 3H, *CH*$_3$ of N*Et*); 1.20-1.23 (br s, 24H, overlapping resonances of *CH*$_3$ groups of 2 N*BPin*); 3.47 (q, *J* = 7.0 Hz, 2H, *CH*$_2$ of N*Et*); 6.90 (d, *J* = 8.8 Hz, 2H of *C*$_6$*H*$_4$); 7.10 (d, *J* = 8.8 Hz, 2H of *C*$_6$*H*$_4$). ^{13}C{^{1}H}-NMR (128.5 MHz; C_6D_6; δ, ppm): 15.9 (s); 24.5 (s); 42.0 (s); 51.3 (s); 82.3 (s); 82.4 (s); 120.0 (s); 127.2 (s); 136.7 (s); 142.4 (s). ^{11}B{^{1}H}-NMR (160.5 MHz; C_6D_6; δ, ppm): 24.2 (very br s, 2 *B*Pin). Methanolysis of this reaction mixture resulted in the conversion of **8o** to 4-(ethylamino)aniline.[17]

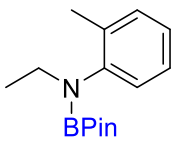

8p

76% NMR yield. ^{1}H-NMR (500 MHz; C_6D_6; δ, ppm): 1.04-1.11 (m, 15H, overlapping resonances of *CH*$_3$ groups of N*BPin* and N*Et*); 2.34 (s, 3H, *CH*$_3$ of *o*-*Tol*N); 3.46 (q, *J* = 7.1 Hz, 2H, *CH*$_2$ of N*Et*); 6.96 (t, *J* = 7.3 Hz, 1H of *o*-*Tol*N); 7.04 (t, *J* = 7.6 Hz, 1H of *o*-*Tol*N); 7.10 (d, *J* = 7.6 Hz, 1H of *o*-*Tol*N); 7.14-7.14 (m, 1H of *o*-*Tol*N overlapping with the residual resonance of C_6D_6). ^{13}C{^{1}H}-NMR (128.5 MHz; C_6D_6; δ, ppm): 15.8 (s); 18.5 (s); 24.8 (s); 45.0 (s); 51.3 (s); 82.3 (s); 125.5 (s); 126.7 (s); 129.1 (s); 131.0 (s); 136.1 (s);

144.8 (s). $^{11}B\{^{1}H\}$-NMR (160.5 MHz; C_6D_6; δ, ppm): 23.0 (br s, *B*Pin).

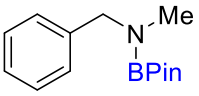

8q

98% NMR yield. ^{1}H-NMR (500 MHz; C_6D_6; δ, ppm): 1.15 (s, 12H, 4 *CH*$_3$ of N*BPin*); 2.58 (s, 3H, *CH*$_3$ of N*Me*); 4.15 (s, 2H, *CH*$_2$ of N*CH*$_2$Ph); 7.09 (t, *J* = 7.3 Hz, 1H, *p*-H of NCH$_2$*Ph*); 7.19 (t, *J* = 7.6 Hz, 2H, 2 *m*-H of NCH$_2$*Ph*); 7.26 (d, *J* = 7.4 Hz, 2H, 2 *o*-H of NCH$_2$*Ph*). $^{11}B\{^{1}H\}$-NMR (160.5 MHz; C_6D_6; δ, ppm): 23.6 (br s, *B*Pin). NMR data are consistent with those previously reported in the literature.[18]

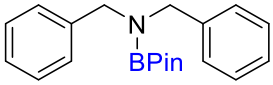

8r

>99% NMR yield. ^{1}H-NMR (500 MHz; C_6D_6; δ, ppm): 1.18 (s, 12H, 4 *CH*$_3$ of N*BPin*); 4.14 (s, 4H, 2 *CH*$_2$ of N(*CH*$_2$Ph)$_2$); 7.10 (t, *J* = 7.2 Hz, 2H, 2 *p*-H of N(CH$_2$*Ph*)$_2$); 7.19 (t, *J* = 7.5 Hz, 4H, 4 *m*-H of N(CH$_2$*Ph*)$_2$); 7.26 (d, *J* = 7.4 Hz, 4H, 4 *o*-H of N(CH$_2$*Ph*)$_2$). $^{11}B\{^{1}H\}$-NMR (160.5 MHz; C_6D_6; δ, ppm): 24.2 (br s, *B*Pin). NMR data are consistent with those previously reported in the literature.[12]

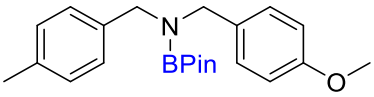

8t

>99% NMR yield. ^{1}H-NMR (500 MHz; C_6D_6; δ, ppm): 1.19 (s, 12H, 4 *CH*$_3$ of N*BPin*); 2.14 (s, 3H, *CH*$_3$ of *p-Tol*CH$_2$N); 3.33 (s, 3H, *CH*$_3$ of *p-MeO*C$_6$H$_4$CH$_2$N); 4.15 (s, 2H, *CH*$_2$ of N*CH*$_2$); 4.17 (s, 2H, *CH*$_2$ of N*CH*$_2$); 6.79-6.83 (m, 2H, *p-MeO*C$_6$H$_4$ / *p-Tol*); 7.04 (d, *J* = 7.7 Hz, 2H, *p-MeO*C$_6$H$_4$ / *p-Tol*); 7.22 (d, *J* = 8.6 Hz, *p-MeO*C$_6$H$_4$ / *p-Tol*); 7.24 (d, *J* = 7.7 Hz, 2H, *p-MeO*C$_6$H$_4$ / *p-Tol*). $^{13}C\{^{1}H\}$-NMR (128.5 MHz; C_6D_6; δ, ppm): 21.1 (s); 24.8 (s); 48.0 (s); 48.3 (s); 54.8 (s); 82.6 (s); 114.2 (s); 128.5 (s); 129.4 (s); 129.6 (s); 132.6 (s); 136.3 (s); 137.7 (s); 159.3 (s). $^{11}B\{^{1}H\}$-NMR (160.5 MHz; C_6D_6; δ, ppm): 24.4 (br s, *B*Pin).

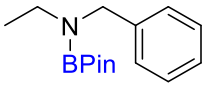

8u

97% NMR yield. ^{1}H-NMR (500 MHz; C_6D_6; δ, ppm): 0.98 (t, *J* = 7.1 Hz, 3H, *CH*$_3$ of N*Et*); 1.15 (s, 12H, 4 *CH*$_3$ of N*BPin*); 3.00 (q, *J* = 7.1 Hz, 2H, *CH*$_2$ of N*Et*); 4.22 (s, 2H, *CH*$_2$ of PhCH$_2$N); 7.09 (t, *J* = 7.3 Hz, 1H, *p*-H of *Ph*CH$_2$N); 7.19 (t, *J* = 7.6 Hz, 2H, 2 *m*-H of *Ph*CH$_2$N); 7.28-7.31 (m, 2H, 2 *o*-H of *Ph*CH$_2$N). $^{13}C\{^{1}H\}$-NMR (128.5 MHz; C_6D_6; δ, ppm): 15.1 (s); 24.8 (s); 39.9 (s); 49.4 (s); 82.3 (s); 126.9 (s); 128.6 (s); 141.5 (s). $^{11}B\{^{1}H\}$-NMR (160.5 MHz; C_6D_6; δ, ppm): 23.8 (br s, *B*Pin).

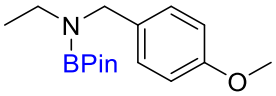

8v

98% NMR yield. ^{1}H-NMR (500 MHz; C_6D_6; δ, ppm): 1.02 (t, J = 7.1 Hz, 3H, CH_3 of N*Et*); 1.17 (s, 12H, 4 CH_3 of N*BPin*); 3.04 (q, J = 7.1 Hz, 2H, CH_2 of N*Et*); 3.34 (s, 3H, CH_3 of *p*-*MeO*$C_6H_4CH_2N$); 4.21 (s, 2H, CH_2 of PhCH_2N); 6.82 (d, J = 8.4 Hz, 2H of C_6H_4); 7.23 (d, J = 8.4 Hz, 2H of C_6H_4). ^{13}C{^{1}H}-NMR (128.5 MHz; C_6D_6; δ, ppm): 15.1 (s); 24.8 (s); 39.6 (s); 48.8 (s); 54.8 (s); 82.2 (s); 114.1 (s); 129.3 (s); 133.4 (s); 159.2 (s). ^{11}B{^{1}H}-NMR (160.5 MHz; C_6D_6; δ, ppm): 23.8 (br s, *B*Pin).

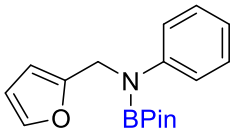

8w

97% NMR yield. ^{1}H-NMR (500 MHz; C_6D_6; δ, ppm): 1.07 (s, 12H, 4 CH_3 of N*BPin*); 4.70 (s, 2H, CH_2 of CH_2N); 5.97-6.10 (m, 2H, 2-*furyl group*); 6.84 (t, J = 7.3 Hz, 1H, *p*-H of N*Ph*); 7.04 (br s, 1H, 2-*furyl group*); 7.11-7.16 (m, 2H, 2 *m*-H of N*Ph*); 7.49 (d, J = 7.8 Hz, 2H, 2 *o*-H of N*Ph*). ^{13}C{^{1}H}-NMR (128.5 MHz; C_6D_6; δ, ppm): 24.6 (s); 45.3 (s); 83.1 (s); 106.7 (s); 110.6 (s); 121.3 (s); 122.1 (s); 128.9 (s); 141.5 (s); 146.6 (s); 154.8 (s). ^{11}B{^{1}H}-NMR (160.5 MHz; C_6D_6; δ, ppm): 24.0 (br s, *B*Pin). NMR data are consistent with those previously reported in the literature.[19]

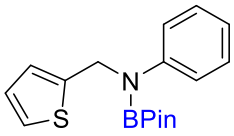

8x

97% NMR yield. ^{1}H-NMR (500 MHz; C_6D_6; δ, ppm): 1.10 (s, 12H, 4 CH_3 of N*BPin*); 4.84 (s, 2H, CH_2 of CH_2N); 5.65-6.68 (m, 1H, *2-thienyl group*); 6.73-6.75 (m, 1H, *2-thienyl group*); 6.78-6.80 (m, 1H, *2-thienyl group*); 6.82 (t, J = 7.4 Hz, 1H, *p*-H of N*Ph*); 7.11 (t, J = 7.9 Hz, 2H, 2 *m*-H of N*Ph*); 7.49 (d, J = 8.4 Hz, 2H, 2 *o*-H of N*Ph*). ^{13}C{^{1}H}-NMR (128.5 MHz; C_6D_6; δ, ppm): 24.7 (s); 47.2 (s); 83.2 (s); 121.6 (s); 122.3 (s); 124.1 (s); 124.4 (s); 126.8 (s); 128.9 (s); 145.4 (s); 146.3 (s). ^{11}B{^{1}H}-NMR (160.5 MHz; C_6D_6; δ, ppm): 24.0 (br s, *B*Pin). NMR data are consistent with those previously reported in the literature.[19]

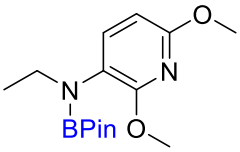

8y

88% NMR yield. ^{1}H-NMR (500 MHz; C_6D_6; δ, ppm): 1.05 (t, J = 7.1 Hz, 3H, CH_3 of N*Et*); 1.11 (s, 12H, 4 CH_3 of N*BPin*); 3.53 (q, J = 7.1 Hz, 2H, CH_2 of N*Et*); 3.63 (s, 3H, O*Me*); 3.72 (s, 3H, O*Me*); 6.27 (d, J = 8.1 Hz, 1H, *Py*); 7.24 (d, J = 8.1 Hz, 1H, *Py*). ^{13}C{^{1}H}-NMR (128.5 MHz; C_6D_6; δ, ppm): 15.8 (s); 24.8 (s); 43.6 (s); 53.0 (s); 53.1 (s); 83.1 (s); 101.2 (s); 121.0 (s); 141.2 (s); 158.9 (s); 160.3 (s). ^{11}B{^{1}H}-NMR (160.5 MHz; C_6D_6; δ, ppm): 23.4 (br s, *B*Pin).

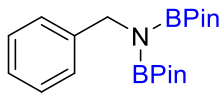

10a

96% NMR yield. ^{1}H-NMR (500 MHz; C_6D_6; δ, ppm): 1.03 (s, 24 H, 8 *CH*$_3$ of 2 NB*Pin*); 4.61 (s, 2 H, *CH*$_2$ of Ph*CH*$_2$N); 7.10 (t, *J* = 7.4 Hz, 1H, *p*-H of *Ph*CH$_2$N); 7.23 (t, *J* = 7.7 Hz, 2H, 2 *m*-H of *Ph*CH$_2$N); 7.54 (d, *J* = 7.5 Hz, 2H, 2 *o*-H of *Ph*CH$_2$N). NMR data are consistent with those previously reported in the literature.[12,13]

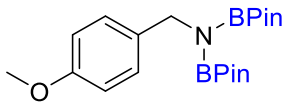

10b

84% NMR yield. ^{1}H-NMR (500 MHz; C_6D_6; δ, ppm): 1.05 (s, 24 H, 8 *CH*$_3$ of 2 NB*Pin*); 3.36 (s, 3H, CH$_3$ of *p*-*MeO*C$_6$H$_4$CH$_2$N); 4.54 (s, 2H, CH$_2$ of *p*-MeOC$_6$H$_4$*CH*$_2$N); 6.85 (d, *J* = 8.5 Hz, 2H of *p*-MeO*C*$_6$*H*$_4$CH$_2$N); 7.54 (d, *J* = 8.5 Hz, 2H of *p*-MeO*C*$_6$*H*$_4$CH$_2$N). NMR data are consistent with those previously reported in the literature.[12,13]

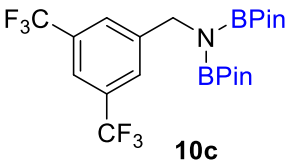

10c

63% NMR yield. ^{1}H-NMR (500 MHz; C_6D_6; δ, ppm): 1.01 (s, 24 H, 8 *CH*$_3$ of 2 NB*Pin*); 4.29 (s, 2H, CH$_2$ of *p*-MeOC$_6$H$_4$*CH*$_2$N); 7.70 (s, 1H, *aromatic*); 7.97 (br s, 2H, *aromatic*). ^{19}F{^{1}H}-NMR (471 MHz; C_6D_6; δ, ppm): -62.63 (s, 2 *CF*$_3$).

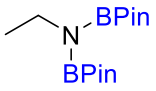

10d

93% NMR yield. ^{1}H-NMR (500 MHz; C_6H_6; δ, ppm): 1.07 (br s, 24H, 8 *CH*$_3$ of 2 NB*Pin*); 1.31 (br t, *J* = 7.0 Hz, 3H, *CH*$_3$ of N*Et*); 3.46 (br q, *J* = 7.0 Hz, *CH*$_2$ of N*Et*). NMR data are consistent with those previously reported in the literature.[20]

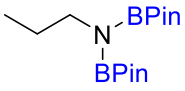

10e

86% NMR yield. ^{1}H-NMR (500 MHz; C_6H_6; δ, ppm): 0.94-0.97 (m, 3H, *CH*$_3$CH$_2$CH$_2$N); 1.07 (br s, 24 H, 8 *CH*$_3$ of 2 NB*Pin*); 1.71-1.80 (m, 2H, CH$_3$*CH*$_2$CH$_2$N); 3.41 (t, *J* = 7.2 Hz, 2H, CH$_3$CH$_2$*CH*$_2$N). NMR data are consistent with those previously reported in the literature.[13,21]

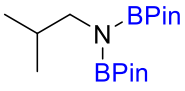

10f

73% NMR yield. ^{1}H-NMR (500 MHz; C_6D_6; δ, ppm): 1.02 (resonance partially overlaps with the resonance for (Pin)$_2$O, 6H, 2 *CH*$_3$ of NCH$_2$^{i}*Pr*); 2.02 (m, 1H, CH of NCH$_2$^{i}*Pr*); 3.25 (d, J = 6.9 Hz, 2 H, *CH*$_2$ of N*CH*$_2$^{i}Pr). NMR data are consistent with those previously reported in the literature.[21]

6. NMR spectra of deoxygenative hydroboration products

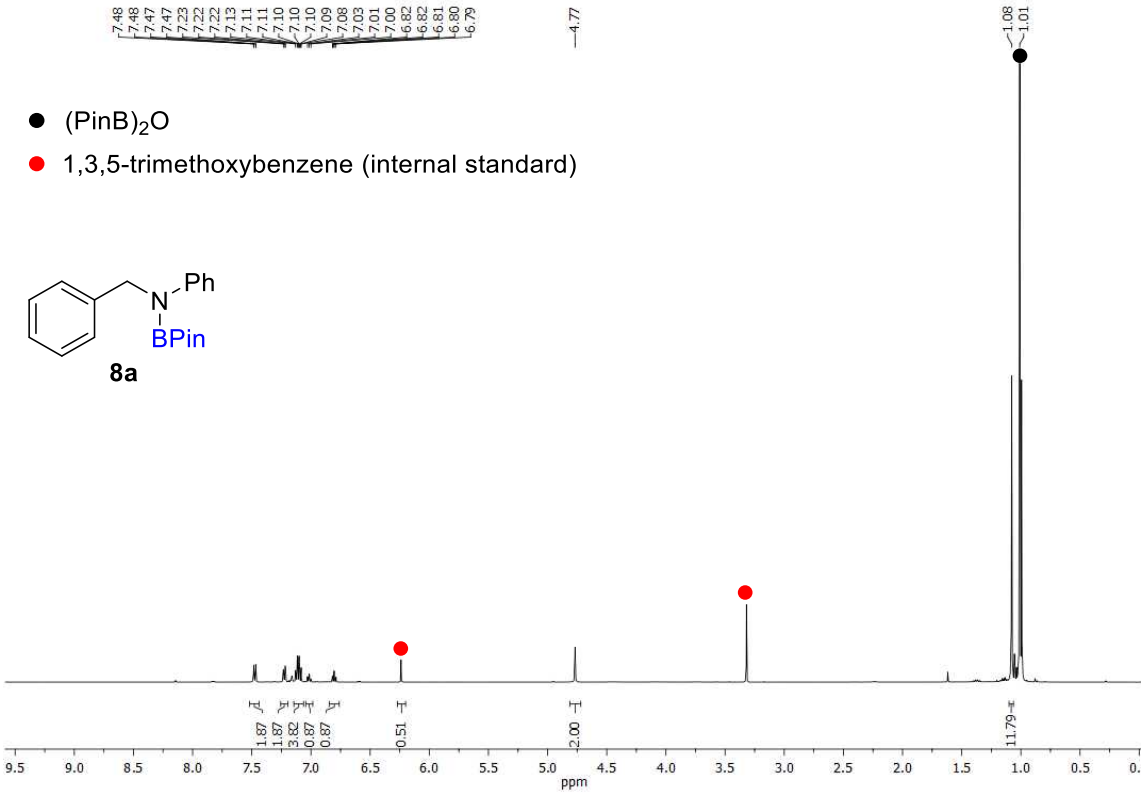

Figure 40. ^{1}H-NMR spectrum of **8a** taken directly from the reaction mixture upon **6-H**-catalyzed hydroboration of *N*-phenylbanzamide with HBPin in C_6D_6.

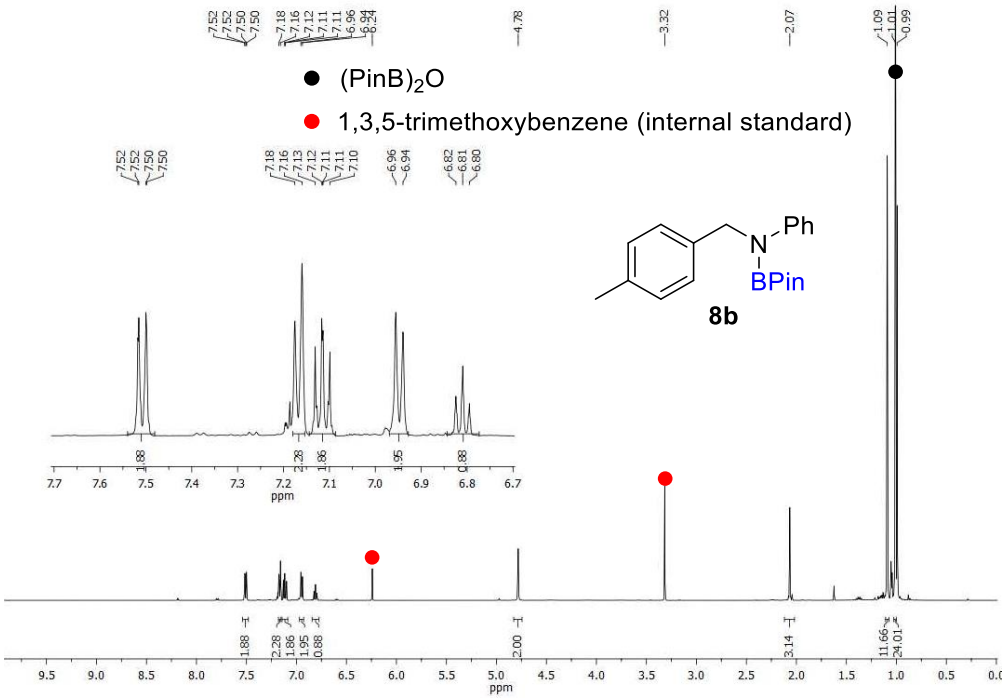

Figure 41. ^{1}H-NMR spectrum of **8b** taken directly from the reaction mixture upon **6-H**-catalyzed hydroboration of 4-methyl-*N*-phenylbenzamide with HBPin in C_6D_6.

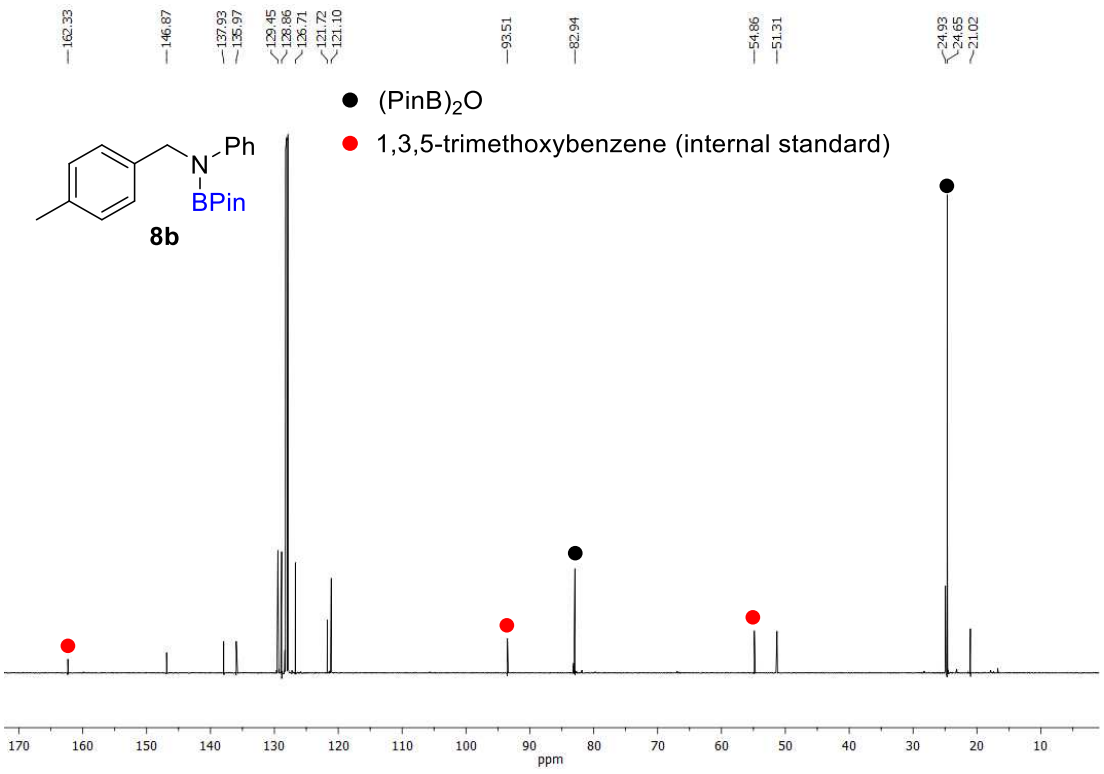

Figure 42. $^{13}C\{^{1}H\}$-NMR spectrum of **8b** taken directly from the reaction mixture upon **6-H**-catalyzed hydroboration of 4-methyl-*N*-phenylbenzamide with HBPin.

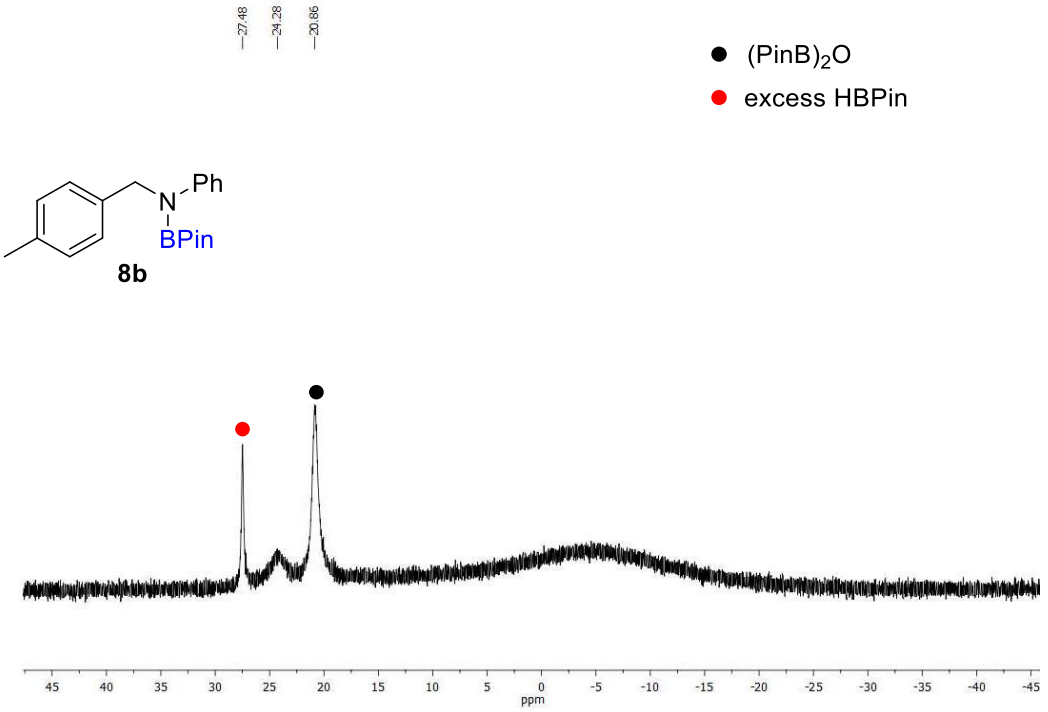

Figure 43. $^{11}B\{^{1}H\}$-NMR spectrum of **8b** taken directly from the reaction mixture upon **6-H**-catalyzed hydroboration of 4-methyl-*N*-phenylbenzamide with HBPin.

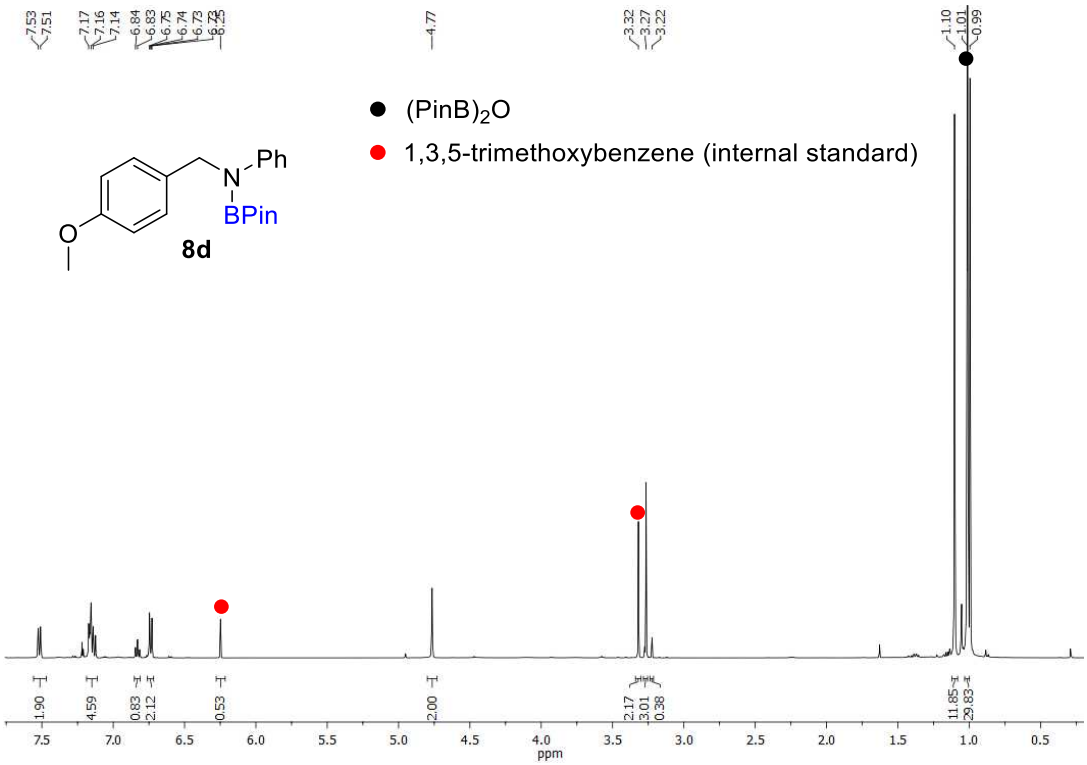

Figure 44. ^{1}H-NMR spectrum of **8d** taken directly from the reaction mixture upon **6-H**-catalyzed hydroboration of 4-methoxy-*N*-phenylbenzamide with HBPin in C_6D_6.

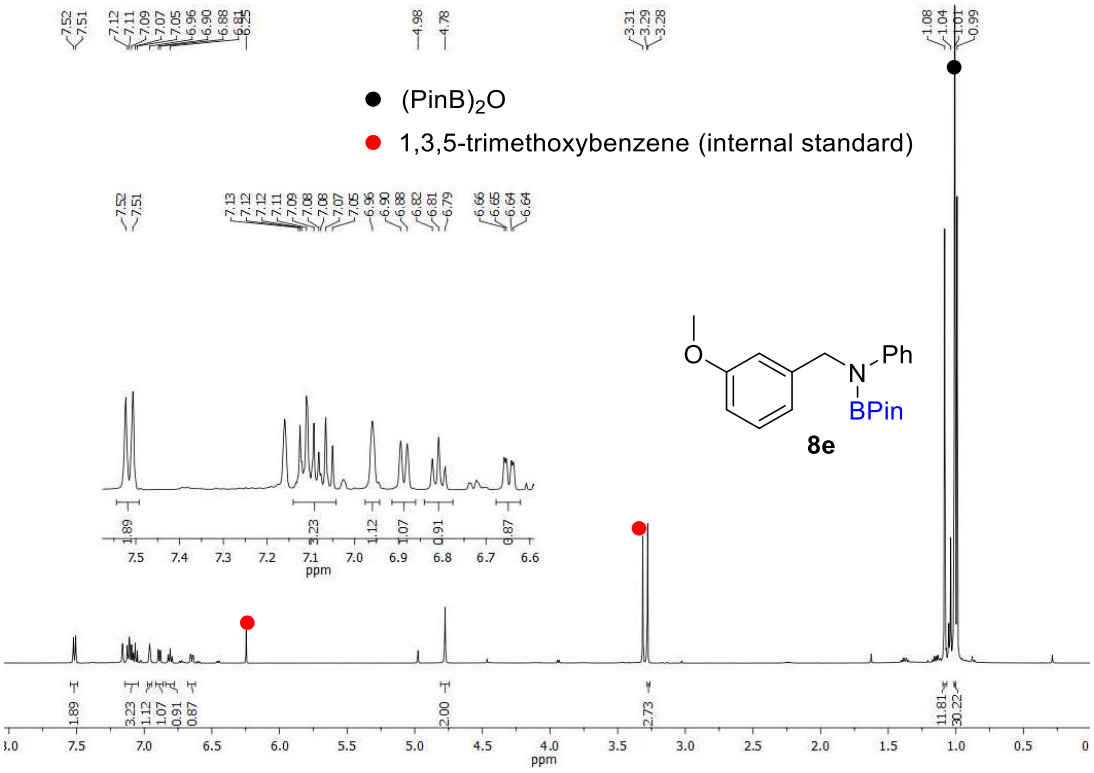

Figure 45. ^{1}H-NMR spectrum of **8e** taken directly from the reaction mixture upon **6-H**-catalyzed hydroboration of 3-methoxy-*N*-phenylbenzamide with HBPin in C_6D_6.

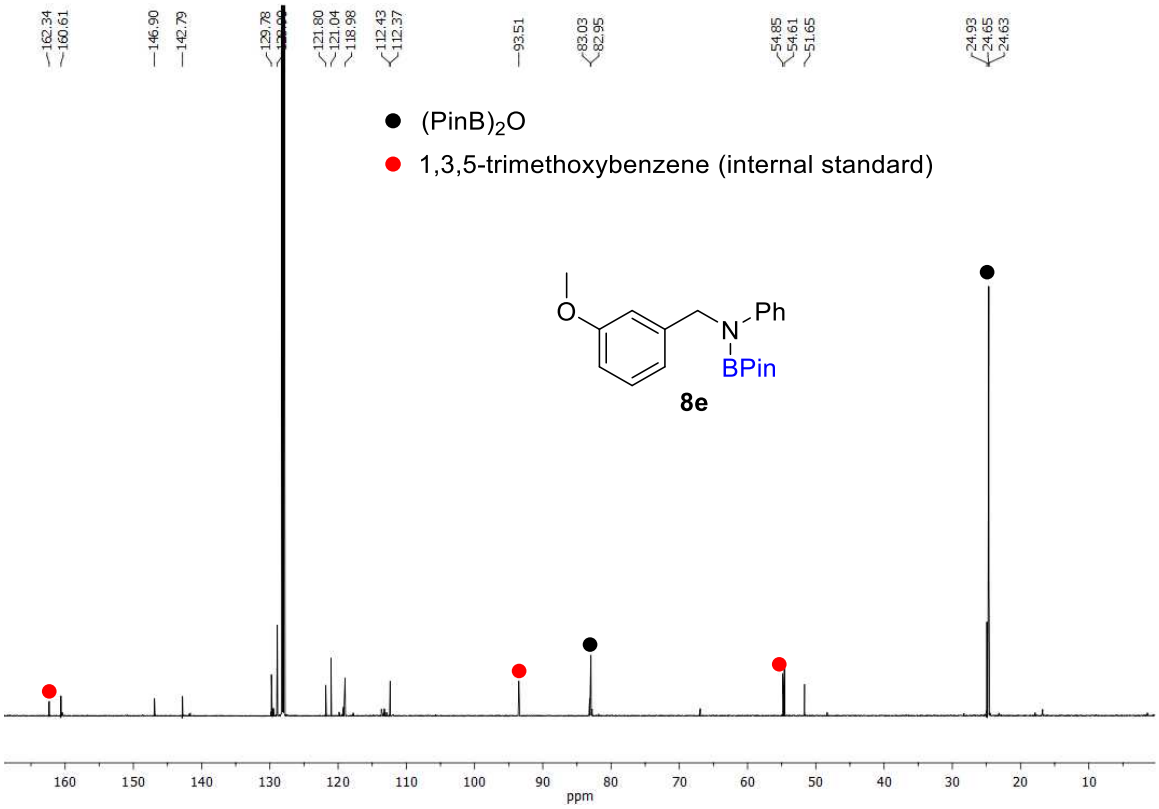

Figure 46. $^{13}C\{^{1}H\}$-NMR spectrum of **8e** taken directly from the reaction mixture upon **6-H**-catalyzed hydroboration of 3-methoxy-*N*-phenylbenzamide with HBPin in C_6D_6.

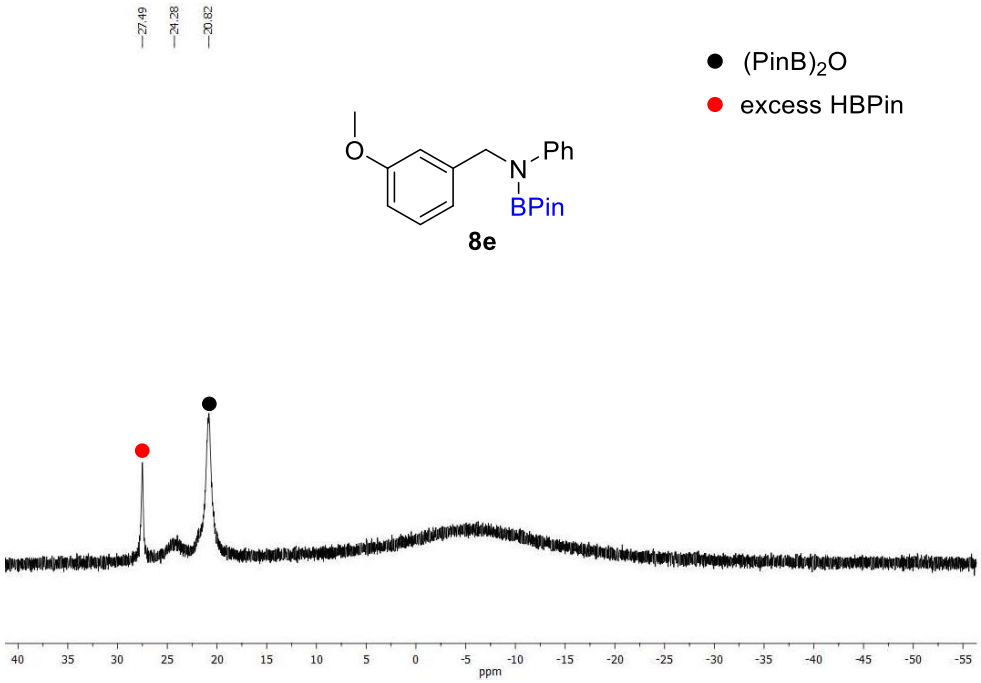

Figure 47. $^{11}B\{^{1}H\}$-NMR spectrum of **8e** taken directly from the reaction mixture upon **6-H**-catalyzed hydroboration of 3-methoxy-*N*-phenylbenzamide with HBPin in C_6D_6.

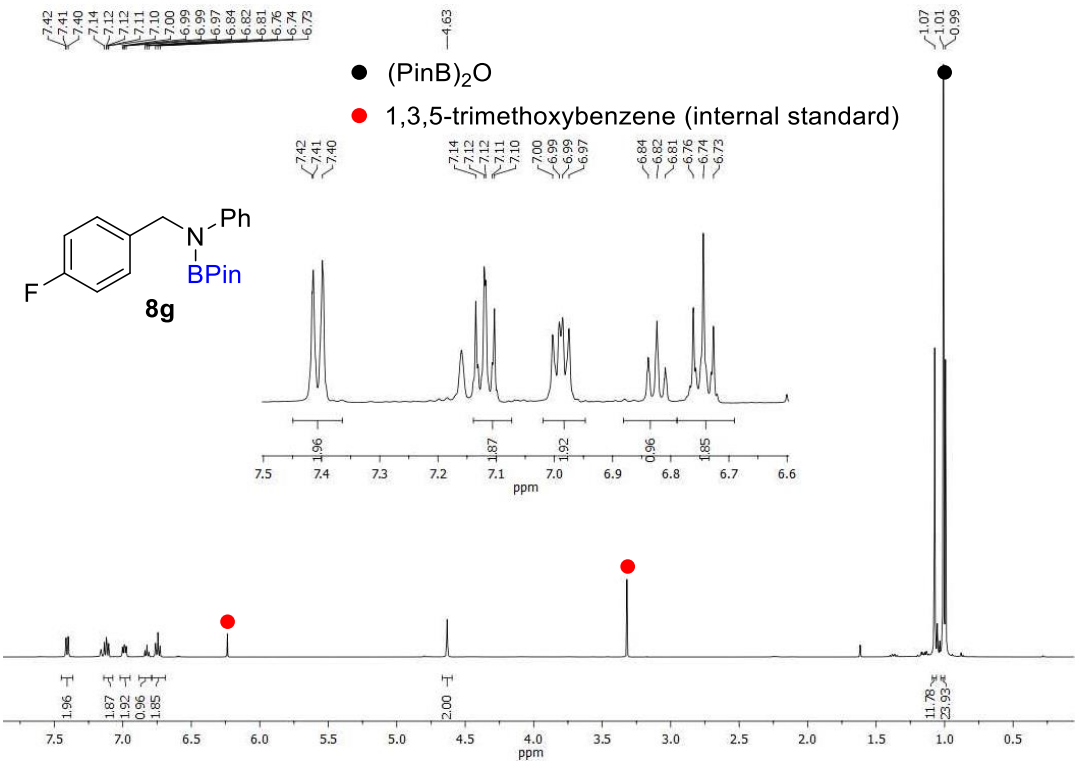

Figure 48. ^{1}H-NMR spectrum of **8g** taken directly from the reaction mixture upon **6-H**-catalyzed hydroboration of 4-fluoro-*N*-phenylbenzamide with HBPin in C_6D_6.

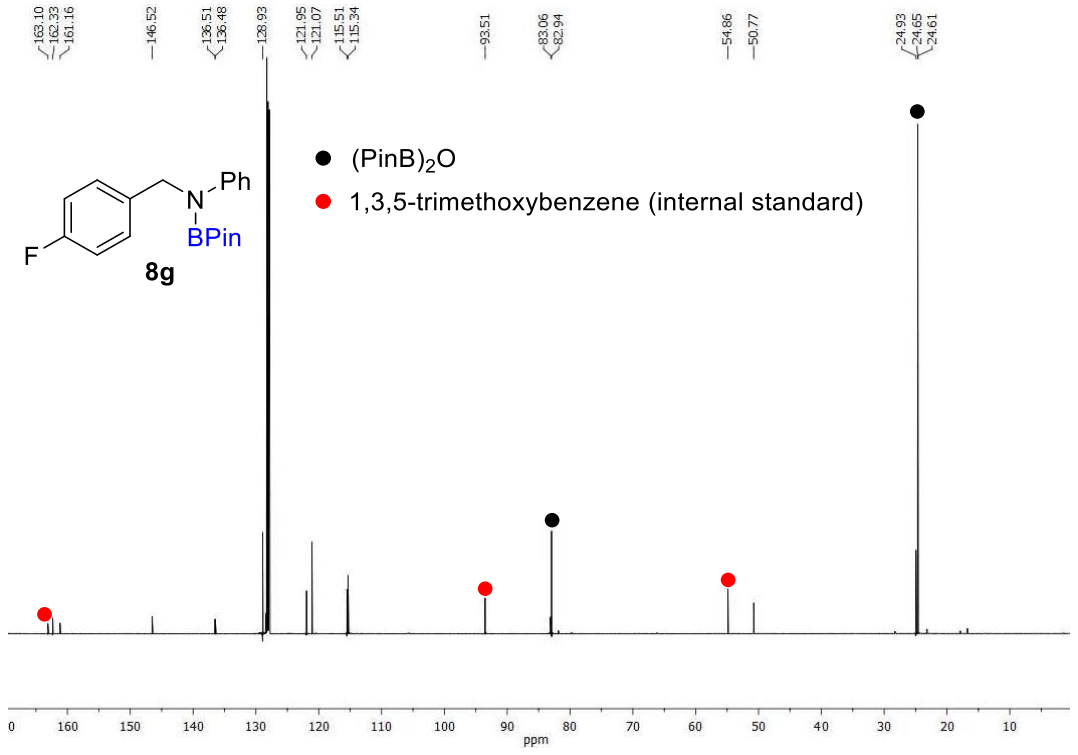

Figure 49. ^{13}C{^{1}H}-NMR spectrum of **8g** taken directly from the reaction mixture upon **6-H**-catalyzed hydroboration of 4-fluoro-*N*-phenylbenzamide with HBPin in C_6D_6

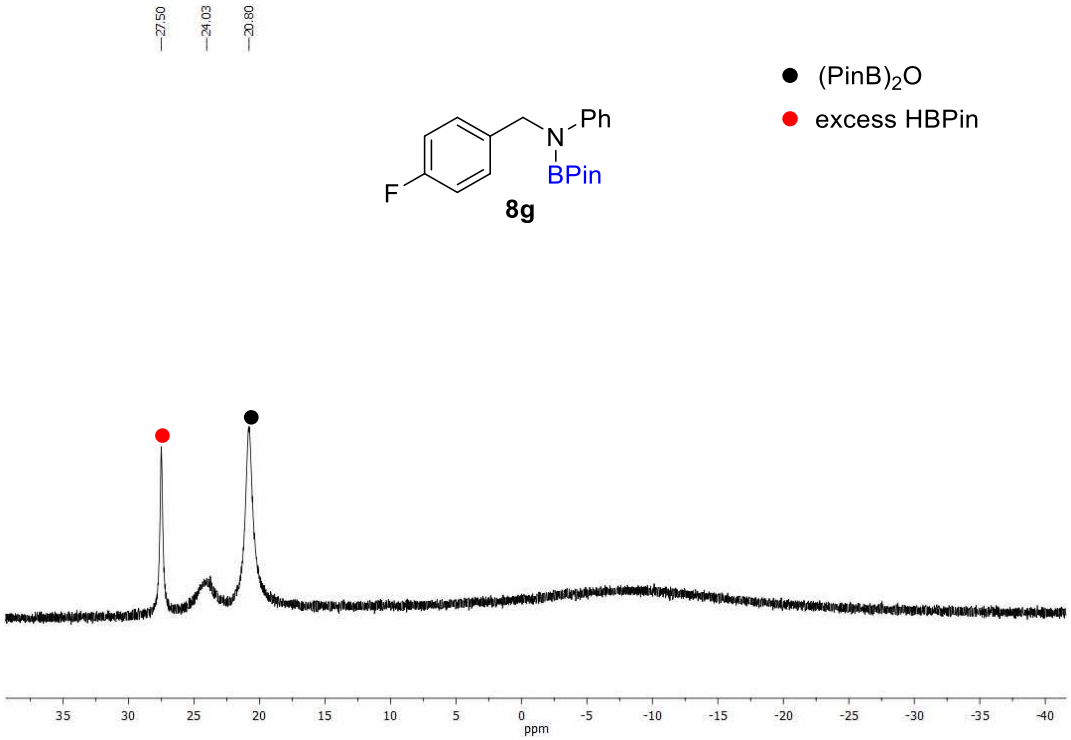

Figure 50. $^{11}B\{^{1}H\}$-NMR spectrum of **8g** taken directly from the reaction mixture upon **6-H**-catalyzed hydroboration of 4-fluoro-*N*-phenylbenzamide with HBPin in C_6D_6

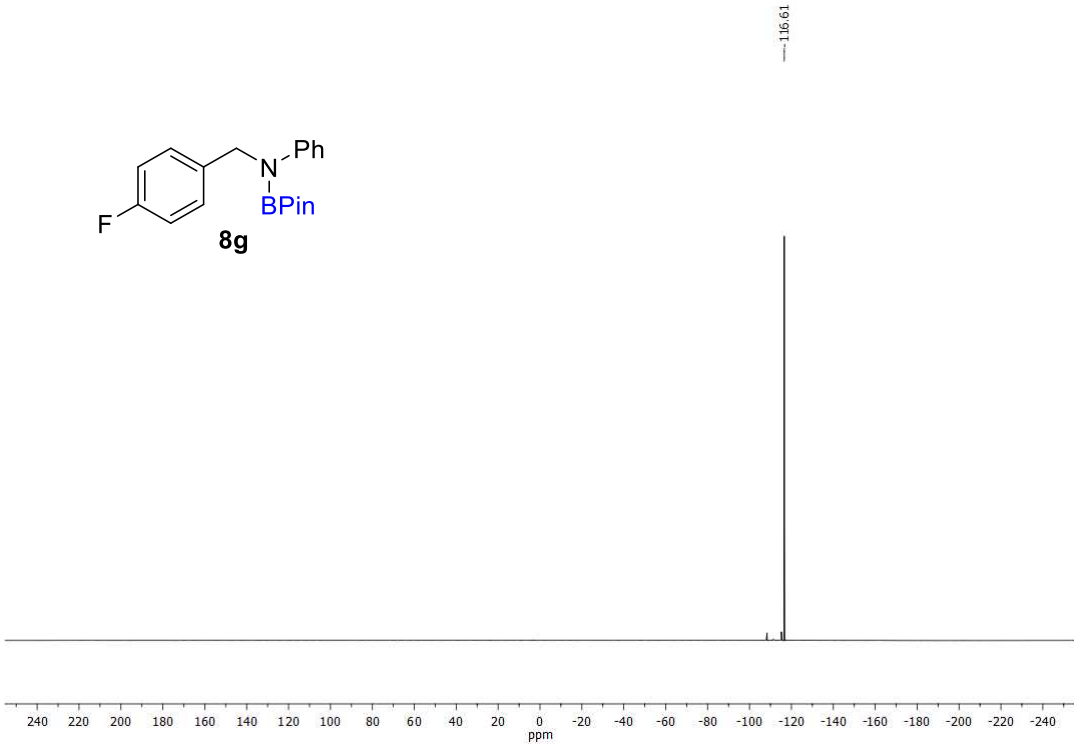

Figure 51. $^{19}F\{^{1}H\}$-NMR spectrum of **8g** taken directly from the reaction mixture upon **6-H**-catalyzed hydroboration of 4-fluoro-*N*-phenylbenzamide with HBPin in C_6D_6

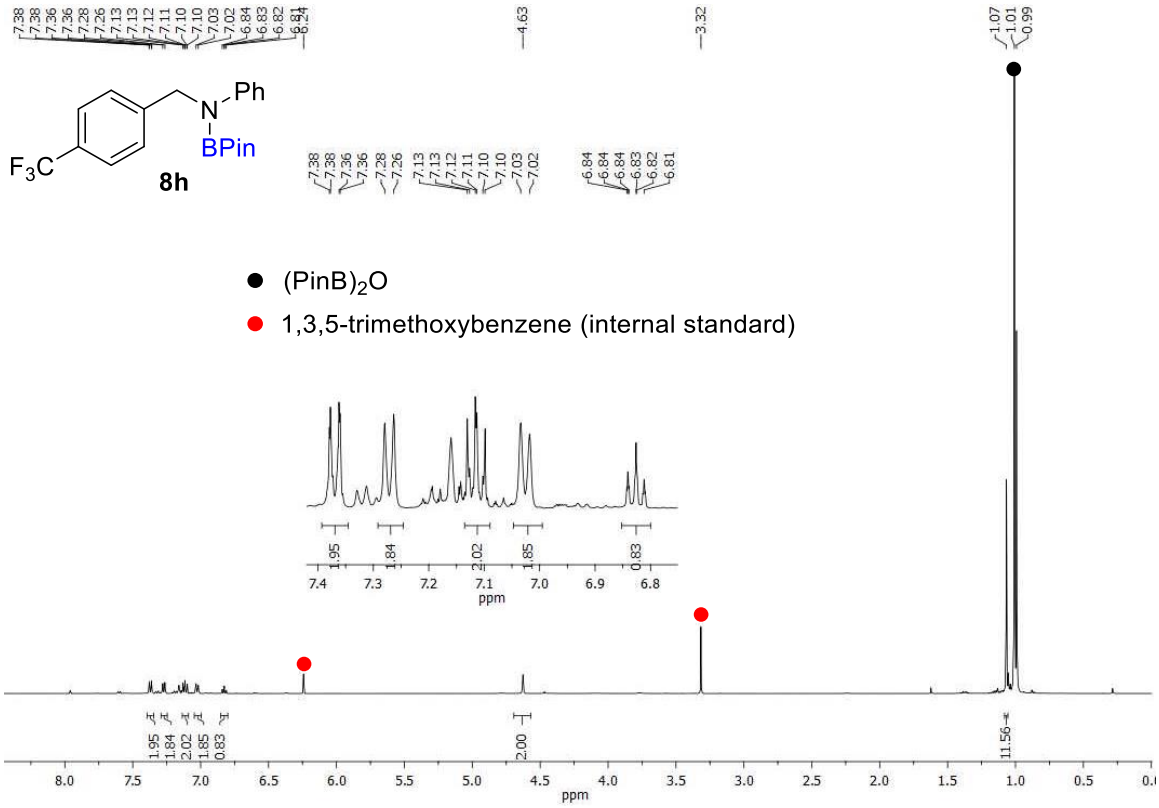

Figure 52. ^{1}H-NMR spectrum of **8h** taken directly from the reaction mixture upon **6-H**-catalyzed hydroboration of 4-(trifluoromethyl)-*N*-phenylbenzamidewith with HBPin in C_6D_6.

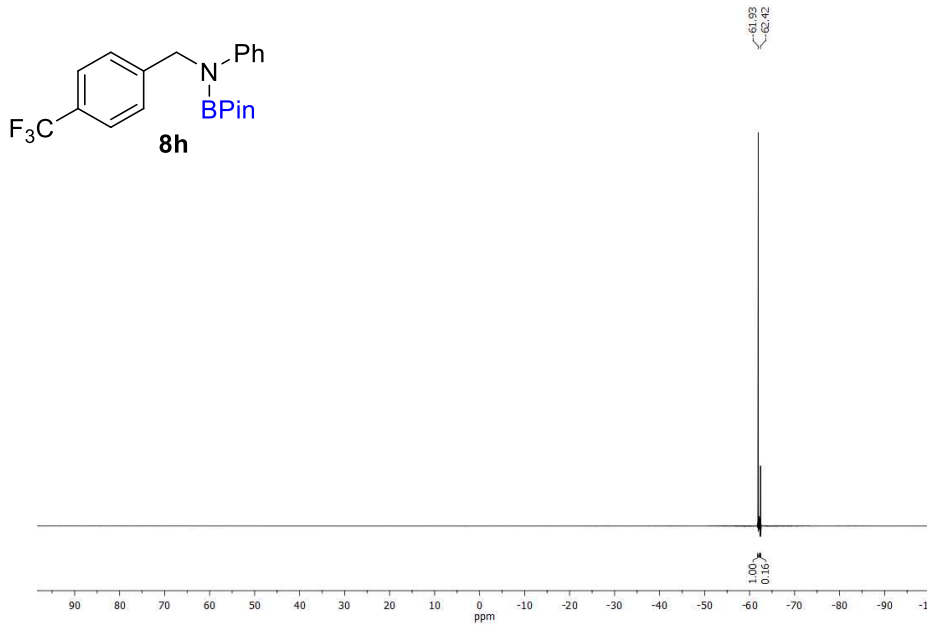

Figure 53. ^{19}F{^{1}H}-NMR spectrum of **8h** taken directly from the reaction mixture upon **6-H**-catalyzed hydroboration of 4-(trifluoromethyl)-*N*-phenylbenzamidewith with HBPin in C_6D_6.

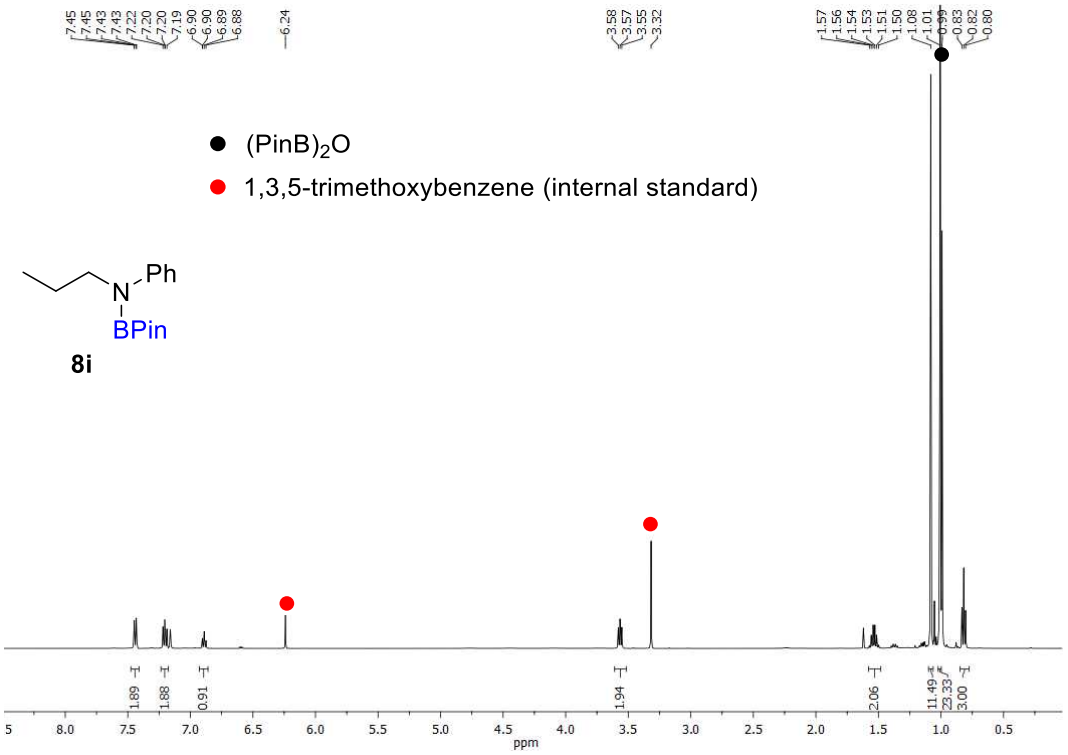

Figure 54. ^{1}H-NMR spectrum of **8i** taken directly from the reaction mixture upon **6-H**-catalyzed hydroboration of *N*-phenylpropanamide with HBPin in C_6D_6.

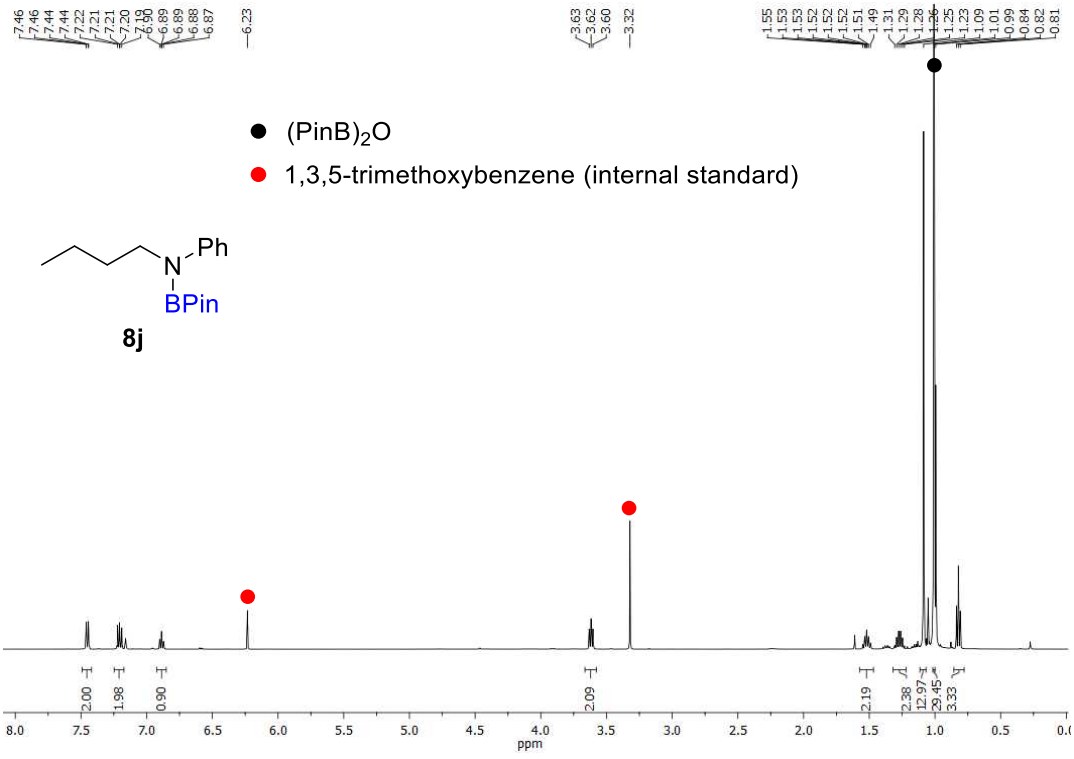

Figure 55. ^{1}H-NMR spectrum of **8j** taken directly from the reaction mixture upon **6-H**-catalyzed hydroboration of *N*-phenylbutananamide with HBPin in C_6D_6.

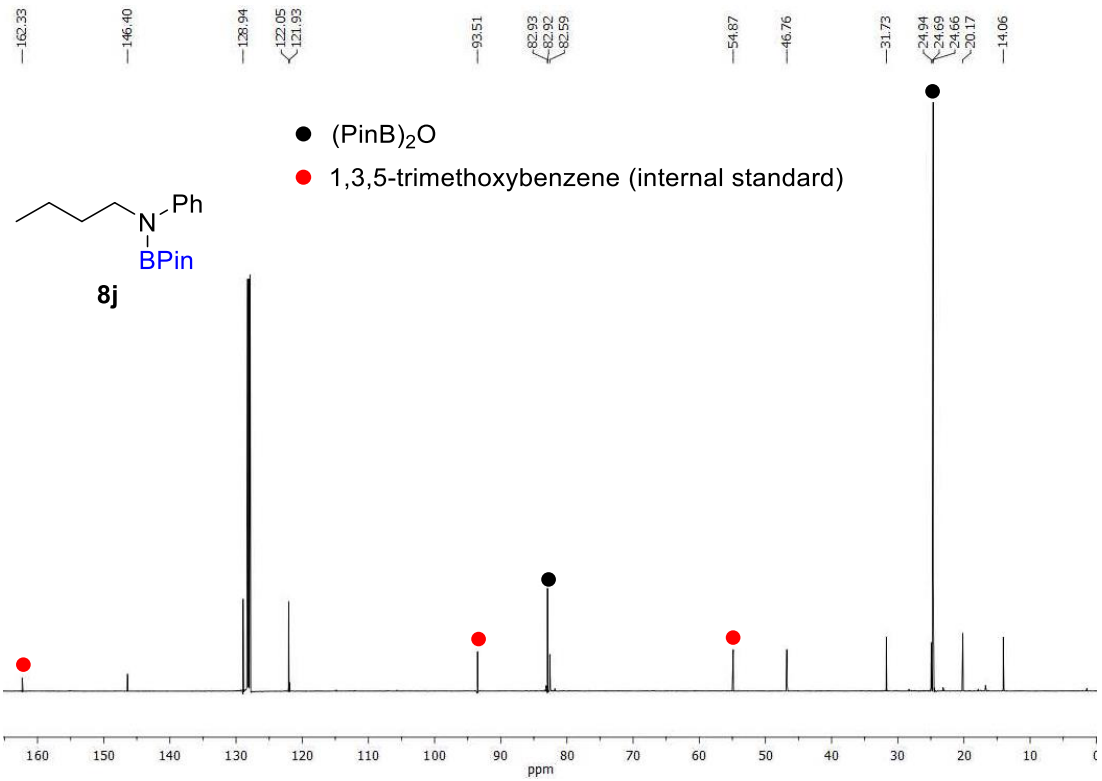

Figure 56. $^{13}C\{^{1}H\}$-NMR spectrum of **8j** taken directly from the reaction mixture upon **6-H**-catalyzed hydroboration of *N*-phenylbutananamide with HBPin in C_6D_6.

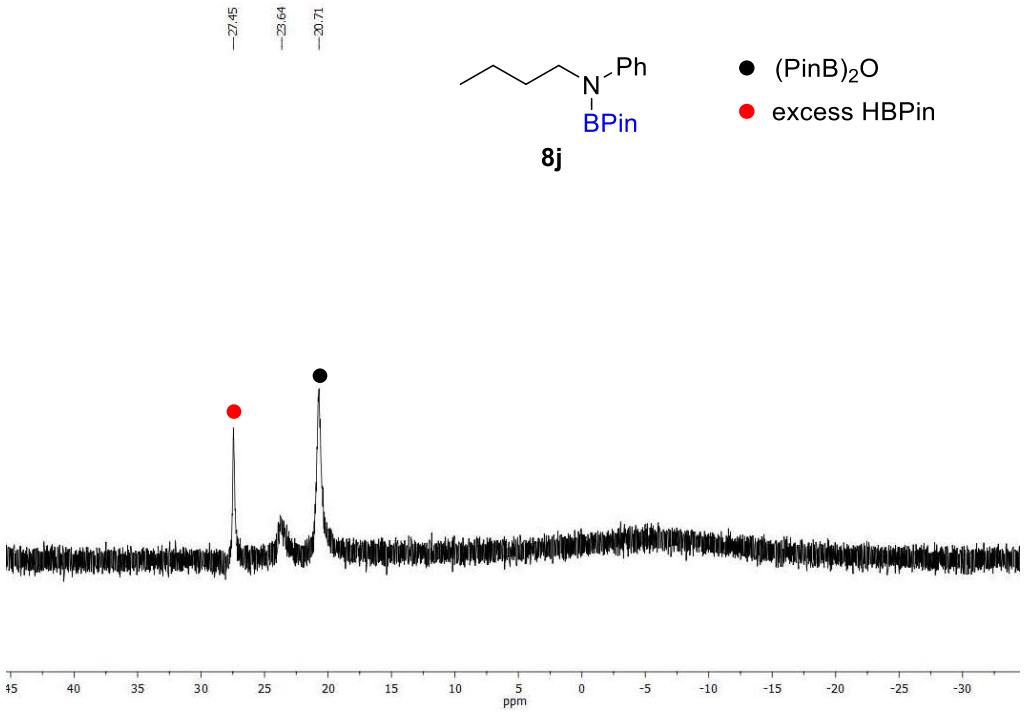

Figure 57. $^{11}B\{^{1}H\}$-NMR spectrum of **8j** taken directly from the reaction mixture upon **6-H**-catalyzed hydroboration of *N*-phenylbutananamide with HBPin in C_6D_6.

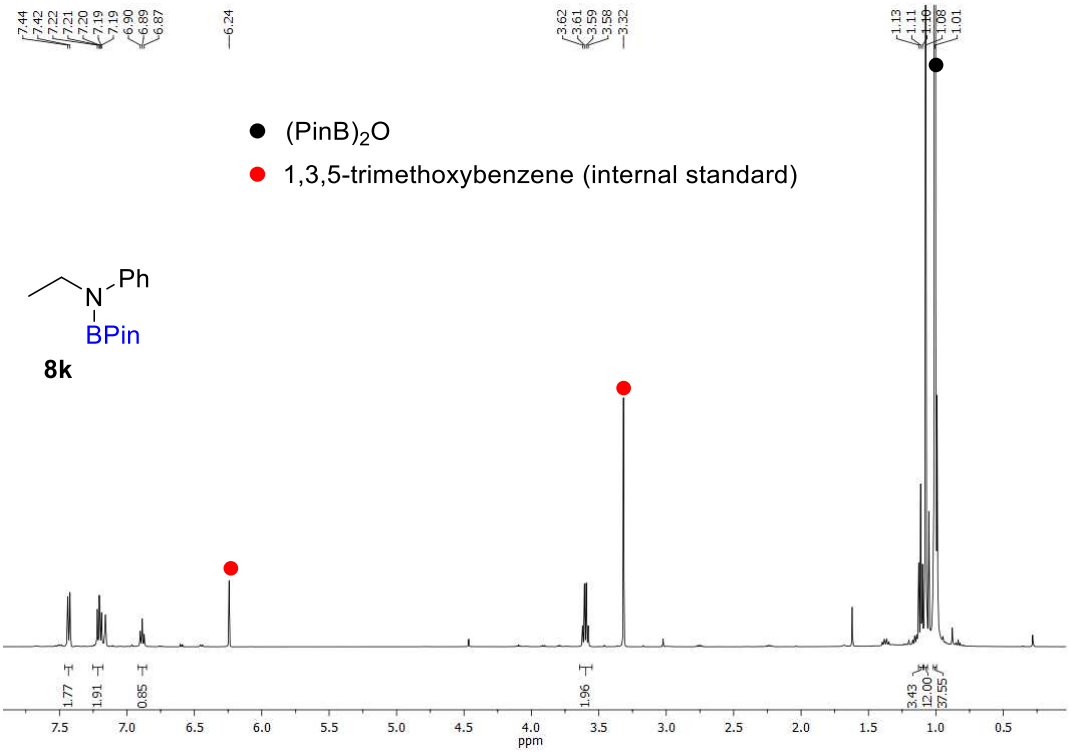

Figure 58. ^{1}H-NMR spectrum of **8k** taken directly from the reaction mixture upon **6-H**-catalyzed hydroboration of *N*-phenylacetamide with HBPin in C_6D_6.

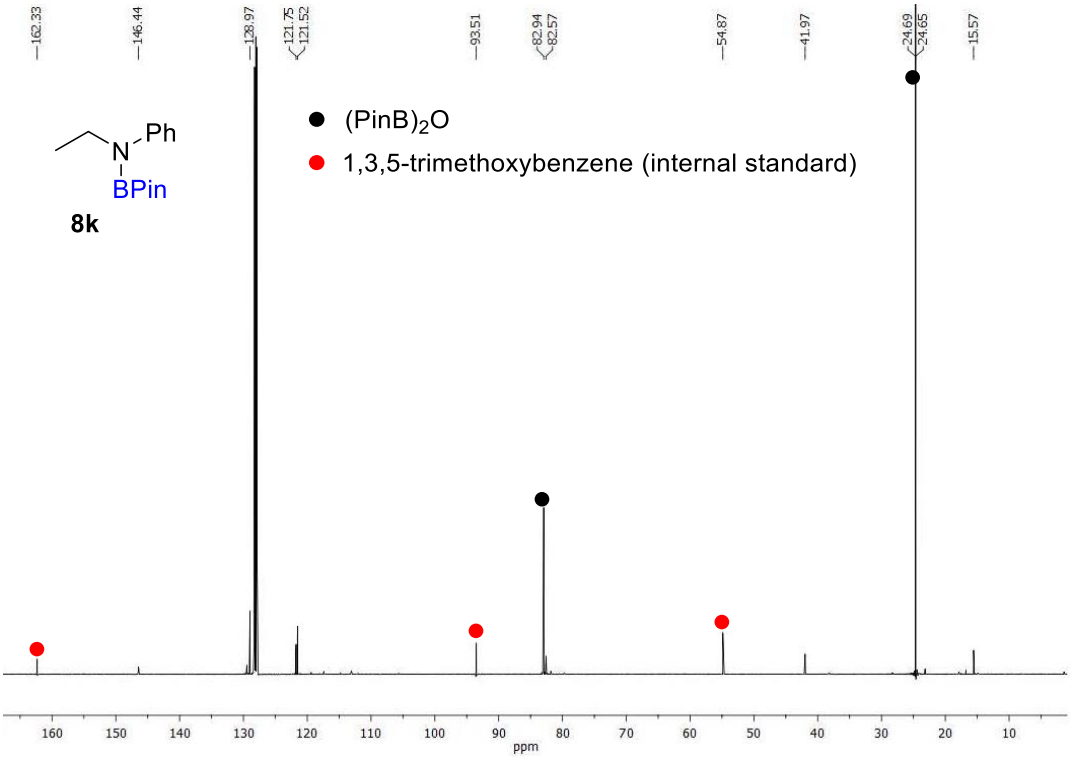

Figure 59. ^{13}C{^{1}H}-NMR spectrum of **8k** taken directly from the reaction mixture upon **6-H**-catalyzed hydroboration of *N*-phenylacetamide with HBPin in C_6D_6.

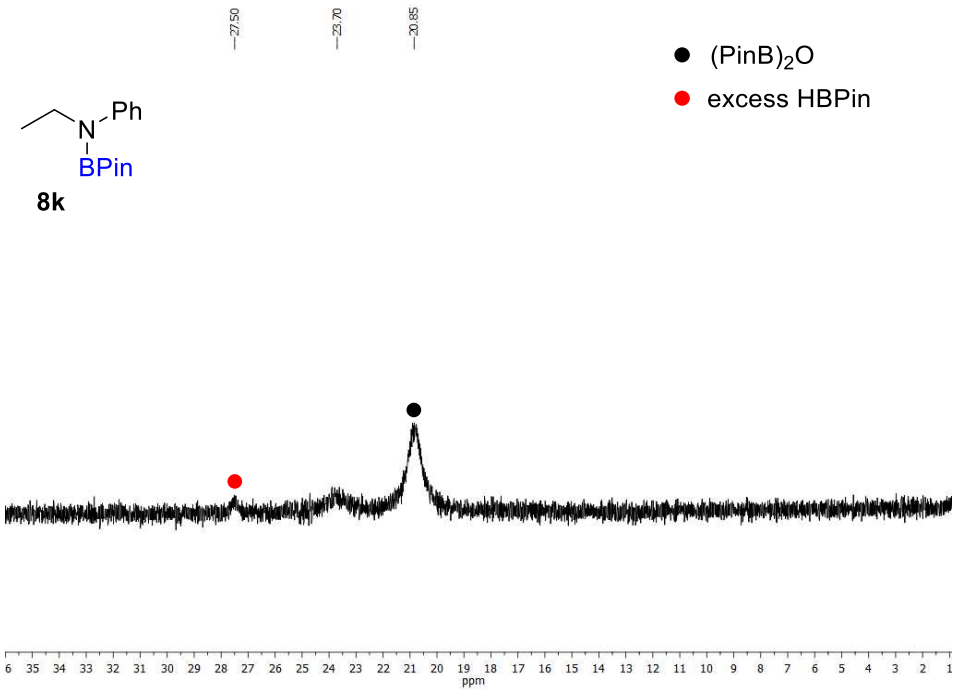

Figure 60. $^{11}B\{^{1}H\}$-NMR spectrum of **8k** taken directly from the reaction mixture upon **6-H**-catalyzed hydroboration of *N*-phenylacetamide with HBPin in C_6D_6.

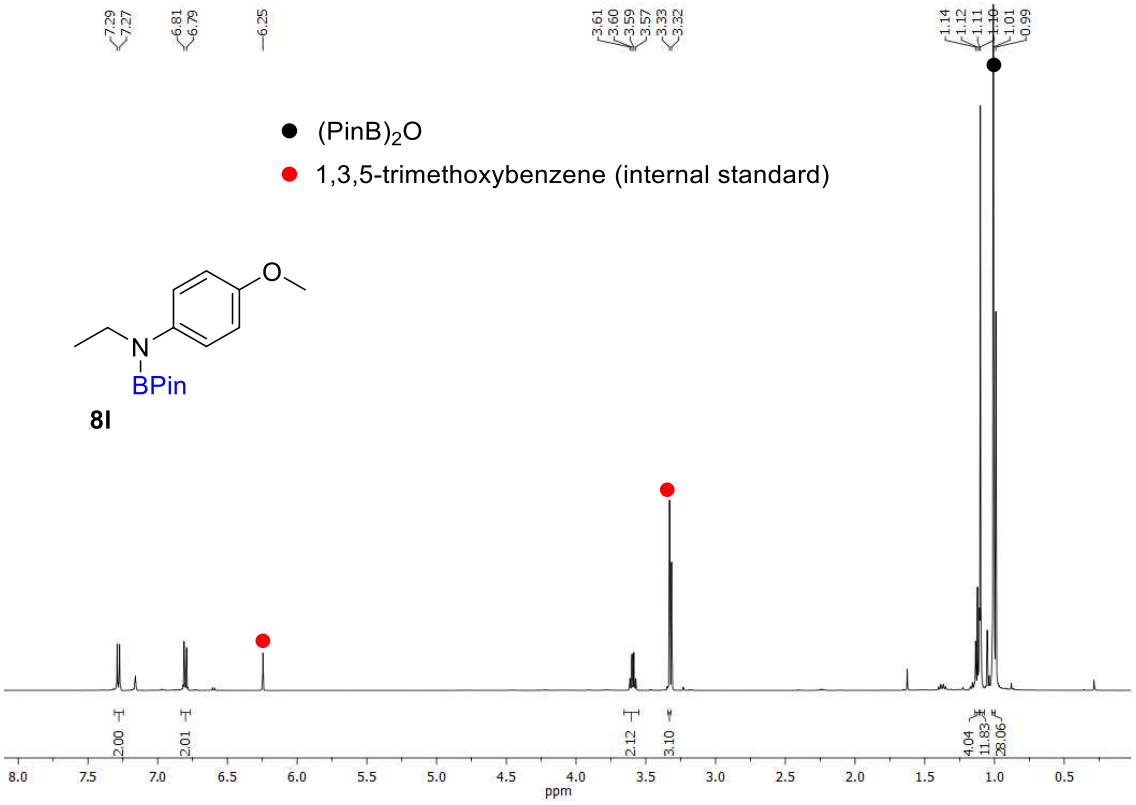

Figure 61. ^{1}H-NMR spectrum of **8l** taken directly from the reaction mixture upon **6-H**-catalyzed hydroboration of *N*-(4-methoxyphenyl)acetamide with HBPin in C_6D_6.

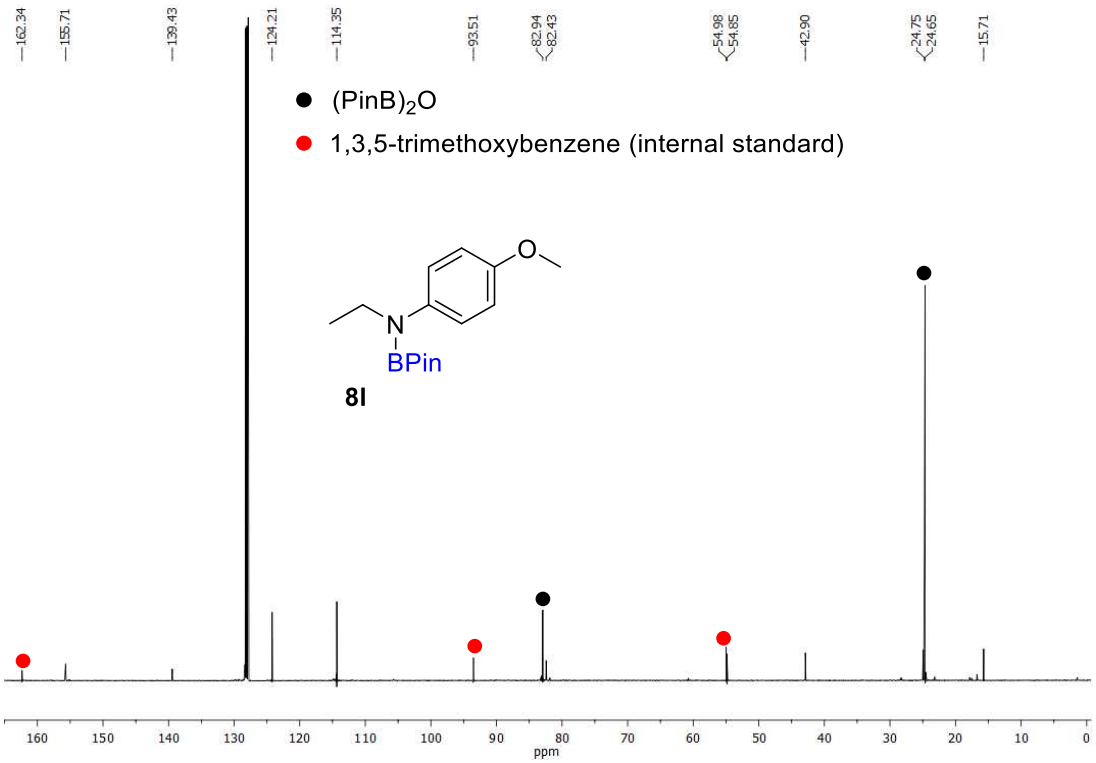

Figure 62. $^{13}C\{^{1}H\}$-NMR spectrum of **8l** taken directly from the reaction mixture upon **6-H**-catalyzed hydroboration of *N*-(4-methoxyphenyl)acetamide with HBPin in C_6D_6.

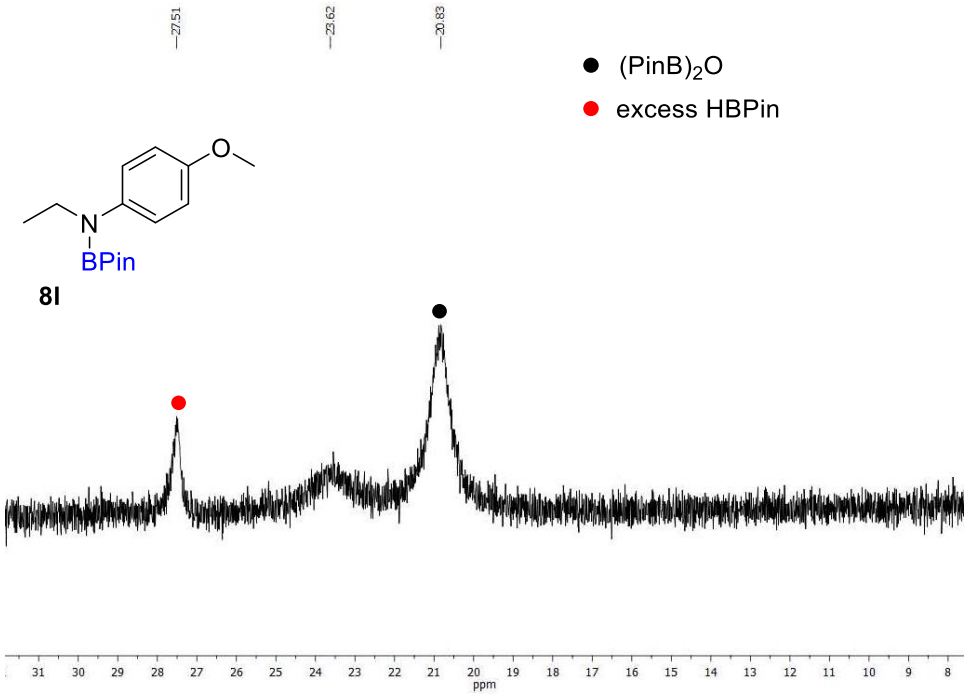

Figure 63. $^{11}B\{^{1}H\}$-NMR spectrum of **8l** taken directly from the reaction mixture upon **6-H**-catalyzed hydroboration of *N*-(4-methoxyphenyl)acetamide with HBPin in C_6D_6.

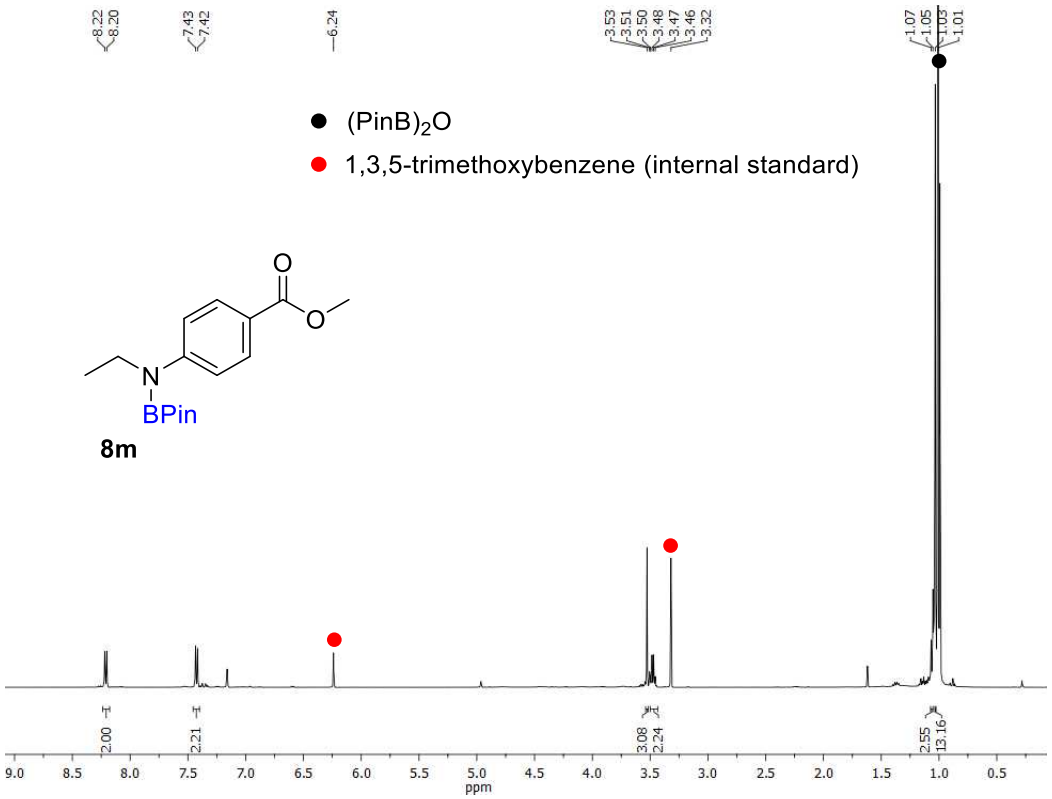

Figure 64. ^{1}H-NMR spectrum of **8m** taken directly from the reaction mixture upon **6-H**-catalyzed hydroboration of methyl 4-acetamidobenzoate with HBPin in C_6D_6.

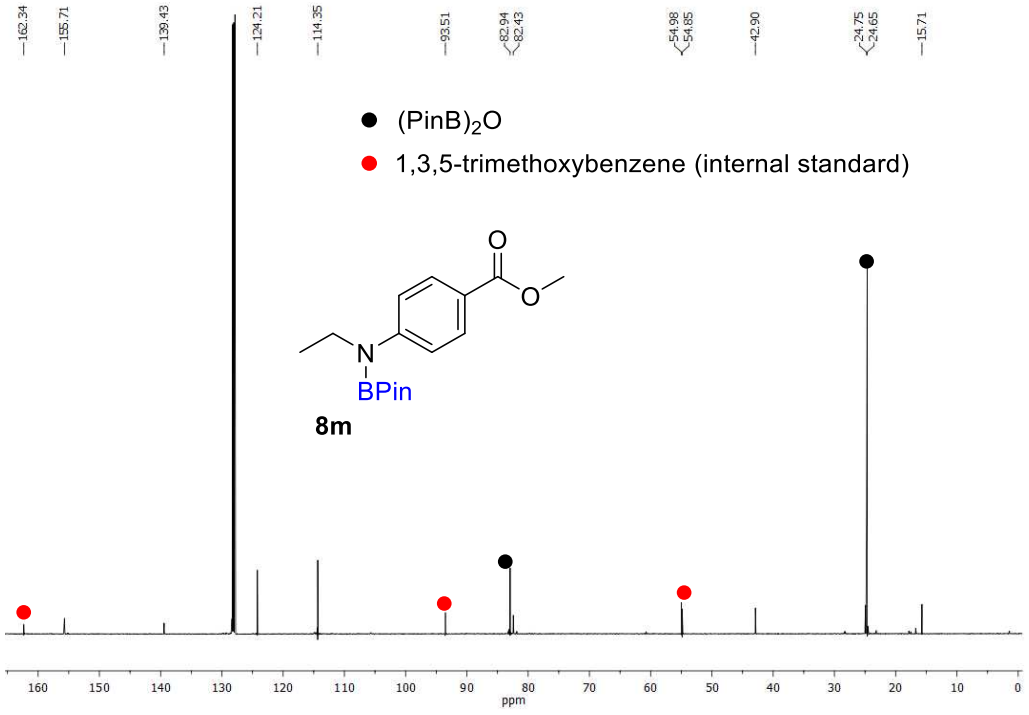

Figure 65. ^{13}C{^{1}H}-NMR spectrum of **8m** taken directly from the reaction mixture upon **6-H**-catalyzed hydroboration of methyl 4-acetamidobenzoate with HBPin in C_6D_6.

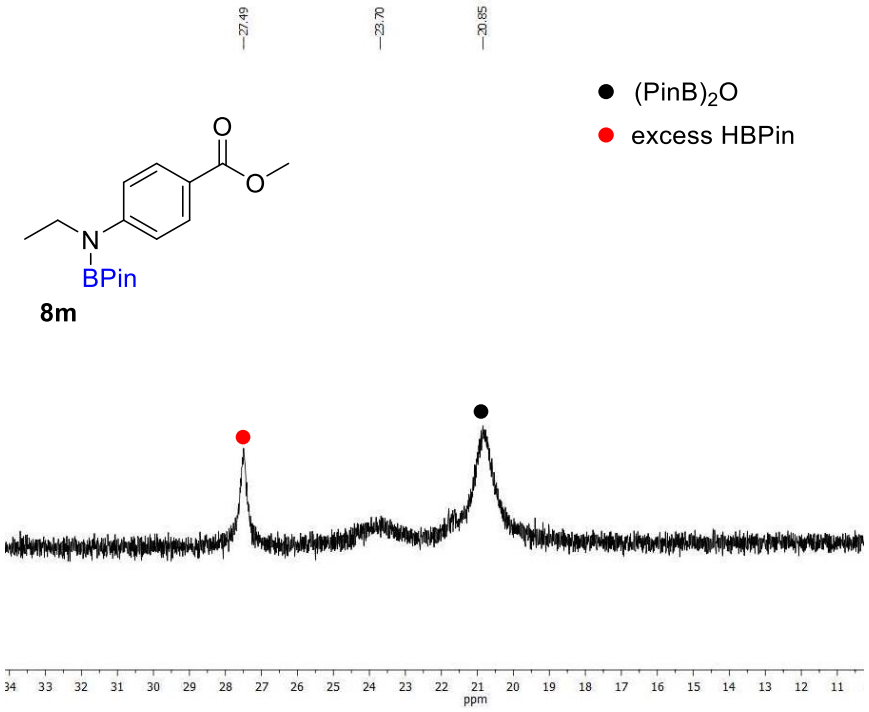

Figure 66. $^{11}B\{^{1}H\}$-NMR spectrum of **8m** taken directly from the reaction mixture upon **6-H**-catalyzed hydroboration of methyl 4-acetamidobenzoate with HBPin in C_6D_6.

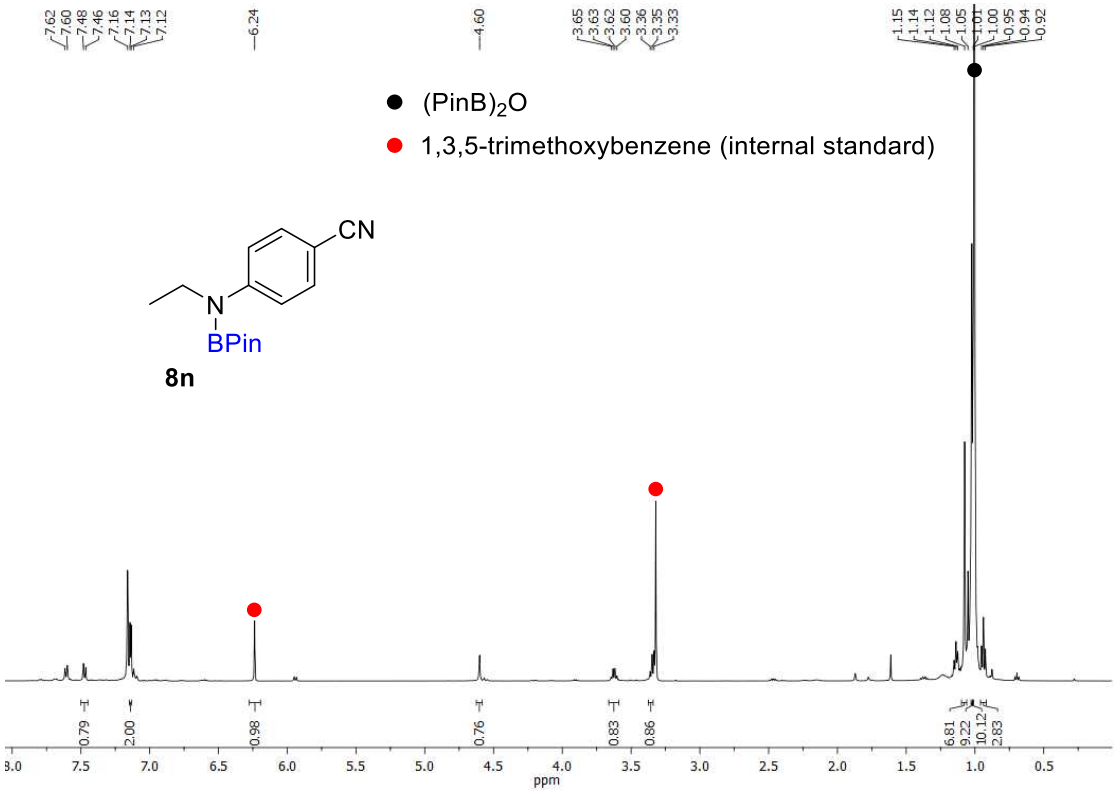

Figure 67. ^{1}H-NMR spectrum of **8n** taken directly from the reaction mixture upon **6-H**-catalyzed hydroboration of *N*-(4-cyanophenyl)acetamide with HBPin in C_6D_6.

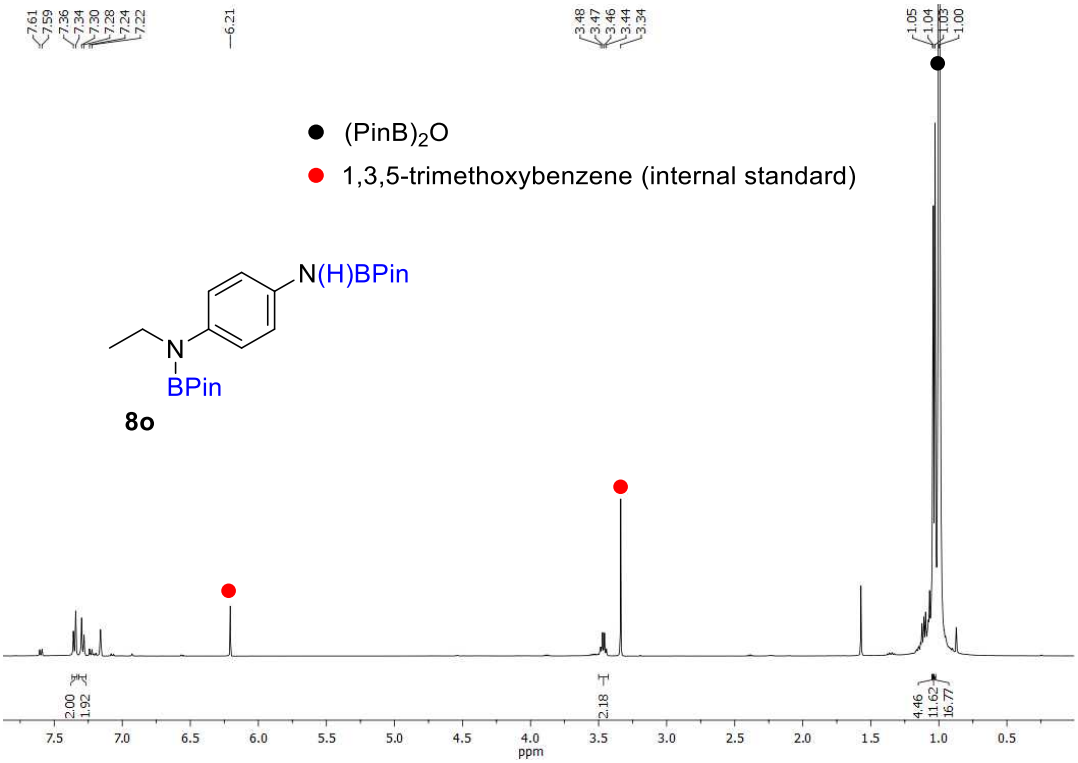

Figure 68. ^{1}H-NMR spectrum of **8o** taken directly from the reaction mixture upon **6-H**-catalyzed hydroboration of *N*-(4-nitrophenyl)acetamide with HBPin in C_6D_6.

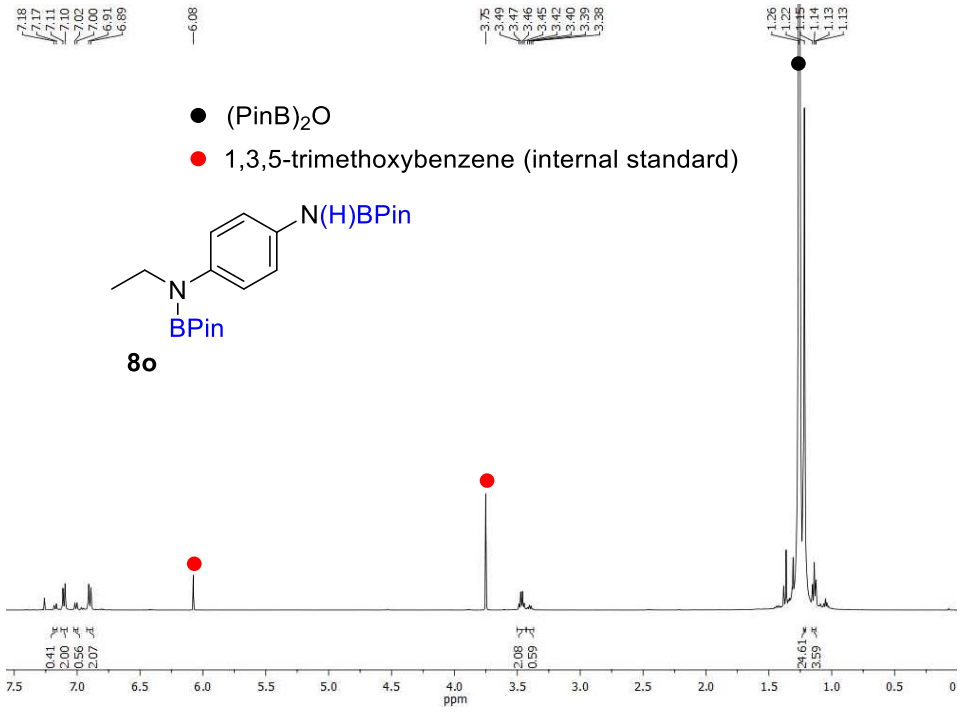

Figure 69. ^{1}H-NMR spectrum (in $CDCl_3$ after removal of C_6D_6) of **8o** taken directly from the reaction mixture upon **6-H**-catalyzed hydroboration of *N*-(4-nitrophenyl)acetamide with HBPin in C_6D_6.

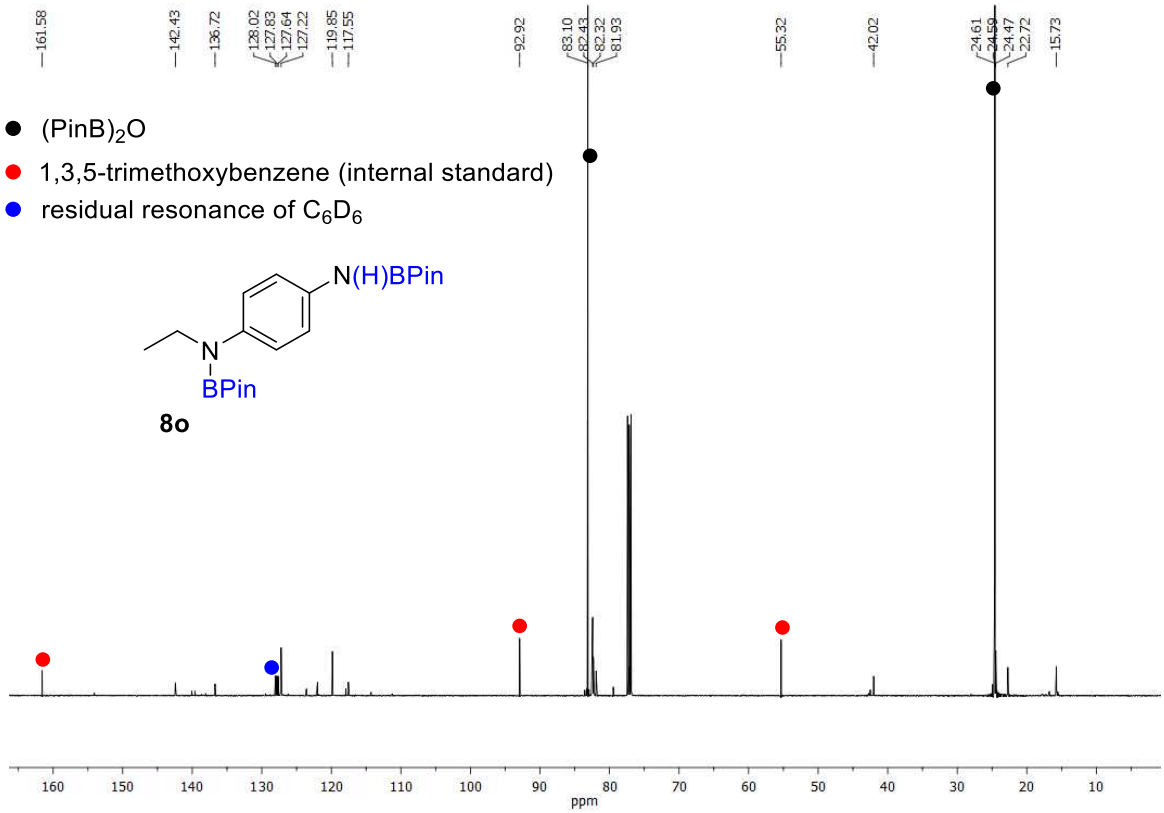

Figure 70. $^{13}C\{^{1}H\}$-NMR spectrum (in $CDCl_3$ after removal of C_6D_6) of **8o** taken directly from the reaction mixture upon **6-H**-catalyzed hydroboration of *N*-(4-nitrophenyl)acetamide with HBPin in C_6D_6.

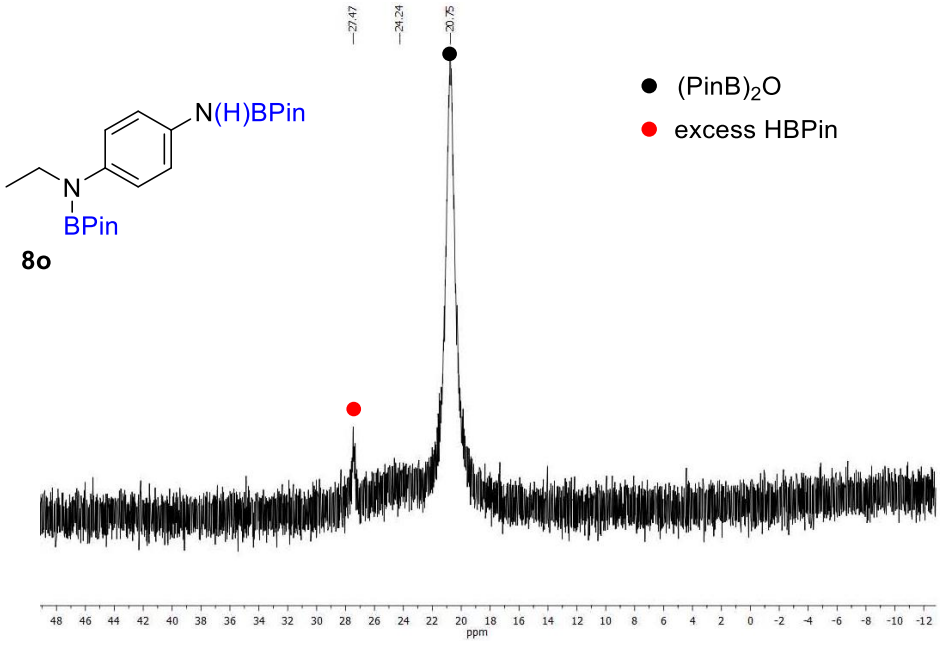

Figure 71. $^{11}B\{^{1}H\}$-NMR spectrum of **8o** taken directly from the reaction mixture upon **6-H**-catalyzed hydroboration of *N*-(4-nitrophenyl)acetamide with HBPin in C_6D_6.

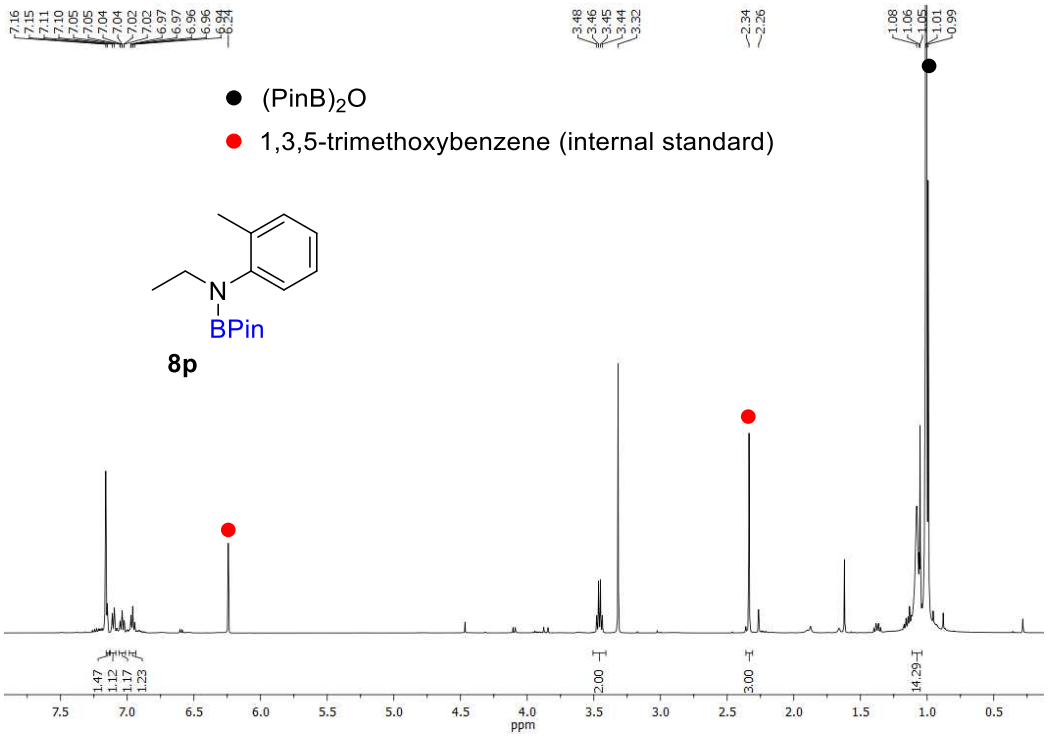

Figure 72. ^{1}H-NMR spectrum of **8p** taken directly from the reaction mixture upon **6-H**-catalyzed hydroboration of *N*-(o-tolyl)acetamide with HBPin in C_6D_6.

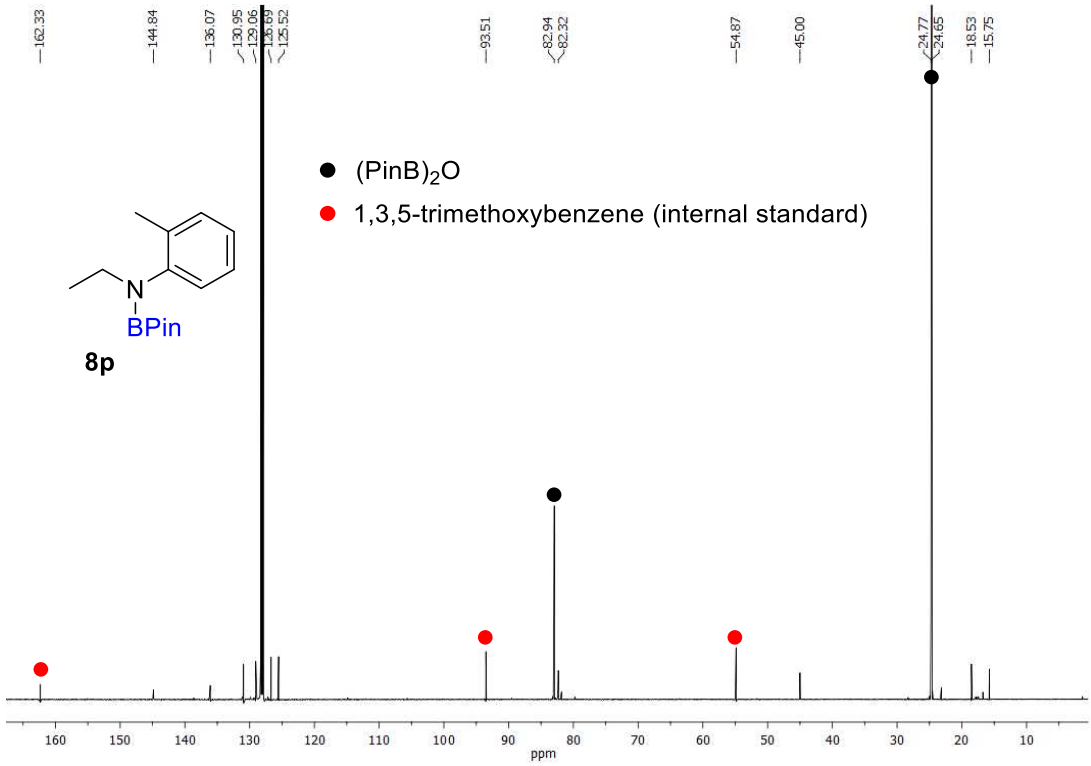

Figure 73. ^{13}C{^{1}H}-NMR spectrum of **8p** taken directly from the reaction mixture upon **6-H**-catalyzed hydroboration of *N*-(o-tolyl)acetamide with HBPin in C_6D_6.

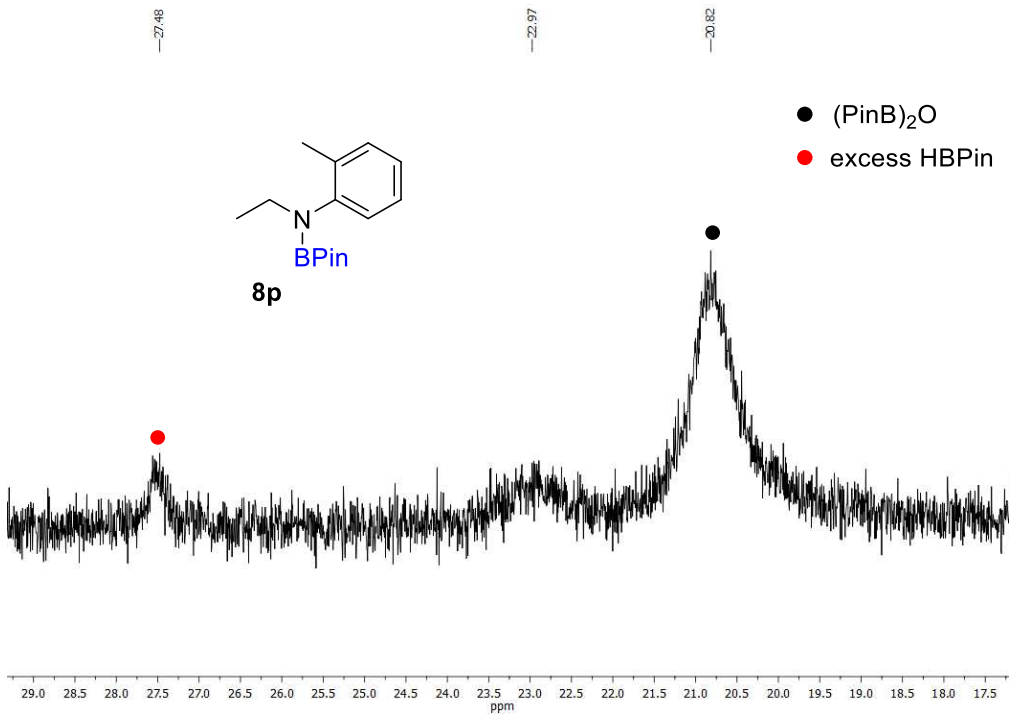

Figure 74. $^{11}B\{^{1}H\}$-NMR spectrum of **8p** taken directly from the reaction mixture upon **6-H**-catalyzed hydroboration of *N*-(o-tolyl)acetamide with HBPin in C_6D_6.

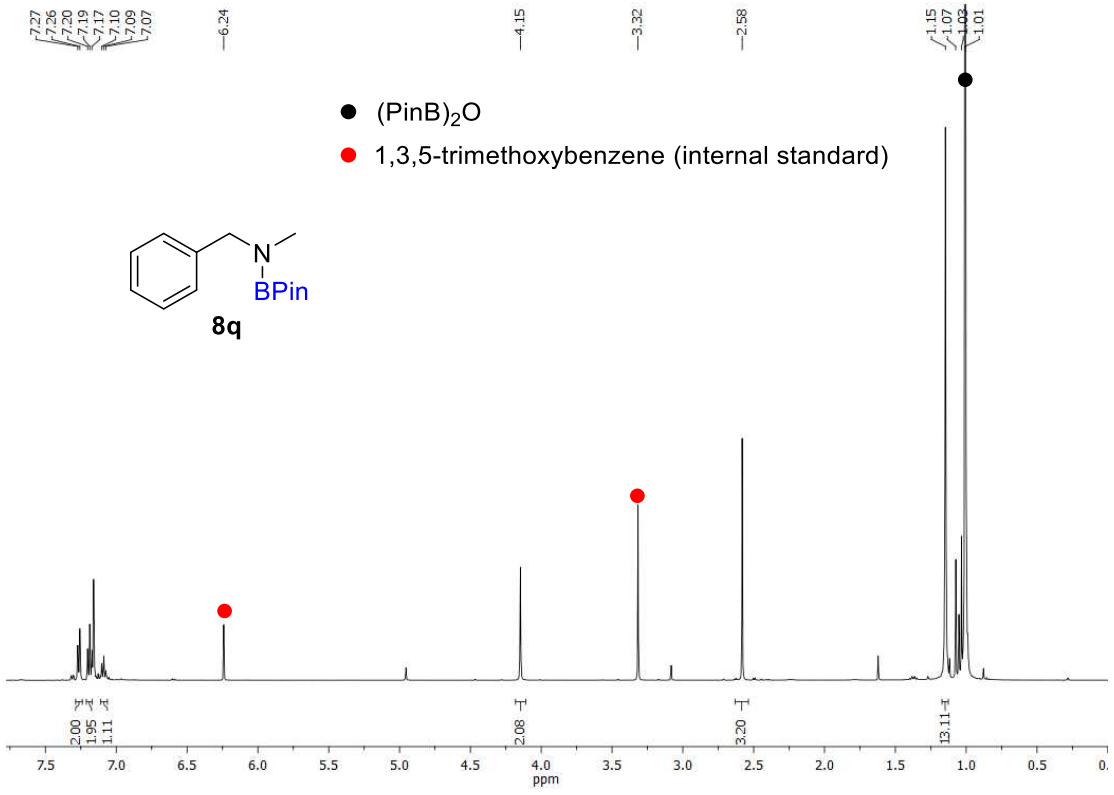

Figure 75. ^{1}H-NMR spectrum of **8q** taken directly from the reaction mixture upon **6-H**-catalyzed hydroboration of *N*-methylbenzamide with HBPin in C_6D_6.

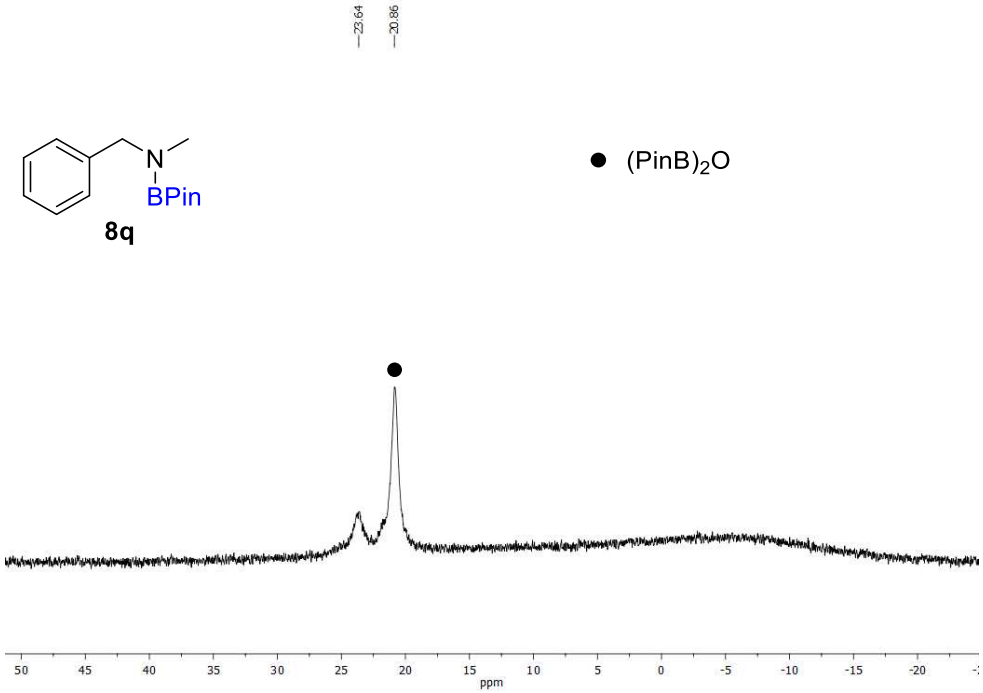

Figure 76. $^{11}B\{^{1}H\}$-NMR spectrum of **8q** taken directly from the reaction mixture upon **6-H**-catalyzed hydroboration of *N*-methylbenzamide with HBPin in C_6D_6.

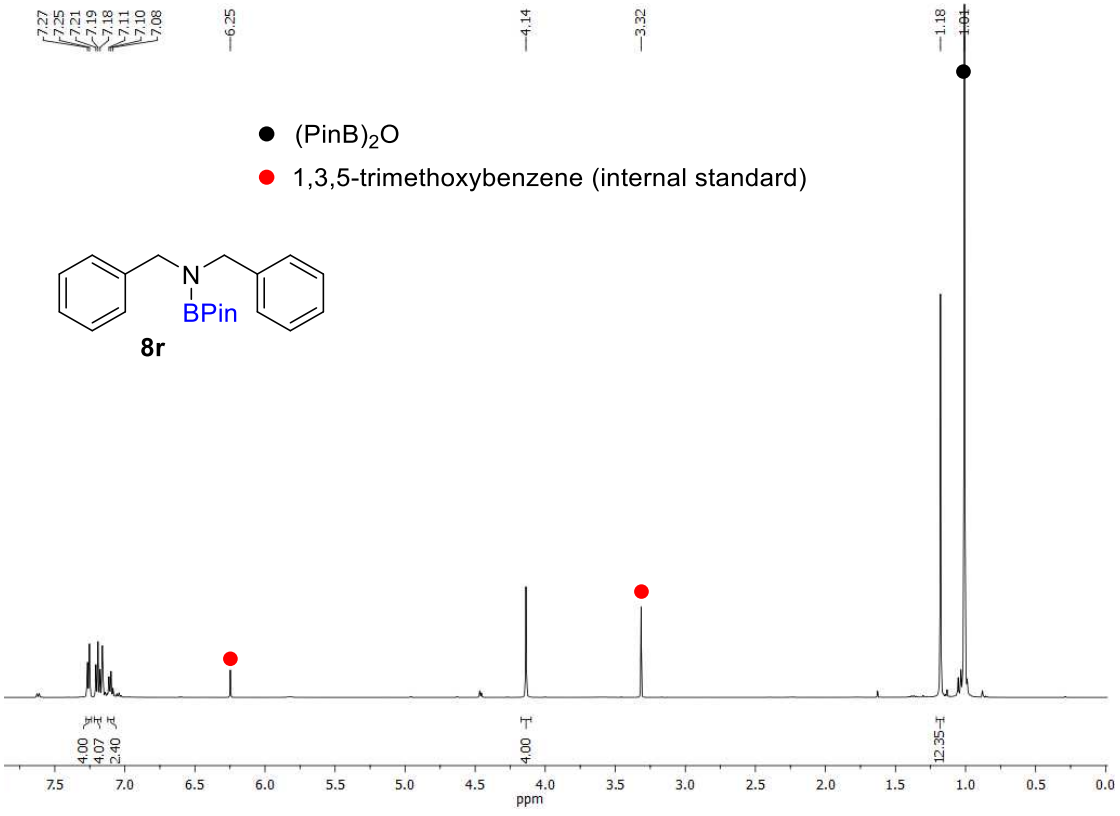

Figure 77. ^{1}H-NMR spectrum of **8r** taken directly from the reaction mixture upon **6-H**-catalyzed hydroboration of *N*-benzylbenzamide with HBPin in C_6D_6.

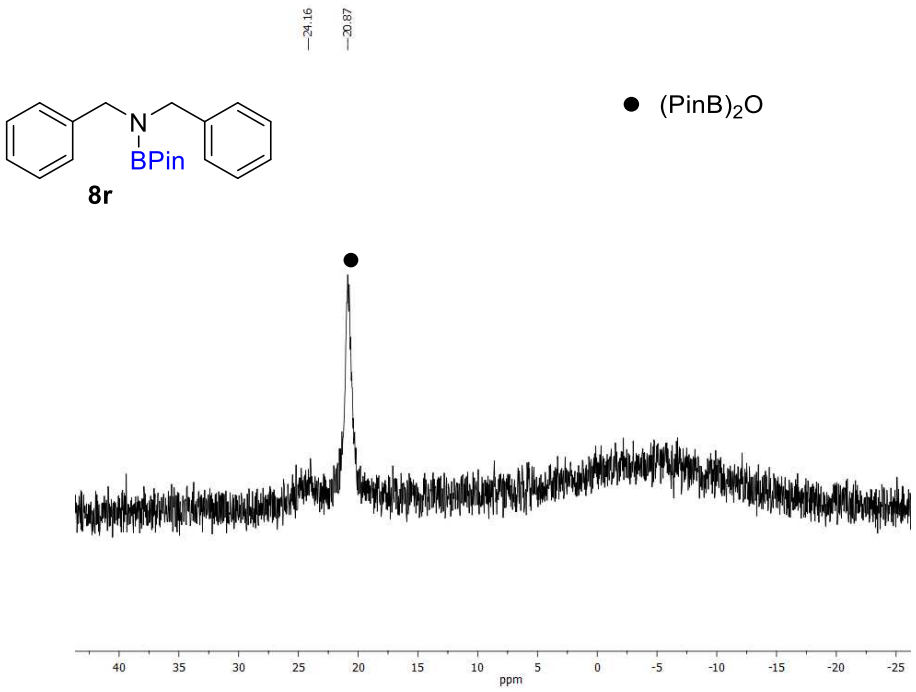

Figure 78. $^{11}B\{^{1}H\}$-NMR spectrum of **8r** taken directly from the reaction mixture upon **6-H**-catalyzed hydroboration of *N*-benzylbenzamide with HBPin in C_6D_6.

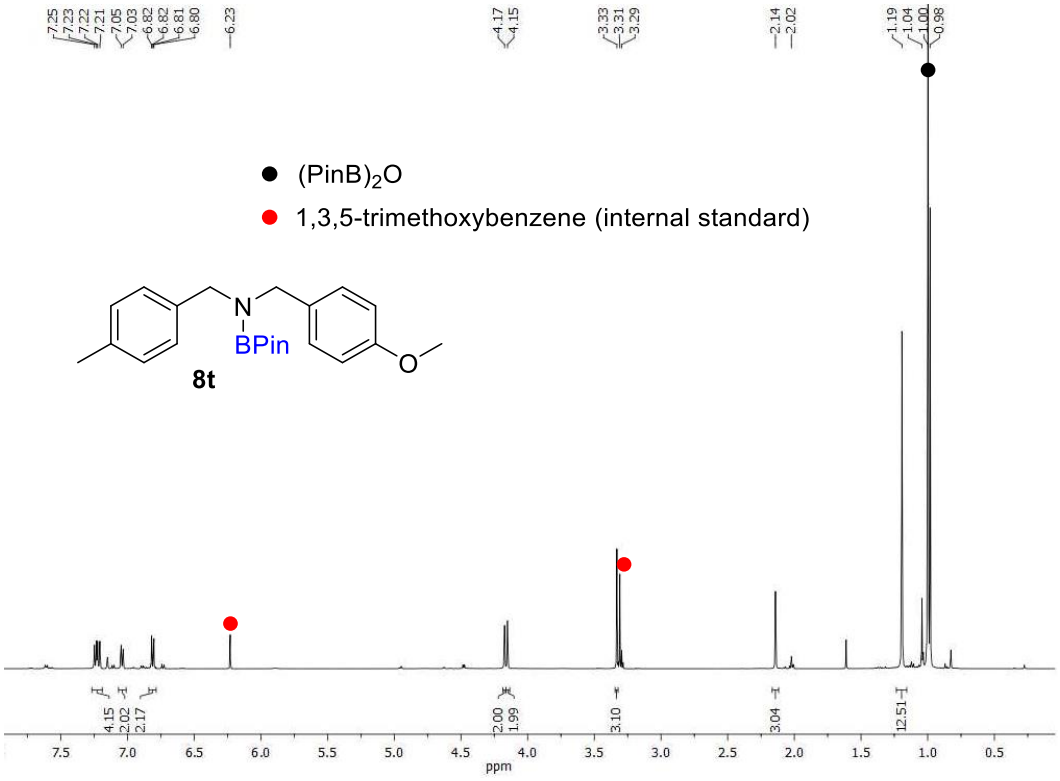

Figure 79. ^{1}H-NMR spectrum of **8t** taken directly from the reaction mixture upon **6-H**-catalyzed hydroboration of *N*-(4-methoxybenzyl)-4-methylbenzamide with HBPin in C_6D_6.

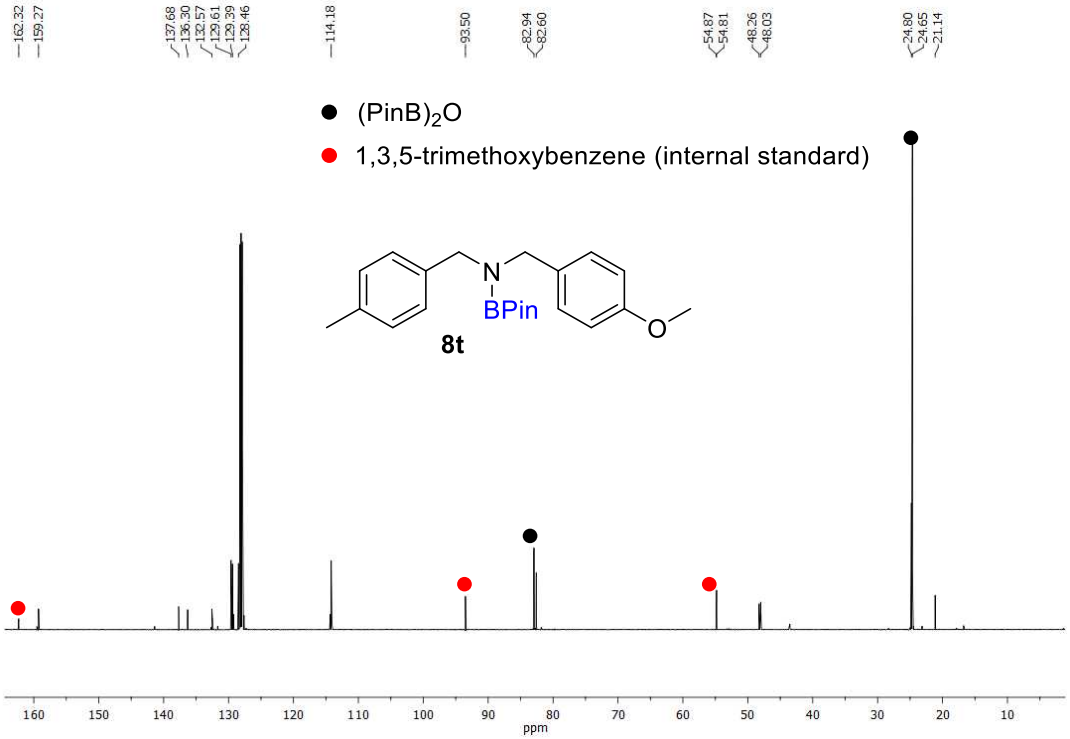

Figure 80. $^{13}C\{^{1}H\}$-NMR spectrum of **8t** taken directly from the reaction mixture upon **6-H**-catalyzed hydroboration of *N*-(4-methoxybenzyl)-4-methylbenzamide with HBPin in C_6D_6.

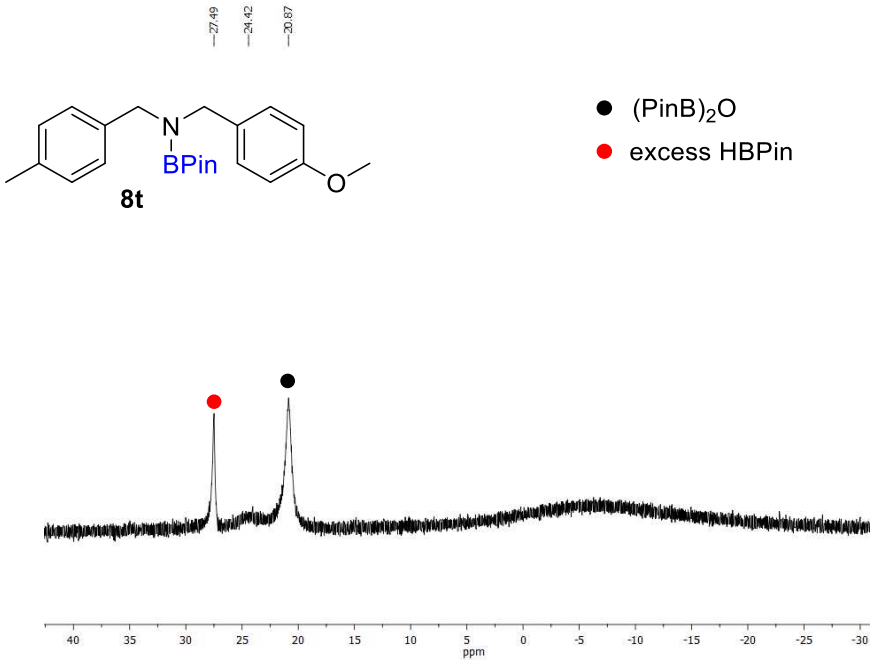

Figure 81. $^{11}B\{^{1}H\}$-NMR spectrum of **8t** taken directly from the reaction mixture upon **6-H**-catalyzed hydroboration of *N*-(4-methoxybenzyl)-4-methylbenzamide with HBPin in C_6D_6.

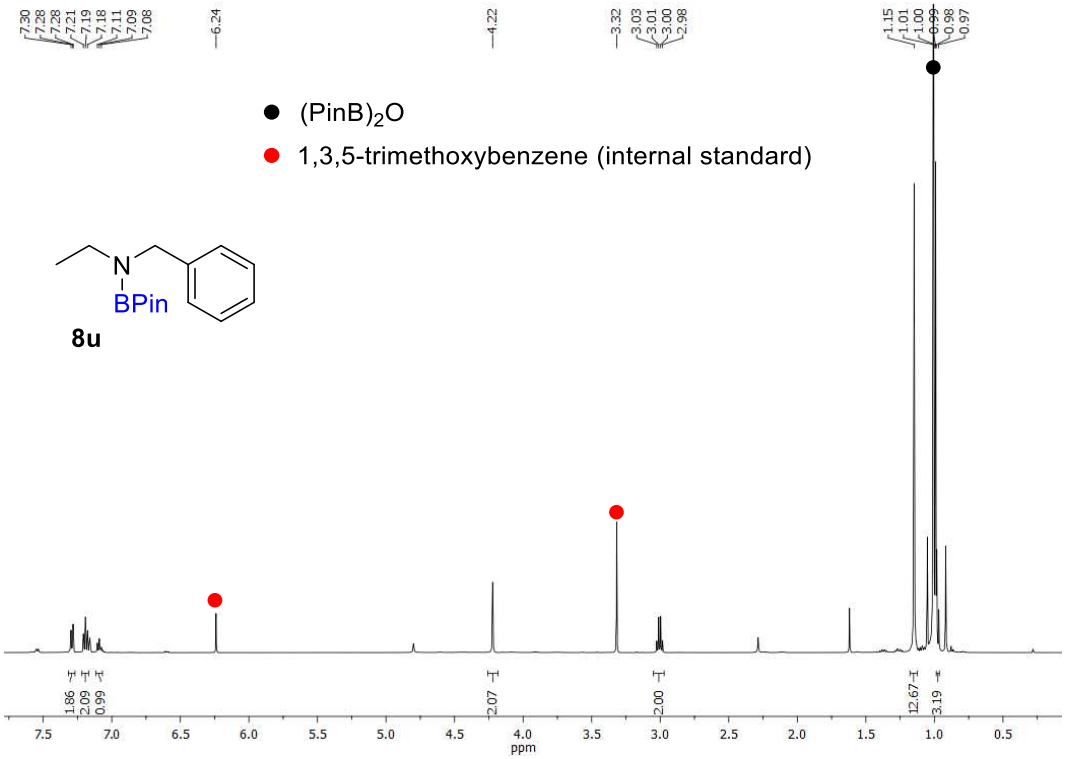

Figure 82. ^{1}H-NMR spectrum of **8u** taken directly from the reaction mixture upon **6-H**-catalyzed hydroboration of *N*-benzylacetamide with HBPin in C_6D_6

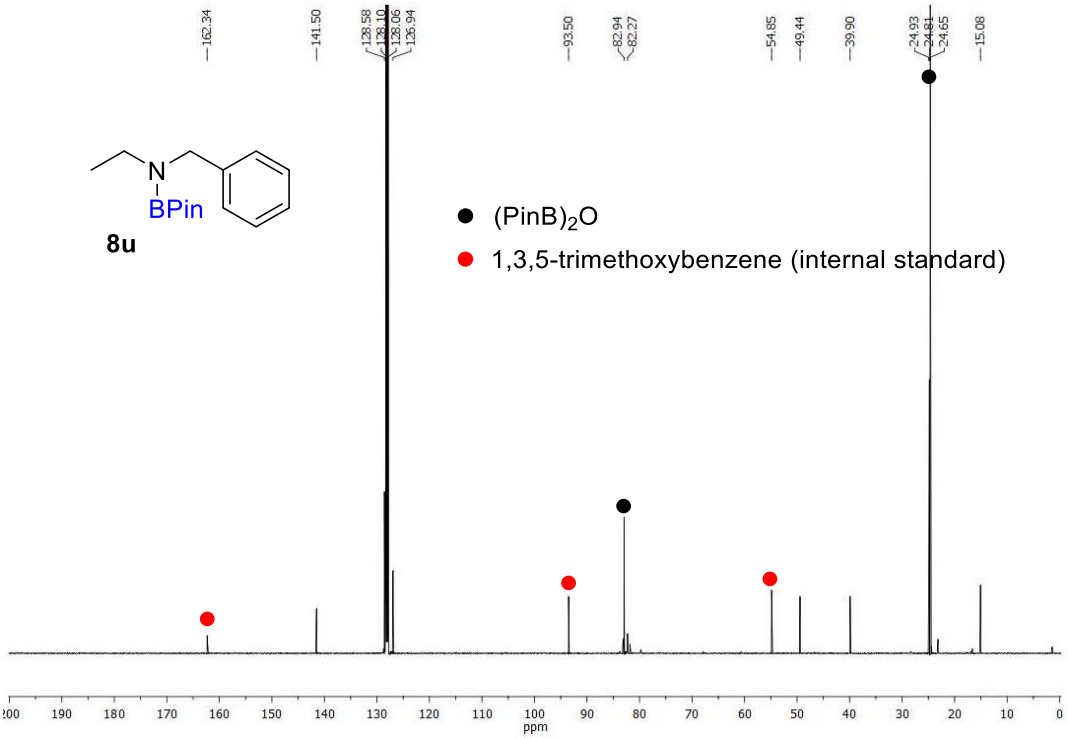

Figure 83. ^{13}C{^{1}H}-NMR spectrum of **8u** taken directly from the reaction mixture upon **6-H**-catalyzed hydroboration of *N*-benzylacetamide with HBPin in C_6D_6

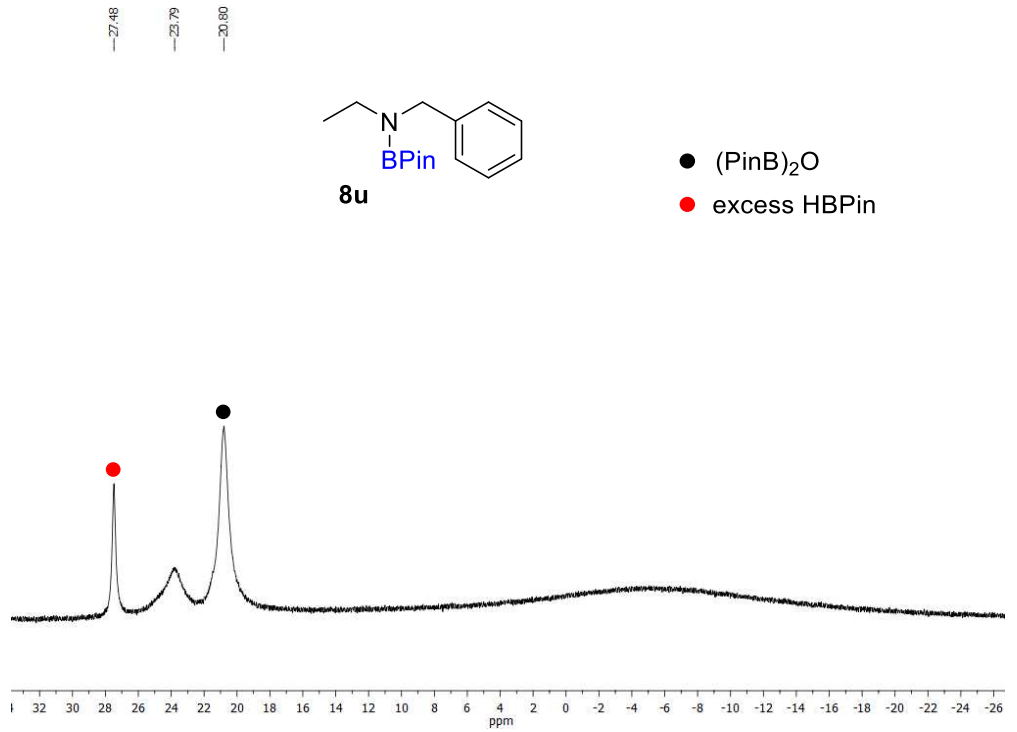

Figure 84. $^{11}B\{^{1}H\}$-NMR spectrum of **8u** taken directly from the reaction mixture upon **6-H**-catalyzed hydroboration of *N*-benzylacetamide with HBPin in C_6D_6

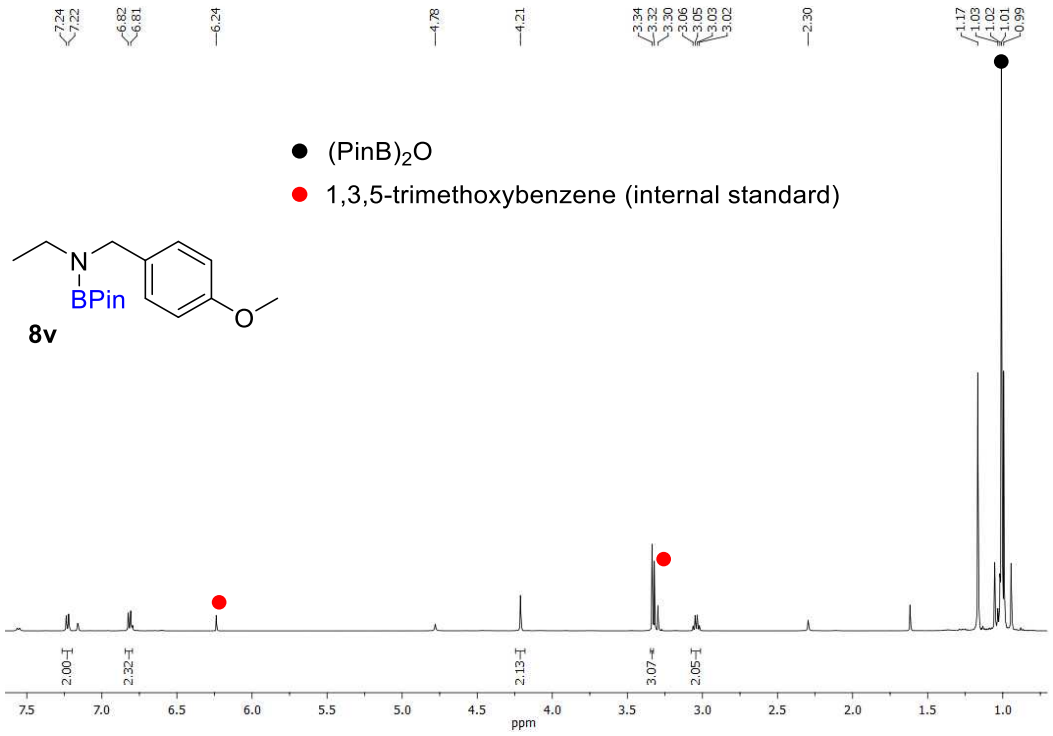

Figure 85. ^{1}H-NMR spectrum of **8v** taken directly from the reaction mixture upon **6-H**-catalyzed hydroboration of *N*-(4-methoxybenzyl)acetamide with HBPin in C_6D_6.

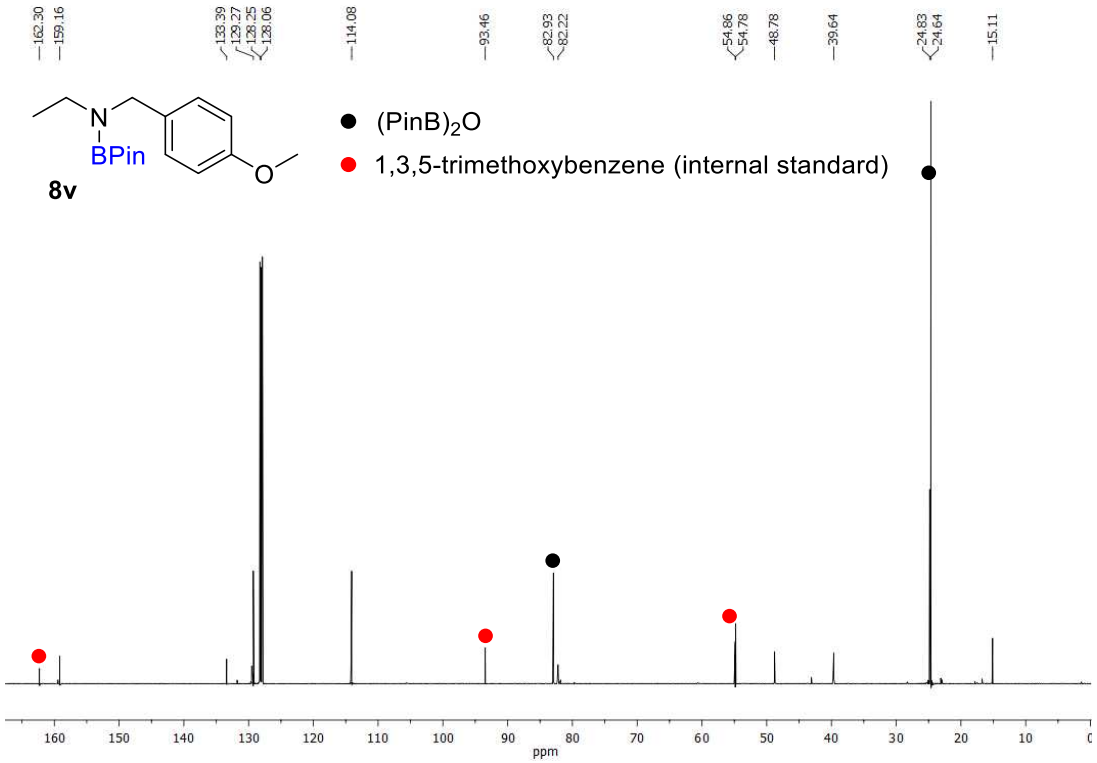

Figure 86. $^{13}C\{^{1}H\}$-NMR spectrum of **8v** taken directly from the reaction mixture upon **6-H**-catalyzed hydroboration of *N*-(4-methoxybenzyl)acetamide with HBPin in C_6D_6.

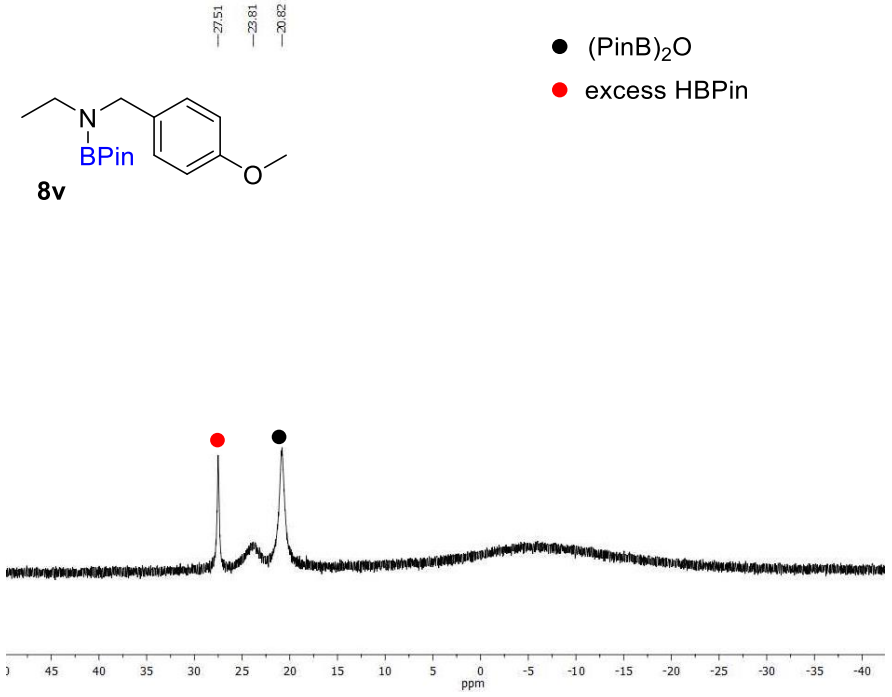

Figure 87. $^{11}B\{^{1}H\}$-NMR spectrum of **8v** taken directly from the reaction mixture upon **6-H**-catalyzed hydroboration of *N*-(4-methoxybenzyl)acetamide with HBPin in C_6D_6.

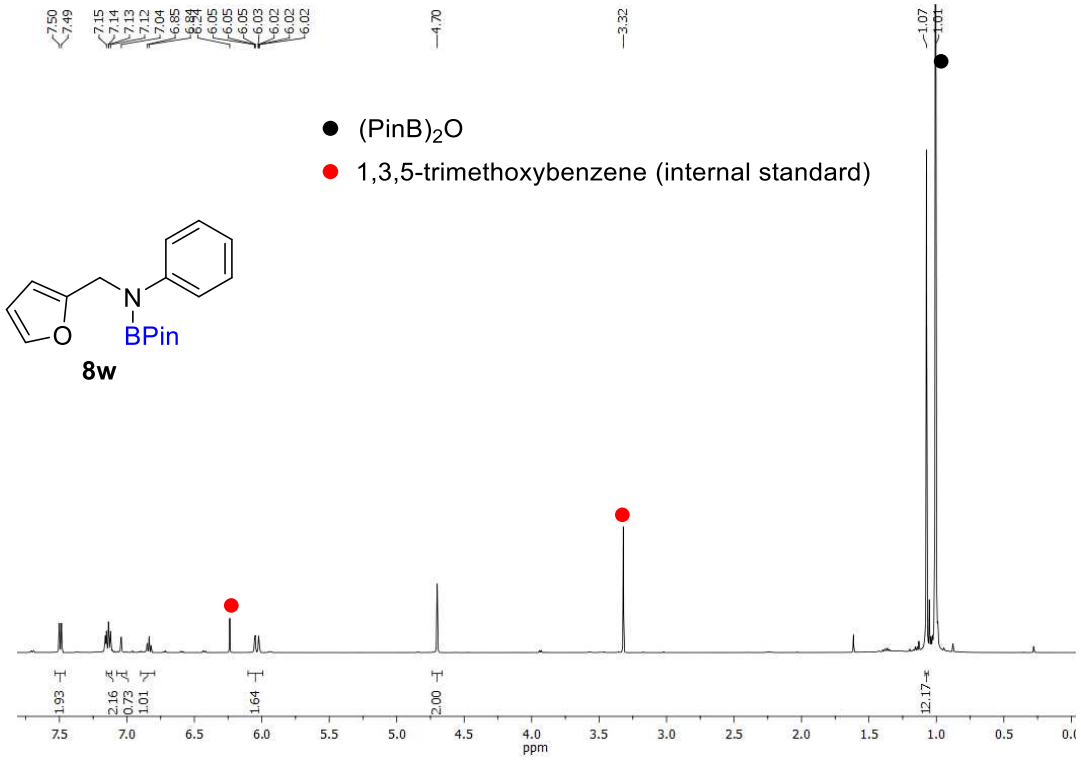

Figure 88. ^{1}H-NMR spectrum of **8w** taken directly from the reaction mixture upon **6-H**-catalyzed hydroboration of *N*-phenylfuran-2-carboxamide with HBPin in C_6D_6.

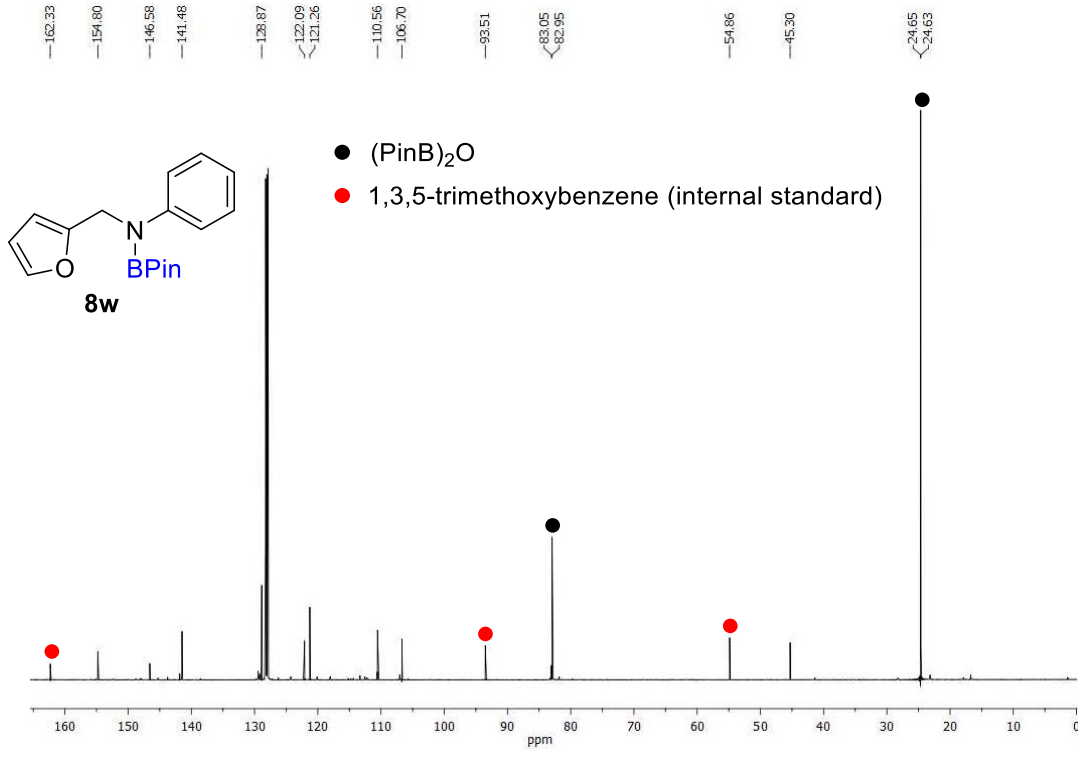

Figure 89. ^{13}C{^{1}H}-NMR spectrum of **8w** taken directly from the reaction mixture upon **6-H**-catalyzed hydroboration of *N*-phenylfuran-2-carboxamide with HBPin in C_6D_6.

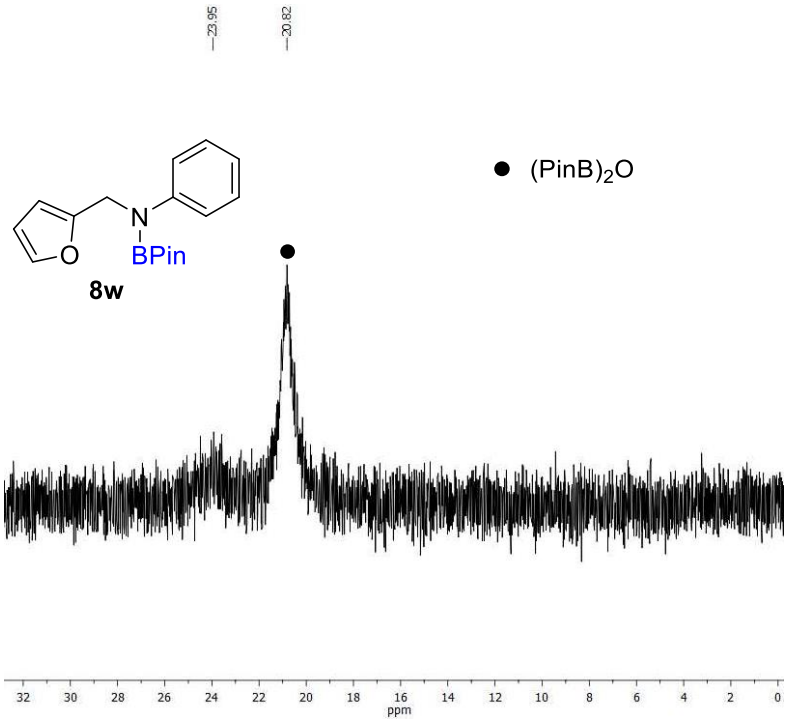

Figure 90. $^{11}B\{^{1}H\}$-NMR spectrum of **8w** taken directly from the reaction mixture upon **6-H**-catalyzed hydroboration of *N*-phenylfuran-2-carboxamide with HBPin in C_6D_6.

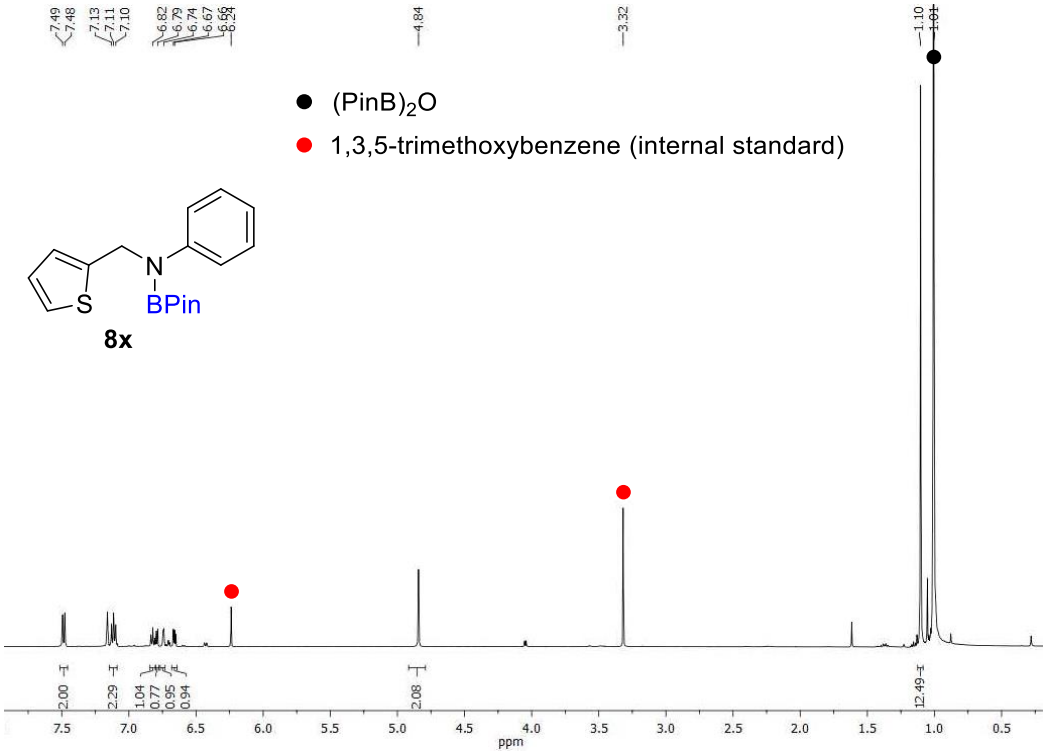

Figure 91. ^{1}H-NMR spectrum of **8x** taken directly from the reaction mixture upon **6-H**-catalyzed hydroboration of *N*-phenylthiophene-2-carboxamide with HBPin in C_6D_6.

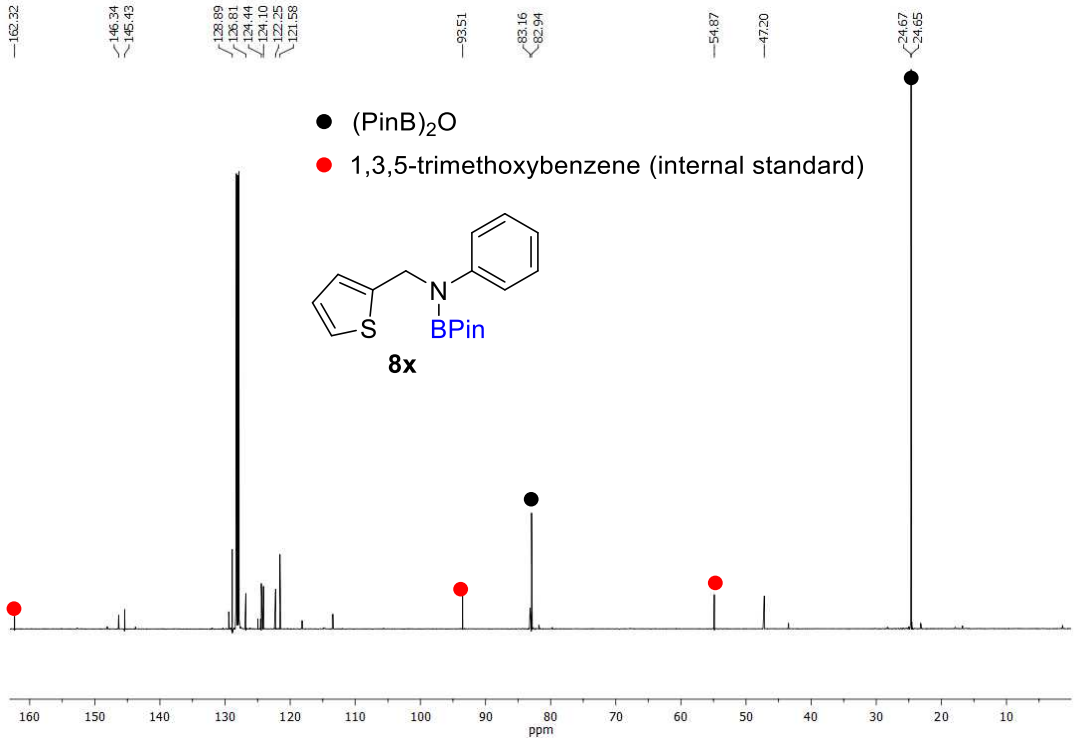

Figure 92. $^{13}C\{^{1}H\}$-NMR spectrum of **8x** taken directly from the reaction mixture upon **6-H**-catalyzed hydroboration of *N*-phenylthiophene-2-carboxamide with HBPin in C_6D_6.

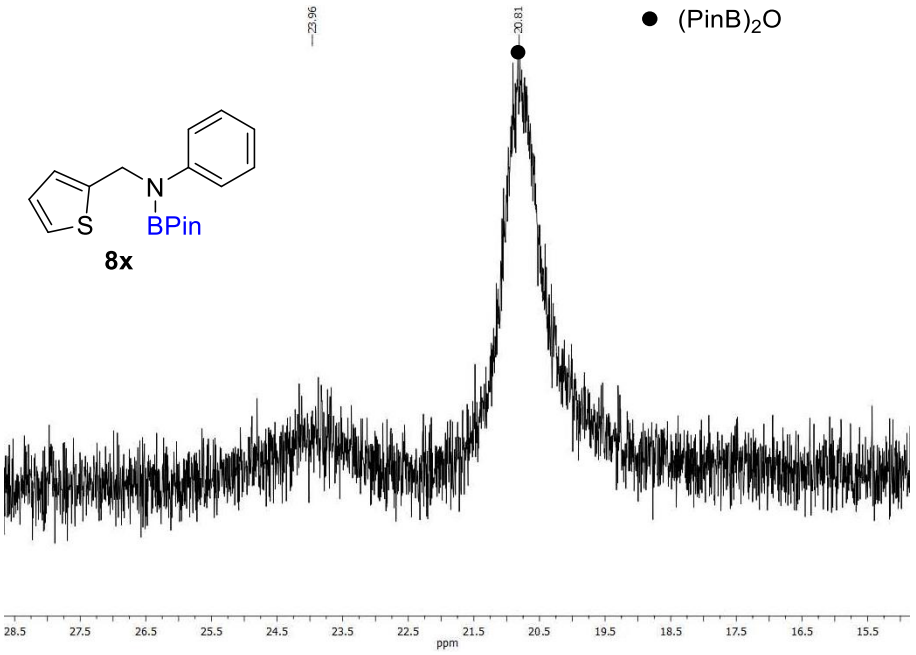

Figure 93. $^{11}B\{^{1}H\}$-NMR spectrum of **8x** taken directly from the reaction mixture upon **6-H**-catalyzed hydroboration of *N*-phenylthiophene-2-carboxamide with HBPin in C_6D_6.

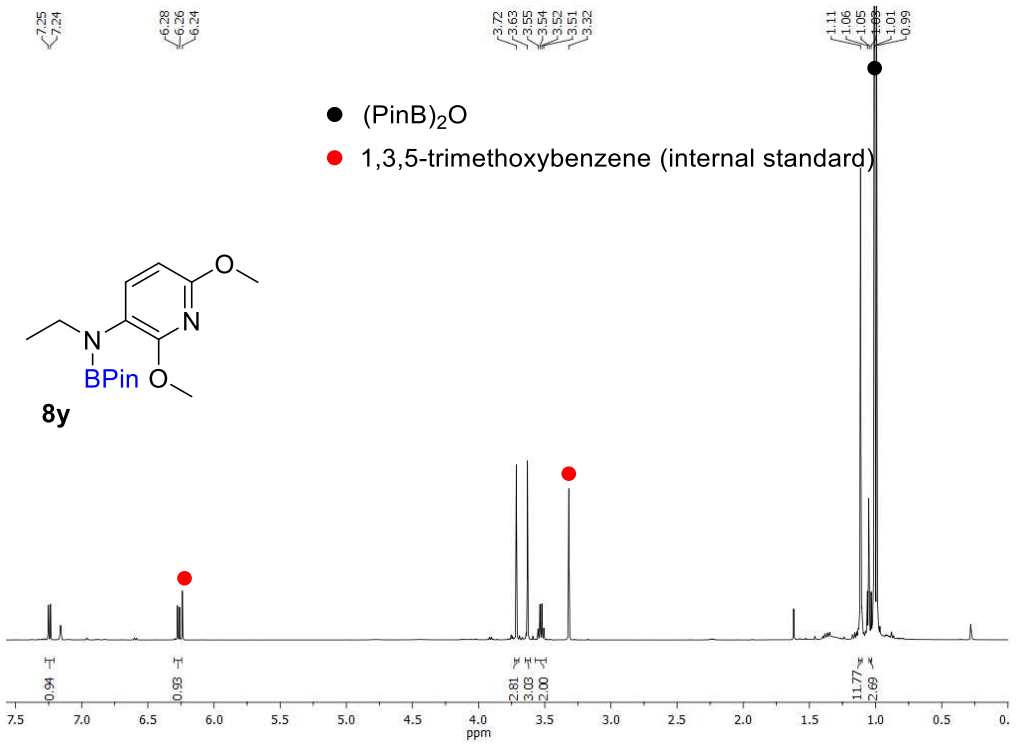

Figure 94. ^{1}H-NMR spectrum of **8y** taken directly from the reaction mixture upon **6-H**-catalyzed hydroboration of *N*-(2,6-dimethoxypyridin-3-yl)acetamide with HBPin in C_6D_6.

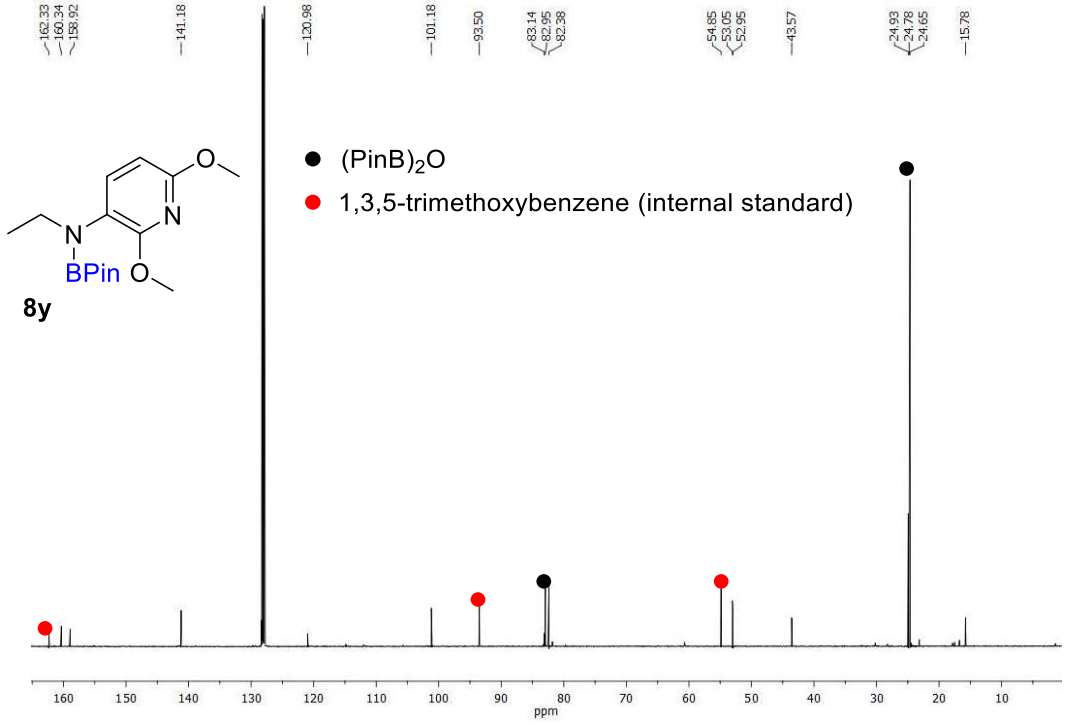

Figure 95. ^{13}C{^{1}H}-NMR spectrum of **8y** taken directly from the reaction mixture upon **6-H**-catalyzed hydroboration of *N*-(2,6-dimethoxypyridin-3-yl)acetamide with HBPin in C_6D_6.

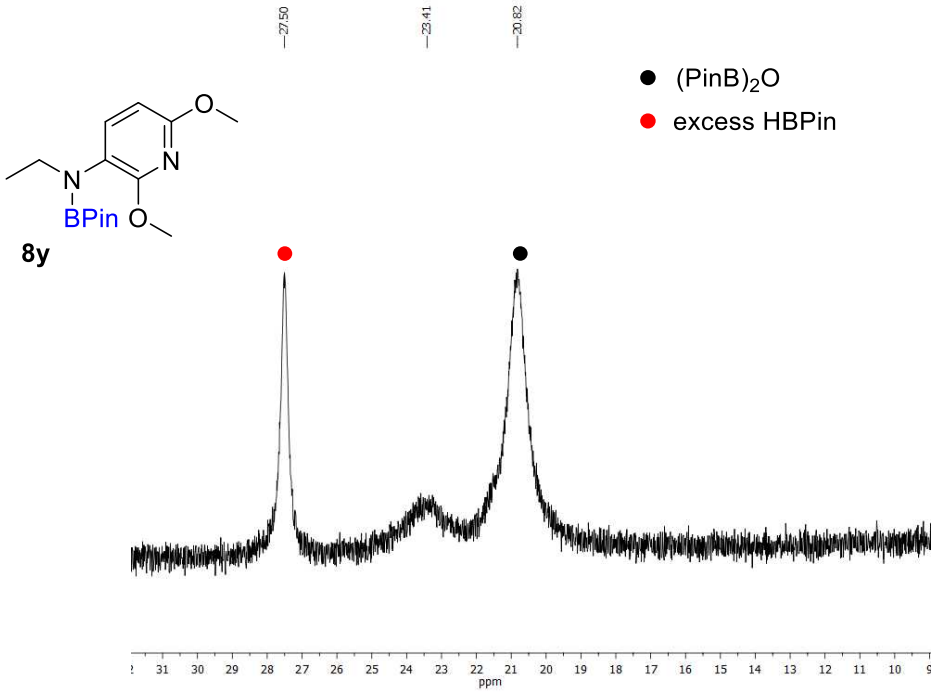

Figure 96. $^{11}B\{^{1}H\}$-NMR spectrum of **8y** taken directly from the reaction mixture upon **6-H**-catalyzed hydroboration of *N*-(2,6-dimethoxypyridin-3-yl)acetamide with HBPin in C_6D_6.

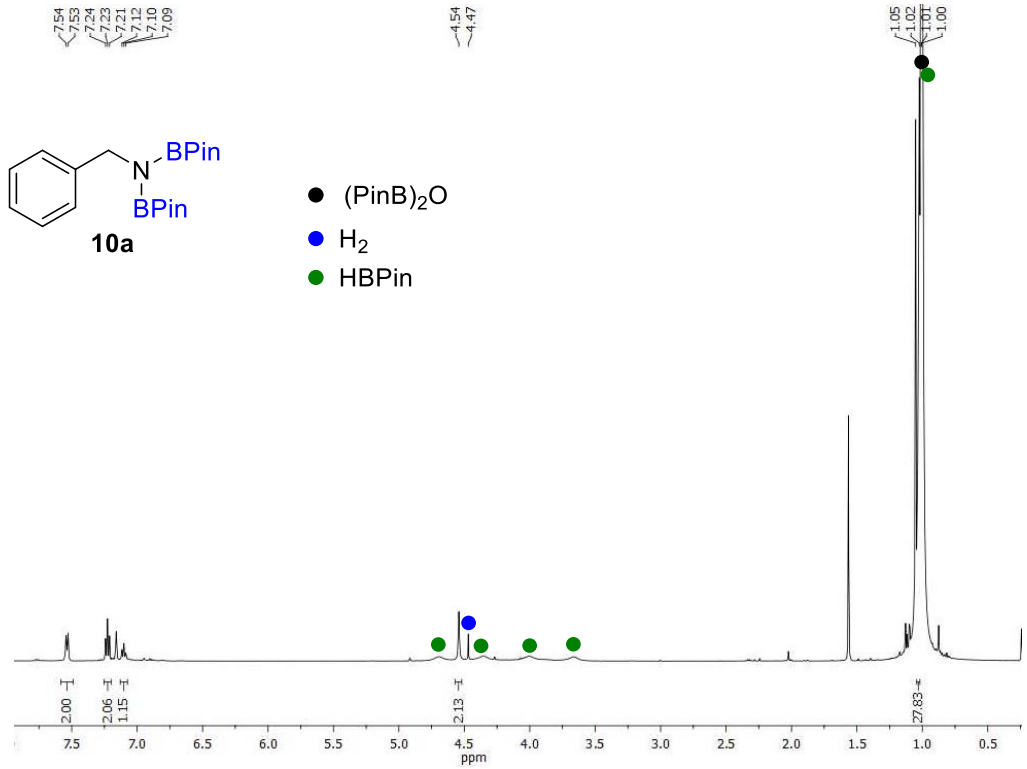

Figure 97. ^{1}H-NMR spectrum of **10a** taken directly from the reaction mixture upon **2-CH_2TMS**-catalyzed hydroboration of benzamide with HBPin in C_6D_6.

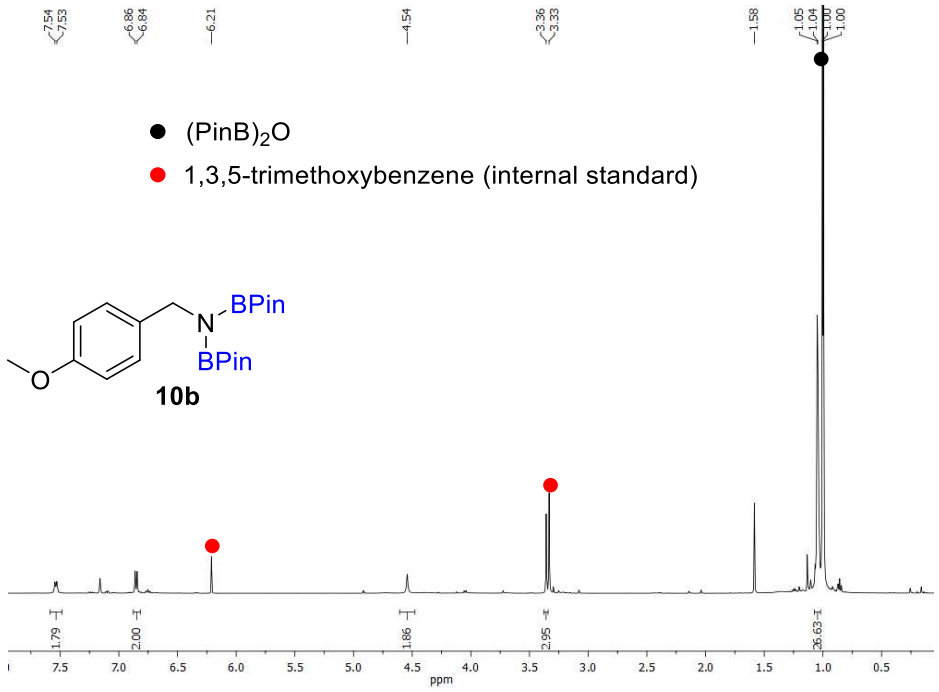

Figure 98. ^{1}H-NMR spectrum of **10b** taken directly from the reaction mixture upon **2-CH$_2$TMS**-catalyzed hydroboration of 4-methoxybenzamide with HBPin in C_6D_6.

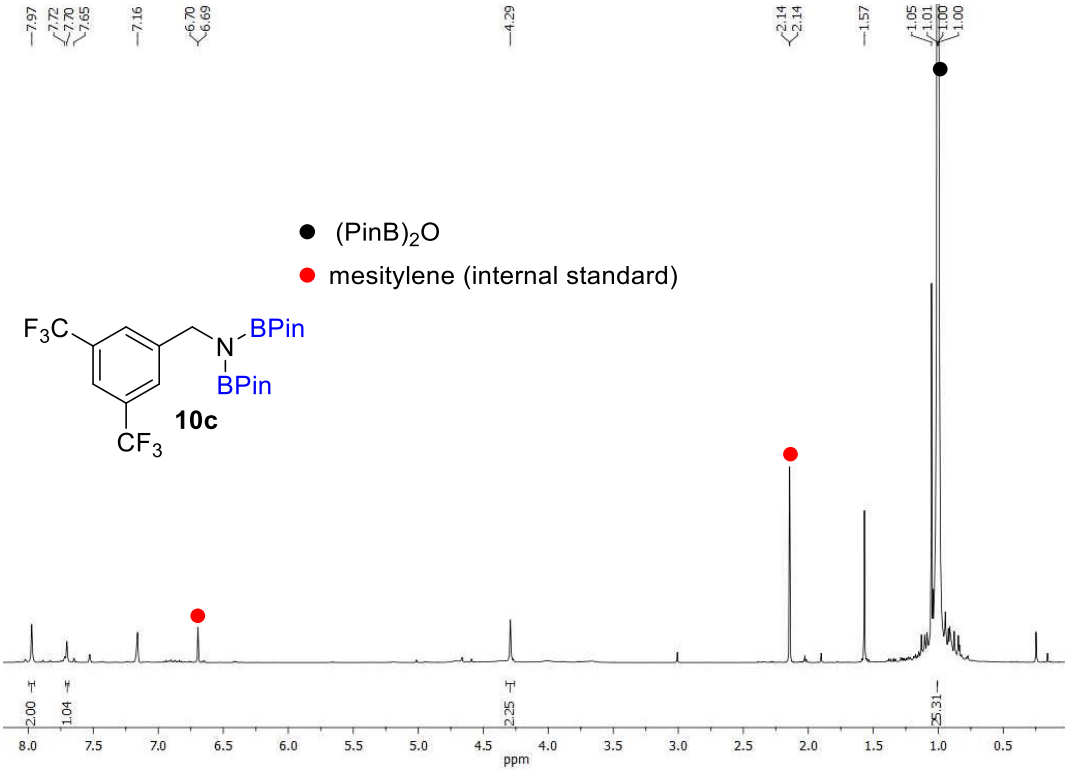

Figure 99. ^{1}H-NMR spectrum of **10c** taken directly from the reaction mixture upon **2-CH$_2$TMS**-catalyzed hydroboration of 3,5-bis(trifluoromethyl)benzamide with HBPin in C_6D_6.

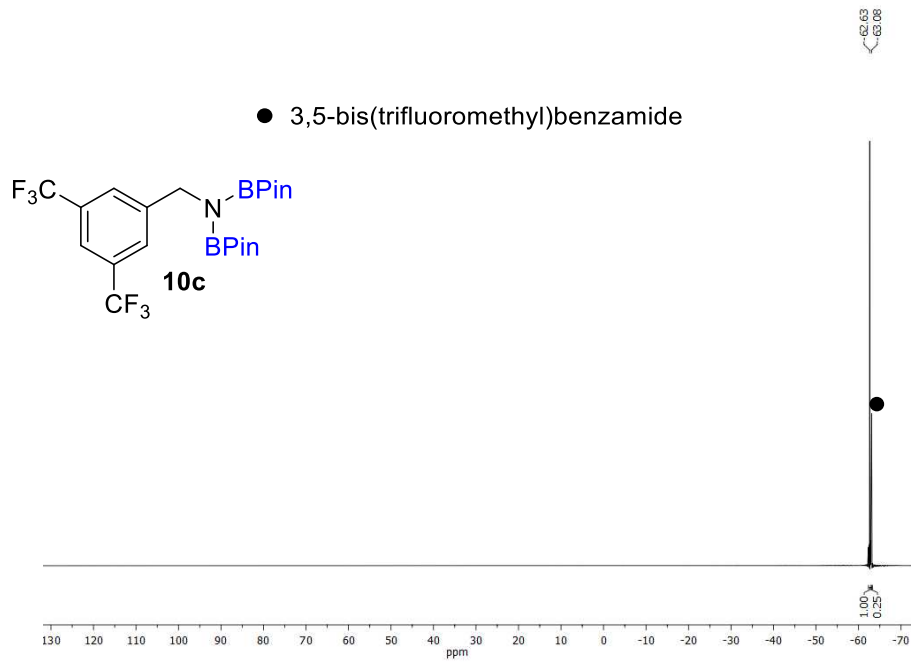

Figure 100. $^{19}F\{^{1}H\}$-NMR spectrum of **10c** taken directly from the reaction mixture upon **2-CH$_2$TMS**-catalyzed hydroboration of 3,5-bis(trifluoromethyl)benzamide with HBPin in C_6D_6.

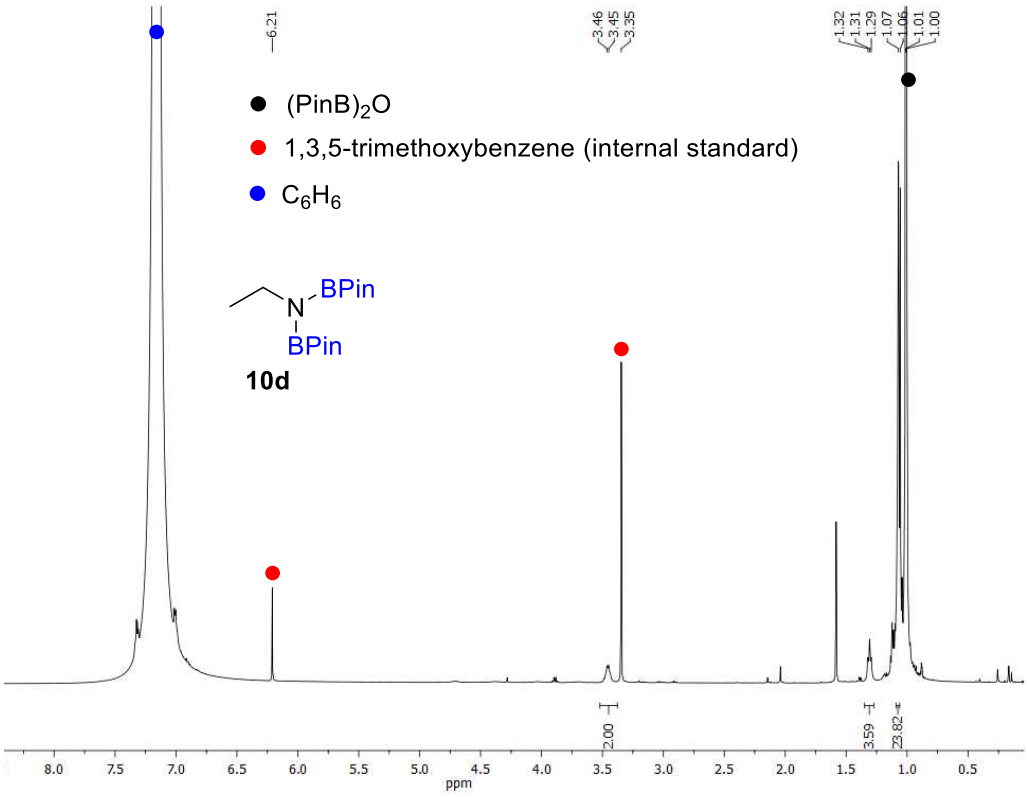

Figure 101. ^{1}H-NMR spectrum of **10d** taken directly from the reaction mixture upon **2-CH$_2$TMS**-catalyzed hydroboration of acetamide with HBPin in C_6H_6.

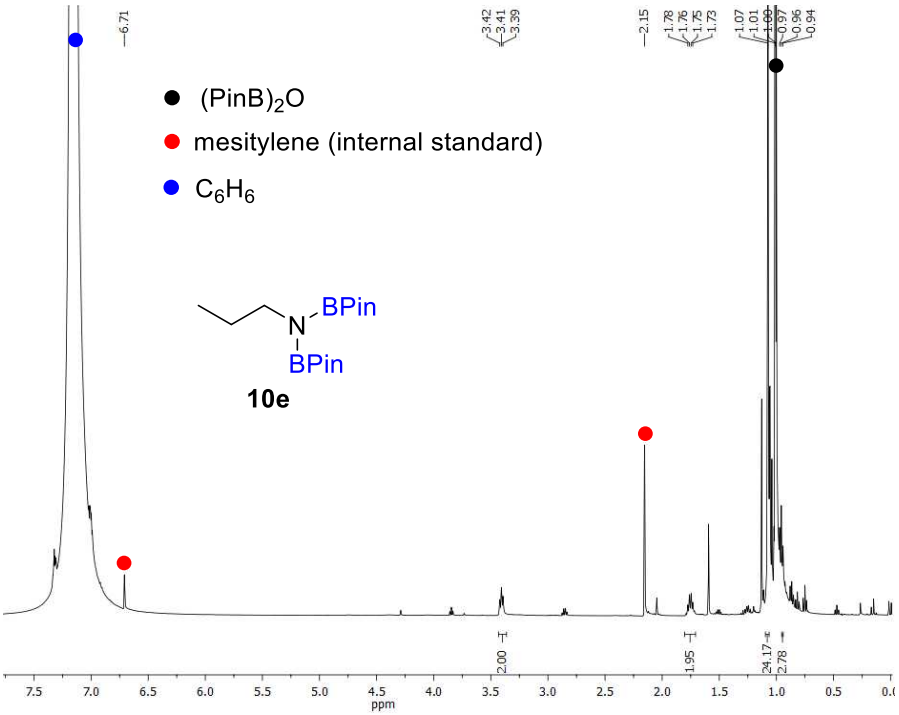

Figure 102. ^{1}H-NMR spectrum of **10e** taken directly from the reaction mixture upon **2-CH$_2$TMS**-catalyzed hydroboration of propanamide with HBPin in C_6H_6.

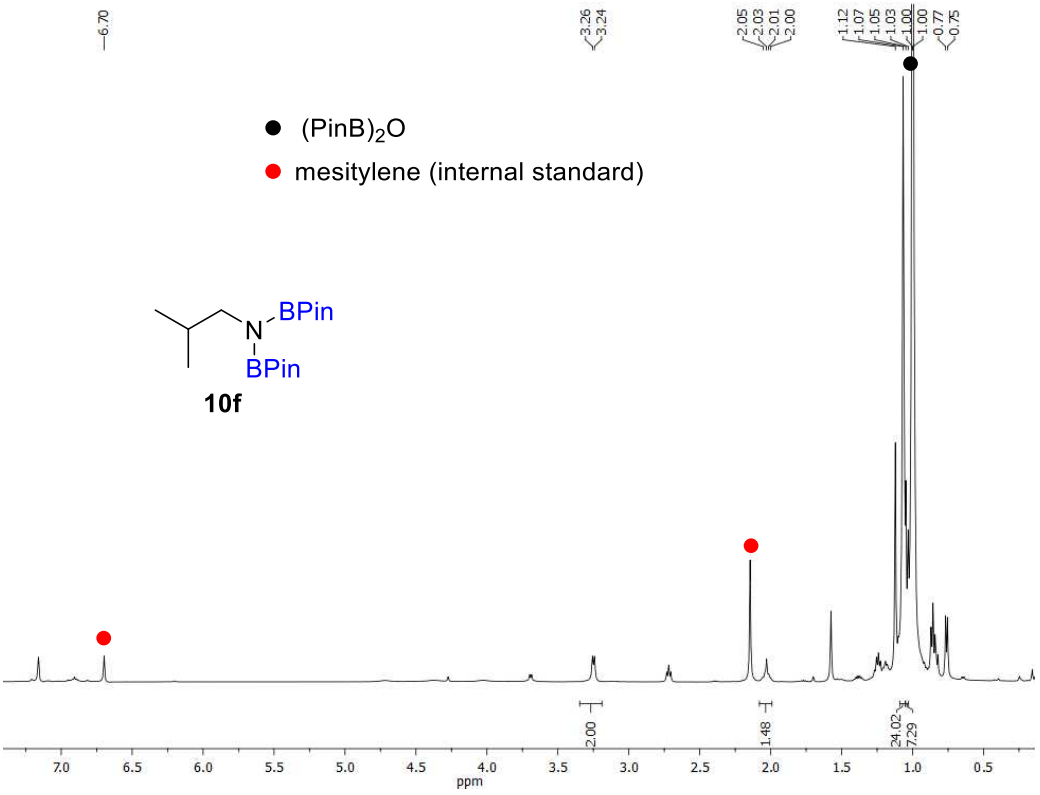

Figure 103. ^{1}H-NMR spectrum of **10f** taken directly from the reaction mixture upon **2-CH$_2$TMS**-catalyzed hydroboration of isobutyramide with HBPin in C_6D_6.

7. References

1 (*a*) D. M. Spasyuk, D. Zargarian and A. van der Est, *Organometallics*, 2009, **28**, 6531-6540; (*b*) D. M. Spasyuk, S. I. Gorelsky, A. van der Est and D. Zargarian, *Inorg. Chem.*, 2011, **50**, 2661–2674; (*c*) B. Mougang-Soumé, F. Belanger-Gariépy and D. Zargarian, *Organometallics*, 2014, **33**, 5990–6002.

2 V. Pandarus and D. Zargarian, *Chem. Commun.*, 2007, 978-980.

3 D. Morales-Morales, C. Grause, K. Kasaoka, R. Redon, R.E. Cremer and C.M. Jensen, *Inorg. Chim. Acta*, 2000, **300-302**, 958-963.

4 K. A. Gudun, M. Segizbayev, A. Adamov, P. N. Plessow, K. A. Lyssenko, M. P. Balanay and A. Y. Khalimon, *Dalton Trans.*, 2019, **48**, 1732–1746

5 (*a*) S. Chakraborty, J. A. Krause and H. Guan, *Organometallics*, 2009, **28**, 582-586; (*b*) N. P. N. Wellala, H. T. Dong, J. A. Krause and H. Guan, *Organometallics*, 2018, **37**, 4032-4039.

6 For synthesis of **6-H** from **6-Br**, $LiHBEt_3$ (1.1 equiv. to **6-Br**) was used instead of excess $LiAlH_4$ as in the original method described in ref. 5.

7 F. Zhang, M.Gong, H. Xie and Y. Luo, *New J. Chem.*, 2021, **45**, 17654-17659.

8 N. R. Anastasi, K. M. Waltz, W. L. Weerakoon and J. F. Hartwig, *Organometallics*, 2003, **22**, 365-369.

9 S. Saha and M. Eisen, *Dalton Trans.*, 2020, **49**, 12835-12841.

10 (*a*) M. Bhunia, S. R. Sahoo, A. Das, J. Ahmed, Sreejyothi P. and S. K. Mandal, *Chem. Sci*.**,** 2020, **11**, 1848-1854; (*b*) R. Kumar, M. K. Bisai, S. Jain, K. Vanka and S. S. Sen, *Chem. Commun.*, 2021, **57**, 10596-10599; (c) M. K. Bisai, K. Gour, T. Das, K. Vanka and S. S. Sen, *Dalton Trans.*, 2021, **50**, 2354-2358.

11 K. A. Gudun, A. Slamova, D. Hayrapetyan and A. Y. Khalimon, *Chem. Eur. J.*, 2020, **26**, 4963-4968.

12 X. Wang and X. Xu, *RSC Adv.*, 2021, **11**, 1128-1133.

13 S. Saha and M. S. Eisen, *ACS Catal.*, 2019, **9**, 5947-5956.

14 Z. Moutaoukil, E. Serrano-Díez, I. G. Collado, M. Jiménez-Tenorio and J. M. Botubol-Ares, *Org. Biomol. Chem.*, 2022, **20**, 1103-1111.

15 S. Mahato, P. Rawal, A. K. Devadkar, M. Joshi, A. R. Choudhury, B. Biswas, P. Gupta and T. K. Panda, *Org. Biomol. Chem.*, 2022, **20**, 831-839.

16 C. Lu, Z. Qiu, M. Xuan, Y. Huang, Y. Lou, Y. Zhu, H. Shen and B.-L. Lin, *Adv. Synth. Catal.*, 2020, **362**, 4551-4158.

17 D. Nagaraja and M. A. Pasha, *Indian J. Chem., Sect B.*, 2004, **43B**, 593-594

18 C. R. Aversa-Fleener, D. K. Chang and A. L. Liberman-Martin, *Organometallics*, 2021, **40**, 4050-4054.

19 Q. Xie and G. Dong, *J. Am. Chem. Soc.*, 2021, **143**, 14422-14427.

20 (*a*) A. Kaithal, B. Chatterjee and C. Gunanathan, *J. Org. Chem.*, 2016, **81**, 11153-11161; (*b*) M. Ito, M. Itazaki and H. Nakazawa, *Inorg. Chem.*, 2017, **56**, 13709-

13714; (*c*) H. Ben-Daat, C. L. Rock, M. Flores, T. L. Groy, A. C. Bowman and R. J. Trovich, *Chem. Commun.*, 2017, **53**, 7333-7336.

21 C. Weetman, M. D. Anker, M. Arrowsmith, M. S. Hill, G. Kociok-Köhn, D. J. Liptrot and M. F. Mahon, *Chem. Sci.*, 2016, **7**, 628-641.